



UNILASALLE 
CENTRO UNIVERSITÁRIO LA SALLE

CÉSAR MOACIR NORIEGA LEAL CUTRUNEO

**ESPECIAÇÃO QUÍMICA E MINERALÓGICA DOS RESÍDUOS DO
BENEFICIAMENTO DE CARVÕES BRASILEIROS**

CANOAS, 2014

CÉSAR MOACIR NORIEGA LEAL CUTRUNEO

**ESPECIAÇÃO QUÍMICA E MINERALÓGICA DOS RESÍDUOS DO
BENEFICIAMENTO DE CARVÕES BRASILEIROS**

Dissertação apresentada à banca examinadora do Programa de Pós-Graduação, Mestrado em Avaliação de Impactos Ambientais do Centro Universitário La Salle - Unilasalle.

Orientação: Prof. Dr. Luís Felipe Silva Oliveira

Prof. Dr. Marcos Leandro Silva Oliveira

CANOAS, 2014

Dados Internacionais de Catalogação na Publicação (CIP)

C989e Cutruneo, César Moacir Noriega Leal.

Especiação química e mineralógica dos resíduos do beneficiamento de carvões brasileiros [manuscrito] / César Moacir Noriega Leal Cutruneo. – 2014.

81f. ; 30 cm.

Dissertação (mestrado em Avaliação de impactos ambientais) – Centro Universitário La Salle, Canoas, 2014.

“Orientação: Prof. Dr. Luis Felipe Silva Oliveira”.

1. Carvão mineral.
 2. Difração - Carvão.
 3. Microscopia eletrônica.
 4. Geoquímica.
- I. Oliveira, Luis Felipe Silva. II. Título.

CDU: 504:553.94

Bibliotecário responsável: Melissa Rodrigues Martins - CRB 10/1380

CÉSAR MOACIR NORIEGA LEAL CUTRUNEO

**ESPECIAÇÃO DOS ELEMENTOS CONSTITUINTES
DOS CARVÕES ROM E DOS RESÍDUOS DO BENEFICIAMENTO**

Dissertação apresentada a banca examinadora do Programa de Pós-Graduação, Mestrado em Avaliação de Impactos Ambientais do Centro Universitário La Salle - Unilasalle.

Aprovado pela banca examinadora 4 de agosto de 2014.

BANCA EXAMINADORA

Prof. Dra. Gelsa Edith Navarro Hidalgo
Unilasalle

Prof. Dr. Silvio Roberto Taffarel
Unilasalle

Prof. Dra. Kátia da Boit Martinello
UFRGS

Prof. Dr. Luis Felipe Silva Oliveira
Unilasalle

RESUMO

Os níveis de elementos perigosos no solo superficial de uma área de mineração de carvão dependem, não somente da configuração geológica da região e do solo subjacente, mas também pode ser influenciada por transportes, eólico ou pela água, de resíduos do beneficiamento. Poucos estudos avaliam a relação da composição química e mineralógica de ROM (rom of mine, carvão bruto) e rejeitos do beneficiaento do carvão brasileiro (coal cleaning rejects - CCRs), que podem representar fontes significativas de contaminação da água ou do solo. Neste estudo, foi investigado a distribuição quantitativa de minerais e elementos potencialmente perigosas em CCRs e um carvão ROM dos estados brasileiros do Rio Grande do Sul e Santa Catarina. Os principais minerais identificados por difração de raios-X (XRD), microscopia eletrônica de transmissão de alta resolução (HR-TEM), microscopia eletrônica de varredura com emissão de campo com energia de raios-X (FE-SEM/EDS) foram caulinita, quartzo, camada mixta de ilita-esmectita, pirita, jarosita, melanterita, gesso, rutilo e calcita, enquanto os minerais minoritários incluem barita, hematita, siderita, esfalerita e goethita. Galena, magnetita, zircão, e muitas outras espécies também podem ocorrer como minerais acessórios. Pirita e jarosita são relativamente abundantes em alguns casos, tornando-se cerca de 4% a 5% da matéria mineral. Assim com a jarosita, a melanterita e o gesso, provavelmente são formados pela complexa interação de produtos da oxidação de sulfetos de ferro e argilominerais, além de componentes de carbonatados, iniciado a partir da exposição e armazenagem do material em estudo. Tal exposição à atmosfera, promove a oxidação de sulfeto que em contato com outro minerais libera quando quantidade de substanciais de sulfato, bem como de Ca^{2+} , K^+ , Mg^{2+} , Cl^- , e Al^{3+} . A maior parte dos poluentes nas amostras CCRs exibe uma solubilidade dependente do pH, sendo imobilizado em amostras quase neutras, mas móvel, em condições de baixo pH. Os resultados destacam as complexas interações entre os componentes da matéria mineral do CCRs durante o armazenamento, e o potencial para a liberação de elementos perigosos, em associação com a exposição e armazenamento de longo prazo de tais materiais.

Palavras-chave: Formação docarvão mineral; beneficiamento de carvão; petrologia de carvão; material mineral; Difração de Raio-X; microscopia eletrônica; geoquímica de elementos-traço.

ABSTRACT

The background and anthropogenic levels of hazardous elements in the surface soil of a coal mining area depend on the geological setting of the region and the underlying soil material, but may also be influenced by water-borne or aeolian transport of sediment from adjacent coal-related waste piles. Very few studies have focused on the chemical and mineralogical composition of Brazilian coal cleaning rejects (CCRs), which may represent significant sources of soil or water contamination. In this study, we have investigated the quantitative distribution of minerals and potentially hazardous elements in CCRs and a run-of-mine coal from the Brazilian states of Rio Grande do Sul and Santa Catarina. The major minerals, identified by X-ray diffraction (XRD), high-resolution transmission electron microscopy (HR-TEM), and field-emission scanning electron microscopy/energy dispersive X-ray analysis techniques (FE-SEM/EDS) are kaolinite, quartz, mixed-layer illite-smectite, pyrite, jarosite, melanterite, gypsum, rutile, and calcite, while minor minerals include barite, hematite, siderite, sphalerite, and goethite. Galena, magnetite, zircon, and many other species may also occur as accessory/trace minerals. Pyrite and jarosite are relatively abundant in some cases, making up to around 4% or 5% of the mineral matter, with jarosite, melanterite, and gypsum probably formed by complex interaction of oxidation products from Fe-sulfides and clay or carbonate components, initiated by exposure and storage of the host material. Such atmospheric exposure promotes sulfide oxidation that releases substantial sulfate loads as well as Ca^{2+} , K^+ , Mg^{2+} , Cl^- , and Al^{3+} . Metals with the most severe discharges were Zn, Cu, Mn, Co, Ni, and Cd. Most of the trace pollutants in the CCRs displayed a pH-dependent solubility, being immobile in near-neutral samples but mobile under the low-pH conditions associated with oxidized material. The results highlight the complex interactions among mineral matter components of the CCRs during storage, and the potential for release of potentially hazardous elements in association with longer-term exposure and storage.

Keywords: Coal preparation; coal petrology; mineral matter; X-ray diffraction; electron microscopy; trace element geochemistry.

APRESENTAÇÃO DA ESTRUTURA DA DISSERTAÇÃO

Esta Dissertação de mestrado, intitulada “**ESPECIAÇÃO QUÍMICA E MINERALÓGICA DOS RESÍDUOS DO BENEFICIAMENTO DE CARVÕES BRASILEIROS**”, foi desenvolvida entre março de 2013 e agosto de 2014 no Laboratório de Estudos Ambientais e Nanocompósitos do Centro Universitário La Salle - Unilasalle Canoas, em colaboração com a School of Biological, Earth and Environmental Sciences, University of New South Wales, Sydney, NSW 2052, Australia; University of Kentucky Center for Applied Energy Research, 2540 Research Park Drive, Lexington, KY 40511, USA; Universidade Federal do Rio Grande do Sul, Escola de Engenharia, Departamento de Metalurgia, Centro de Tecnologia, Av. Bento Gonçalves, 9500. Bairro Agronomia. CEP: 91501-970, Porto Alegre, RS, Brazil; Fundação Estadual de Proteção Ambiental Henrique Luis Roessler, Porto Alegre, RS, Brazil.

A Dissertação é composta das seguintes partes:

- Capítulo I: Aspectos introdutórios

Trata sobre os aspectos introdutórios, objetivos, revisão bibliográfica, metodologia.

- Capítulo II: Resultados na forma de artigo científico publicado.

- Capítulo III: Considerações finais.

Apresenta as conclusões, considerações finais e recomendações de futuras pesquisas.

ANEXO A: Trabalho na forma de artigo científico publicado como co-autor.

LISTA DE FIGURAS

Figura 1: Diagrama ilustrando a formação do carvão	13
Figura 2: Formação do carvão mineral.....	15
Figura 3: Natureza dos materiais inorgânicos presentes em carvões	16
Figura 4: Geologia da Bacia do Paraná	18

SUMÁRIO

CAPITULO I	1
INTRODUÇÃO	2
OBJETIVO	6
JUSTIFICATIVA	7
REFERENCIAL TEÓRICO	11
METODOLOGIA	19
Análises Petrográficas	19
Determinação química	20
Determinação mineralógica	22
REFERÊNCIAS.....	25
CAPITULO II.....	31
Resultados na forma de artigo científico publicado.	
CAPITULO III	51
Conclusões, considerações finais e recomendações de futuras pesquisas	
ANEXO A.....	54
Trabalho na forma de artigo científico publicado como co-autor	

CAPITULO I

INTRODUÇÃO,
OBJETIVOS,
JUSTIFICATIVA,
REFERENCIAL
TEÓRICO,
METODOLOGIA.

INTRODUÇÃO

Os principais depósitos do carvão extraído no Brasil encontram-se distribuídos em toda a parte sul do país e se estendem do estado do Paraná até o estado do Rio Grande do Sul (THOMAS, 2002; KALKREUTH et al, 2004). As reservas de carvão do Brasil estão na ordem de 32×10^9 toneladas (KALKREUTH et al., 2006), sendo que a maioria destas (89%) estam localizadas no Rio Grande do Sul, cerca 10% localizados no estado de Santa Catarina, e pequenas quantidades no Paraná e no estado de São Paulo (ABCM, 2014).

O carvão está inserido dentro do contexto geológico da Bacia do Paraná, uma bacia sedimetar intratectônica que evoluiu sobre a plataforma sul americana (HOLZ et al, 1998; KALKREUTH et al, 2006) de cerca de 1.400.000km², que cobre a porção sul do Brasil, o Paraguai, o Uruguai e parte da Argentina, com formato alongado na direção NNE-SSO (1.750 km de comprimento) e largura média de 900km (ZALÁN et. al, 1990). A formação sedimentar iniciou a cerca de 450 milhões de anos, no período Ordoviciano, terminando no Terciário, segundo MINEROPAR (2006). O conjunto de rochas sedimentares e vulcânicas que constituem a Bacia do Paraná representa a superposição de pacotes depositados em três diferentes ambientes tectônicos, decorrentes da dinâmica das placas que conduziu a evolução do Gondwana no tempo geológico (ZALÁN et al., 1990). Seu nome deriva do rio Paraná, o qual percorre paralelo ao seu eixo maior, formando o limite entre Paraguai e Argentina. O preenchimento sedimentar da bacia varia da idade do Ordoviciano-Siluriano ao Cretáceo Superior.

Os estudos petrográficos e seqüências estratigráficas (HOLZ et al, 1998; KALKREUTH et al, 2006) indicam que os veios de carvão, pelo menos na parte sul da bacia, foram formados em turfeiras. Estas turfeiras, a partir do qual se originaram os carvões, foram formadas em pequenas lagoas (KLEPZIG, 2001), com vegetação crescendo e sendo transportado no interior das lagoas, e depositado junto com o solo. O material rico em argila e quartzo tornou-se, assim, intimamente mesclado com a matéria orgânica, o que resulta em carvões com alto teor de cinzas (PIRES e QUEROL, 2004). Os carvões foram comumente recobertos por sedimentos marinhos, um fator que normalmente produz alto teor de enxofre (em média 2,2%) e também de carbonatos (KALKREUTH et al, 2006).

Os carvões na parte sul do Rio Grande do Sul são principalmente sub-betuminosos, mas aqueles mais ao norte, incluindo o carvão em Santa Catarina, são na sua maioria betuminoso alto volátil (KALKREUTH et al, 2004, 2006). Alguns autores (OLIVEIRA et al. 2012) relataram médias máximas de vitrinita e de reflectância para carvões catarinenses variando

entre 0,44 e 1,38%, embora a maior parte dos depósitos costume ter valores entre 0,7 e 1,0%. Kalkreuth et al. (2004) verificaram que a vitrinita em carvões da Bacia do Paraná possui tipicamente características de baixa reflectância.

A produção total de carvão do Brasil está atualmente em torno de 6 Mt por ano (DNPM, 2010). O Rio Grande do Sul é o maior produtor, com 53,1% da produção total; Santa Catarina produz 45,6% e Paraná 1,3%. Atualmente o Brasil, mesmo não sendo o maior produtor, é o maior consumidor de carvão mineral dos países da América do Sul e tal consumo vem crescendo, devido à falta de chuvas no país o que ocasiona uma maior produção energética oriunda de fontes fósseis, a fim de suprir a necessidade energética e manter a economia. No entanto, com o aumento do uso de carvão há uma crescente preocupação sobre os impactos ambientais e na saúde humana, devido o incremento da exposição aos elementos potencialmente perigosos liberados no curso de mineração de carvão, beneficiamento, transporte e combustão de tal mineral (SILVA et al., 2010, 2012).

A região carbonífera brasileira foi classificada como zona de perigo ambiental nacional por um decreto federal de 1980. Deste modo, a área obteve uma assistência especial do governo para tratar do solo e da qualidade da água. Esta assistência permitiu o setor de mineração atender às demandas brasileiras para o carvão mineral, protegendo o ambiente ou ao menos minimizando seus impactos. Em resposta a uma decisão judicial, após uma ação civil pública movida pelo Ministério Público Federal, e em conformidade com os acordos associados, as empresas de mineração de carvão e o governo federal estão dedicando atenção especial para projetos ambientais em áreas degradadas por esta mineração. Por este motivo, a necessidade de pesquisas sobre o comportamento geoquímico dos rejeitos de beneficiamento dos carvões run-of-mine (ROMs) tornou-se mais econômica e ambientalmente relevante. Afinal, devido às altas quantidades de solo e de enxofre, os carvões ROMs, são geralmente beneficiados para se obter um produto com menor percentual de solo e de enxofre, para fins de utilização na geração energética.

Alguns autores (MARCELLO et al. 2008) indicam que cerca de 3,5 Mt por ano, ou aproximadamente 58% da produção de ROM, são resíduos do processo de beneficiamento e por tanto são dispostos em aterros mal preparados, o que gera grandes impactos ambientais. Quase todo o carvão beneficiado é usado para geração de energia, basicamente em cinco plantas térmicas, com uma capacidade total instalada de cerca de 2.000 MW (ANEEL, 2012). A energia gerada a partir destas plantas fornece aproximadamente 11% das necessidades totais de energia elétrica do Brasil (SILVA et al., 2010), sendo três dessas usinas localizadas no Rio Grande do Sul, uma em Santa Catarina e uma no Paraná.

Cabe destacar que a termelétrica a carvão mineral pulverizado, hoje instalada no estado do Ceará é a que possui maior capacidade instalada no Brasil, entretanto a Eneva (www.eneva.com.br), antes designada como MPX Energia S.A. trata-se de uma *joint-venture* do grupo EBX e da empresa alemã E.ON, não utiliza carvão nacional e sim importado especialmente da Colômbia por conter menores quantidades de solo, enxofre e elementos potencialmente carcinogênicos, se comparado com a média do carvão brasileiro. As termelétricas Pecém I e Pecém II estão localizadas no município de São Gonçalo do Amarante (CE) e juntas ampliaram em 90% a produção de energia elétrica no Ceará. Hoje possuem uma capacidade instalada de 1085 MW.

A maioria dos carvões minerados em Santa Catarina possui propriedades coqueificáveis, entretanto a produção atual é praticamente toda utilizada para a geração de eletricidade na termelétrica Jorge Lacerda (Tractebel Suez), localizada na cidade de Capivari de Baixo, no sul do Estado de Santa Catarina, que possui uma capacidade de 875 MW. No entanto, uma pequena quantidade do material beneficiado, principalmente finos de carvão a partir das plantas de preparação, é utilizada em operações de fundição metalúrgica.

Nas plantas de beneficiamento os carvões brasileiros são geralmente menores de 40-50 mm (SAMPAIO et al., 2008, 2011). Devido à mistura de vegetação e solo/barro durante a formação de turfa, o grau de libertação da matéria orgânica esmagadas, presente no ROM é normalmente muito baixo. Os processos de concentração de carvão por gravidade são os mais comuns na região carbonífera brasileira, fazendo uso inclusive de espirais visando a concentração para carvões finos. Apesar do beneficiamento, os carvões obtidos no sul do Brasil com menos de 40% de solo são raramente obtidos e em média são utilizados carvões entre 43-56% de solo (OLIVEIRA et al., 2013).

A fim de proporcionar produtos com baixas quantidades de solo os carvões com pequenos tamanhos costumam ser misturados na blendagem, após beneficiamento, no entanto, isso pode provocar uma diminuição da eficácia dos processos de beneficiamento (SAMPAIO e TAVARES, 2005), e também aumentam o teor de humidade dos produtos diminuindo assim a eficiência energética nas centrais termelétricas, que acabam utilizando óleo diesel para manter as temperaturas das caldeiras. Consequentemente carvões com granulometria maior que 50 mm são os mais utilizados nos processos de beneficiamento e raramente se utilizam carvões com granulometria inferior a 30 mm.

Existe uma relação inversa entre o rendimento de carvão beneficiado e de qualidade de carvão beneficiado, dependendo da natureza das partículas compostas no carvão triturado para ser beneficiado. Altas proporções de partículas com densidades próximas ao ponto de corte

tendem a fazer com que a separação seja difícil, com pequenas variações na densidade do ponto de corte que produzem grandes variações na produtividade e qualidade do produto beneficiado.

Atualmente o beneficiamento do carvão brasileiro oferece duas classes principais de produtos:

- carvões grossos, com tamanho beneficiado tipicamente acima de 2 mm, os quais são vendidos para as termelétricas;
- carvões finos, com tamanho beneficiado geralmente abaixo de 2 mm, São vendidos com as plantas de produção de coque de fundição ou misturados com carvão mais grossos e enviados para temelétricas.

A separação das amostras de carvões trituradas com diferentes frações de densidade tem sido utilizado em vários estudos (GLUSKOTER et al, 1977; SÉNIOR et al, 2000; QUEROL et al 2001; WAGNER e TLOTLENG, 2012) como base para a avaliação dos modos de ocorrência de diferentes elementos-traço. Tal abordagem é geralmente usada para indicar se elementos particulares estão mais fortemente associadas com as partículas densas, matérias minerais do carvão com afinidade inorgânica, ou com as partículas menos densas, frações ricas em macerais com afinidade com a matéria orgânica. Tais estudos são geralmente realizados em amostras trituradas até um tamanho de partículas relativamente finas ($\leq 0.1\text{mm}$), o que propicia uma maior libertação de matéria mineral e de componentes orgânicos, além de uma separação mais eficaz do que seria normalmente obtida sob condições de processamento industrial.

OBJETIVO

Objetivo principal

O objetivo principal do presente estudo é comparar as características químicas¹, mineralógicas² e geoquímicas³ de resíduos de carvões após beneficiamento a partir das principais minas de Santa Catarina e Rio Grande do Sul, a fim de avaliar os principais elementos-traço associados com a concentração de matéria orgânica, nos processos de beneficiamento.

Objetivo secundário

Ajudar na concepção de novas plantas e processos de beneficiamento, para auxiliar o projeto e operação de usinas movidas a carvão. Aumentar o nível de compreensão no desenvolvimento e uso de carvão no Brasil. Espera-se que os resultados forneçam informações para desenvolver uma base técnica para novos planos de recuperação nas áreas de mineração de carvão, bem como para estudos toxicológicos posteriores utilizando tais amostras em estudo na presente dissertação.

¹ Composição total dos elementos constituintes.

² Fração cristalina e ordenada.

³ Estudo das transformações mineralógicas.

JUSTIFICATIVA

Muitos estudos têm sido realizados visando avaliar as variações nas características do carvão associado com a preparação em escala industrial, incluindo variações nas composições químicas (HOWER et al, 1998; MASTALERZ e PADGETT, 1999; VAMVUKA et al, 2001; VASSILEV et al, 2001; WANG et al, 2006; HUGGINS et al, 2009; MOORE e ESMAEILI, 2012; OLIVEIRA et al., 2012, 2013). No entanto, poucos desses estudos têm abordado a variação nas composições químicas e mineralógicas do carvão com a preparação ou focado em mais do que um pequeno número de plantas de beneficiamento. Os minerais são, no entanto, os componentes fundamentais que afetam muitos aspectos do comportamento do carvão, tais como a fusão das cinzas (BRYERS, 1996; REIFENSTEIN et al, 1999; MATJIE et al, 2012a,b), e também a ocorrência e comportamento de determinados elementos-traço, tanto em depósitos (WARD et al, 2011; OLIVEIRA et al, 2012) como durante a utilização (CLARK e SLOSS, 1992; GOODARZI e SWAINE, 1995; QUEROL et al, 1995; QUISPE et al, 2012). Com isso a presente dissertação apresenta grande relevância para a sociedade científica ao aportar melhores dados para as empresas e indústria desse setor mineral.

Autores anteriores (HUGGINS et al. 2009) investigaram as características mineralógicas e geoquímicas do carvão ROM, produtos beneficiados e resíduos do beneficiamento, da Bacia de Illinois, e as variações relacionadas em concentrações de elementos-traço entre essas frações e as variações na abundância relativa de componentes minerais específicos. Moore e Esmaeli (2012) realizou um estudo semelhante de duas minas subterrâneas de carvão no Alborz Coalfield do Irã, mais uma vez com um foco em variações na composição química. Matjie et al. (2008) avaliaram em laboratório de carvão Sul-Africano, o particionamento de minerais entre as frações separadas e os resultados relacionados aos modos de ocorrência mineral de diferentes tamanhos de partículas em carvão triturados para fins industriais.

No Brasil alguns autores (OLIVEIRA et al., 2013, 2012) compararam amostras de ROM e produtos do carvão beneficiados derivados de plantas de preparação em Santa Catarina, tais autores comprovaram reduções significativas de matéria mineral e porcentagens totais de enxofre associados ao beneficiamento, e também nas proporções relativas de pirita dentro da matéria mineral. Com exceção da pirita, a matéria mineral dos carvões beneficiados quantificados por difração de raio-X, é semelhante à dos respectivos materiais ROMs. O quartzo assim como a caulinita, ilita e mesclas de ilita-esmectita, assim como proporções menores de calcita e outras fases mineralógicas acessórias, foram pouco extraídas após o

processo de beneficiamento do carvão mineral. Tais autores comprovaram que apesar da pirita nos ROMs aparecer na forma framboidal, e, portanto, intimamente relacionado com a matéria orgânica, a redução do teor de pirita foi significativa após os processos de beneficiamento. Estes autores ratificaram com a comparação dos ROMs e amostras beneficiadas, que as concentrações da maioria dos elementos-traço potencialmente perigosos (ex.: As, Cd, Cr, Hg, Pb, Zn entre outros) são similares nos dois tipos de materiais, ou são reduzidos no carvão beneficiado por uma proporção similar à redução global do teor de matéria mineral (porcentagem de cinzas obtidas a baixa temperatura, low temperature ash - LTA). As concentrações de As e Pb foram reduzidas quanto maior a redução associada com a pirita, confirmando que estes elementos estão associados com a pirita nos materiais ROMs. A concentração de B também diminui substancialmente com o beneficiamento, indicando possivelmente uma associação com turmalina nos materiais ROMs, mas na maioria dos casos, as concentrações dos elementos-traço são semelhantes nos ROMs e amostras de carvão beneficiado. Entretanto, alguns elementos como U e Th foram concentrados nos produtos beneficiados devido a grande afinidade com a matéria orgânica.

Os impactos na saúde humana e no ambiente, causados pela extração e o uso de carvão, estão relacionados principalmente com o tipo e abundância dos minerais presentes nos ROMs, resíduos do beneficiamento e, principalmente, com os níveis de elementos potencialmente tóxicos contidos nos minerais (FINKELMAN, 1993; FINKELMAN et al., 2002; SILVA et al., 2012). Uma compreensão do modo de associação dos minerais, com a matriz de carvão é importante, antes da aplicação de tecnologia de beneficiamento do carvão ou utilização deste mineral.

Grandes quantidades de minerais derivados do carvão concentram-se nos resíduos dos processos de beneficiamento, especialmente em amostras como os carvões brasileiros, por conterem altas quantidades de solo mesclado com a matéria orgânica. Por tanto, o conhecimento das características mineralógicas também é muito importante para a compreensão da formação de materiais ultrafinos e nanopartículas durante o beneficiamento do carvão, e para desenvolver os passos de controle necessários afim de minimizar impacto na saúde e no ambiente. Os resíduos do beneficiamento dos carvões brasileiros são muitas vezes mal dispostos em aterros com poucas tentativas de entender seus potenciais impactos sobre o ambiente ou mesmo de buscar novas aplicações para os mesmos (MARCELO et al. 2008; OLIVEIRA et al., 2012).

A maioria das empresas de mineração de carvão possuem licenças ambientais de operação válidas para a exploração de plantas de beneficiamento, cabendo destacar que estão

havendo esforços substanciais para atender às normas ambientais relativas às áreas envolvidas nos processos de extração, beneficiamento e estocagem dos carvões bem como de seus resíduos. Uma série de medidas estão sendo aplicadas para reduzir o impacto ambiental das atividades de mineração de carvão, como restringir o tráfego de caminhões durante a noite, regar estradas para reduzir a formação de poeira e cobrindo caminhões para evitar o derramamento (SILVA et al., 2012; OLIVEIRA et al., 2013). No entanto, estas medidas têm se revelado insuficientes para evitar danos causados pela atividade de mineração nas minas de carvão.

Com exceção de produtos secundários associados com oxidação de sulfetos de ferro e dissolução de carbonatos e argilas, os minerais presentes nos resíduos do beneficiamento do carvão são geralmente semelhantes aos encontrados em amostras de ROMs de vários países (DAI et al, 2012, 2013, 2005; SUÁREZ-RUIZ e WARD, 2008; QUEROL et al, 2008, 1995, 2001; RIBEIRO et al, 2013a, b; YOSSIHOVA, 2014). A maioria dos minerais em si não apresentam riscos ambientais ou de saúde humana, a menos que inalados, por exemplo, quartzo ultrafino e várias argilas contendo elementos tóxicos. No entanto, uma abundância de partículas ultrafinas derivadas do carvão, como sulfetos de ferro e nanoparticulates (por exemplo, anatásio, quartzo, sulfatos de ferro, óxidos de ferro e siderita contendo elementos perigosos) pode apresentar algumas preocupações (DAI et al, 2012, 2013;. HUGGINS et al, 2012;. OLIVEIRA et al, 2012;. YOSSIHOVA, 2014). Por exemplo, a sílica cristalina está correlacionada a incidência de câncer de pulmão (TIAN et al., 2008) e, em 1997, da Agência Internacional da Organização Mundial da Saúde para Pesquisa sobre o Câncer (IARC) reclassificou o quartzo e sílica cristalina de classe II para classe I sendo assim taxados como agentes cancerígenos, afirmando que existem provas suficientes para a carcinogenicidade de quartzo em seres humanos e animais experimentais. No entanto, a sílica amorfa também pode ser benéfica, com efeitos positivos sobre a produção de gramíneas (SCHALLER et al., 2012).

Avaliando a composição química e mineralógica de carvão e subprodutos de carvão ou resíduos é importante avaliar o seu potencial impacto na saúde humana e ambiental (FINKELMAN, 1994, 1995; FINKELMAN et al, 2002). Alguns mineiros, pessoas e vegetação em torno de minas carboníferas brasileiras sofreram graves doenças e alterações no DNA causadas pelo contato com o carvão e seus subprodutos (ZOCCHE et al., 2014, 2013). Ren et al. (2004), em um estudo de minas chinesas, relatou que os pulmões dos mineiros contêm Cr em níveis superiores aos das pessoas da mesma região que não são mineiros. Alguns carvões brasileiros são altamente enriquecidos em elementos potencialmente perigosos (por exemplo, Ti em forma de anatasio e rutilo sendo ambos nanométricos; óxidos

de ferro e de alumínio contendo Cd, Cr, Pb e V), o que pode estar relacionado ao câncer de pulmão. No entanto, estudos de impacto direto na saúde humana ainda estão em desenvolvimento e deve ser evitado especulação excessiva no que diz respeito a estes aspectos, afinal afirmações atualmente específicas para determinados carvões brasileiros seria prematura.

Os modos de ocorrência de elementos potencialmente perigosos, são particularmente importantes para as populações expostas a sua influência, como é o caso na área próxima dos aterros de resíduos do beneficiamento. Destaca-se que os resíduos do beneficiamento de carvões brasileiros, derivados do depósito fluvial para ambientes com influência marinha, são geralmente enriquecido em alguns elementos (por exemplo, Cr, V, Rb, Sr), não só porque a água do mar contém maiores concentrações desses elementos do que de água doce (OLIVEIRA et al., 2012), mas também porque o plâncton na água do mar são enriquecidos nesses elementos e também pode alterar o pH, Eh e teor de H₂S, levando a um ambiente favorável para o enriquecimento de tais componentes. Observações semelhantes foram relatadas para carvões chineses (WANG et al, 2007, 2008; DAI et al, 2013).

As concentrações dos elementos perigosos não são o único fator que precisa ser considerado na avaliação do comportamento destes em ROMs e resíduos do beneficiamento. O modo de ocorrência, isto é, se o elemento faz parte um mineral específico, se ele está disperso dentro de um hospedeiro mineral particular, ou nos macerais residuais, podem controlar em grande medida o perigo potencial que representa o elemento. Essas informações, no entanto, foram ignoradas pela maior parte das regulamentações ambientais sobre elementos perigosos em ROMs, produtos beneficiados, resíduos do beneficiamento do carvão mineral e sub-produtos da combustão do carvão brasileiro, o que justifica o desenvolvimento da presente dissertação de mestrado.

REFERENCIAL TEÓRICO

Segundo Schopf (1956) o carvão é uma rocha combustível que contém mais de 50% do seu peso e mais de 70% do volume de material carbonáceo, o qual é formado por compactação ou litificação de plantas remanescentes (BATES, 1987). Trata-se de uma rocha sedimentar, todavia tem uma alta carga de matéria orgânica. Em análises mais detalhadas é possível identificar, por exemplo, estruturas vegetais (e.g. folhas, ramos, raízes, lenhos carbonizados e palinomorfos). Considerando esta característica e o tempo necessário para que se concluam os processos vinculados à gênese do carvão, é possível determinar que ele deriva da deposição e compactação de grandes quantidades de matéria orgânica, sob a forma de macerais⁴, e inorgânica, sob a forma de sais minerais e elementos vestigiais organicamente associados, ocorridos ao longo de milhões de anos.

Para possibilitar a formação do carvão mineral são necessárias condições ambientais adequadas que permitam que uma grande quantidade de matéria orgânica seja acumulada e não seja totalmente decomposta. Em outras palavras, o processo de carbonificação compreende um enriquecimento relativo de carbono fixo à custo de outros elementos, como hidrogênio e oxigênio, expulsos sob forma de água (LEVANDOWSKI, 2009) e interação com fungos e bactérias. A carbonização desenvolve-se sob condições de temperatura e pressão equivalentes aos estágios diagenéticos e epimetamórficos das rochas inorgânicas, e a senilidade da matéria orgânica, frente a pequenas alterações dessas condições, como qualificador ideal para as fases iniciais do metamorfismo tanto da matéria orgânica como inorgânica, a partir de restos de plantas superiores, posteriores macerais, sejam depositadas em áreas alagadas como pântanos e turfeiras.

A água estagnada dos pântanos e turfeiras é pobre em oxigênio, de maneira que não é possível a decomposição completa (oxidação) da matéria orgânica. Em contrapartida, os restos das estruturas reacionam com organismos anaeróbios que os decompõem em parte.

Entre os fatores essenciais para a formação de turfeiras são (MENDONÇA FILHO, 2010a,b):

- clima que controla a produção de matéria vegetal;
- ambiente tectono-sedimentar que controla a subsidência e o equilíbrio entre a produção e a deposição da matéria vegetal;

⁴ Segundo ICCP (1971), macerais são remanescentes de plantas carbonificadas, as quais representam forma e/ou estrutura ainda preservada no estágio do carvão betuminoso (grau de evolução térmica) ou ainda produtos de degradação os quais a origem vegetal não pode mais ser reconhecida.

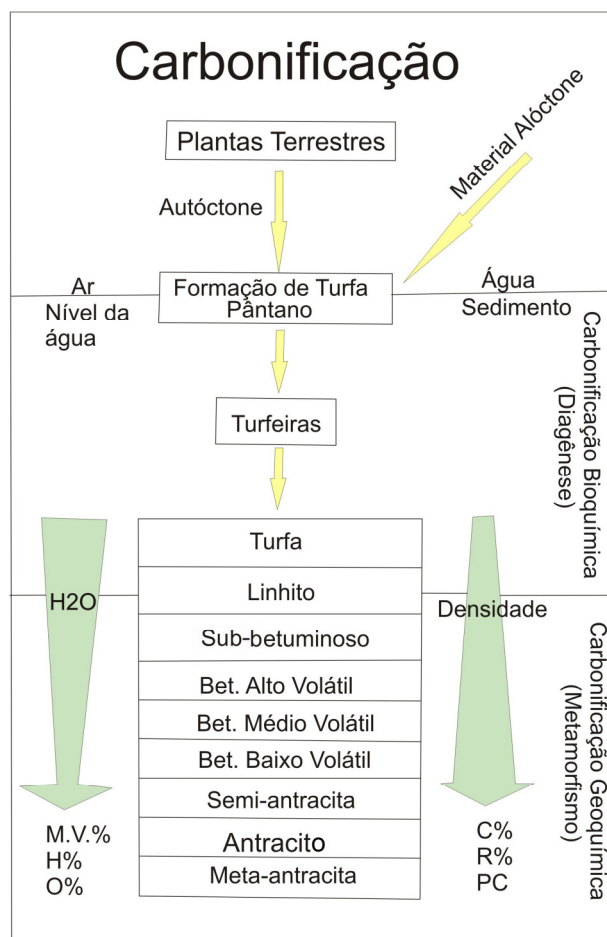
- aporte sedimentar e/ou detritico que dilui ou não a concentração de material orgânico;
- taxa de soterramento que controla a degradação bioquímica e preserva a matéria orgânica;
- ambiente sedimentar que controla a umidade (dependente do nível do lençol freático), a acidez que controla a atividade bacteriana, disponibilidade de nutrientes e a deposição química;
- potencial de oxi-redução da matéria orgânica depositada.

Posteriormente, o sedimento clástico (não orgânico) cumpre a função de isolar o material orgânico acumulado, auxiliando, também, em sua compactação. Isto permite que os materiais voláteis sejam eliminados, sob o efeito da temperatura, da pressão e do tempo. Segundo a MINEROPAR (1980), a matéria vegetal é posteriormente transformada em carvão pelo processo de carbonicação, ou seja: No início a massa vegetal acumulada e soterrada sofre a transformação gradual através de processos bioquímicos, processos esses que ocorrem na turfeira seguindo a deposição e o soterramento durante a diagênese, onde a turfa se transforma em linhito. Posteriormente esse material passa por processos geoquímicos, que ocorrem a profundidades muito pequenas nas turfeiras, na forma de atividade bacteriana que degrada a turfa (Figura 1). Caso estes níveis de material sejam recobertos profundamente por processos geológicos, que podem levar milhões de anos permitirá, então, a maturação do material (litificação), ou seja, a progressão de matéria orgânica a partir do estágio de turfa à antracito (Figura 2).

A etapa inicial do processo de formação de carvões húmicos⁵, consiste, no acúmulo de grandes quantidades de restos de seres vivos (principalmente vegetais) em condições especiais, entre elas a ausência de oxigênio. O maior componente orgânico da maioria dos carvões húmicos é um material brilhante marrom escuro ou preto, visível a olho nu e derivado principalmente da humificação de tecidos lenhosos (MENDONÇA FILHO, 2010a,b). Em carvões com baixo grau de carbonificação, este material é representado por um grupo de macerais chamado huminita, e em carvões betuminosos a antracíticos é chamado vitrinita (MENDONÇA FILHO, 2010b).

⁵ Carvões húmicos são originários essencialmente a partir de vegetais terrestres superiores com alto teor de hidratos de carbono, são tipicamente estratificados. Os carvões húmicos, propriamente ditos, passam através do estágio de turfa com processos que acompanham a humificação após a acumulação no lugar onde a planta cresceu. (Mendonça Filho, 2010).

Figura 1: Diagrama ilustrando a formação do carvão, com mudança nos parâmetros principais usados na determinação do *rank*. M.V. – Material volátil, R- reflectância da vitrinita e PC – poder calorífico.



Fonte: Adaptado de Levandowski, 2009.

Considerando a evolução húmica da matéria orgânica, à medida que o teor de substâncias minerais for se reduzindo e o teor de matéria orgânica aumentado, os folhelhos tendem a se carbonificar tornando-se folhelhos carbonosos a carvões húmicos. De acordo com a escala de carbonificação (maturação) os carvões húmicos são formados das seguintes categorias: turfa, linhito, sub-betuminoso, betuminoso, semi-antracita e antracito (MENDONÇA FILLO, 2010b).

À medida que a matéria orgânica é recoberta, os voláteis são liberados por pressão aumentando de maneira gradual a porcentagem de carbono no material restante (Figura 1). Nesta etapa (Figura 2A), as bactérias não são capazes de realizar a decomposição completa da matéria orgânica por serem destruídas pelos ácidos produzidos pelo próprio metabolismo. Ocorre, então, uma estabilização do material criando camadas do que é conhecido como **turfa** (Figura 2 B), que é a forma mais compacta do acúmulo superficial sedimentado em

decomposição, com teor d'água é entre 65-90%, e poder calorífico é de 3.000- 5.000 kcal/kg (MENDONÇA FILHO, 2010b).

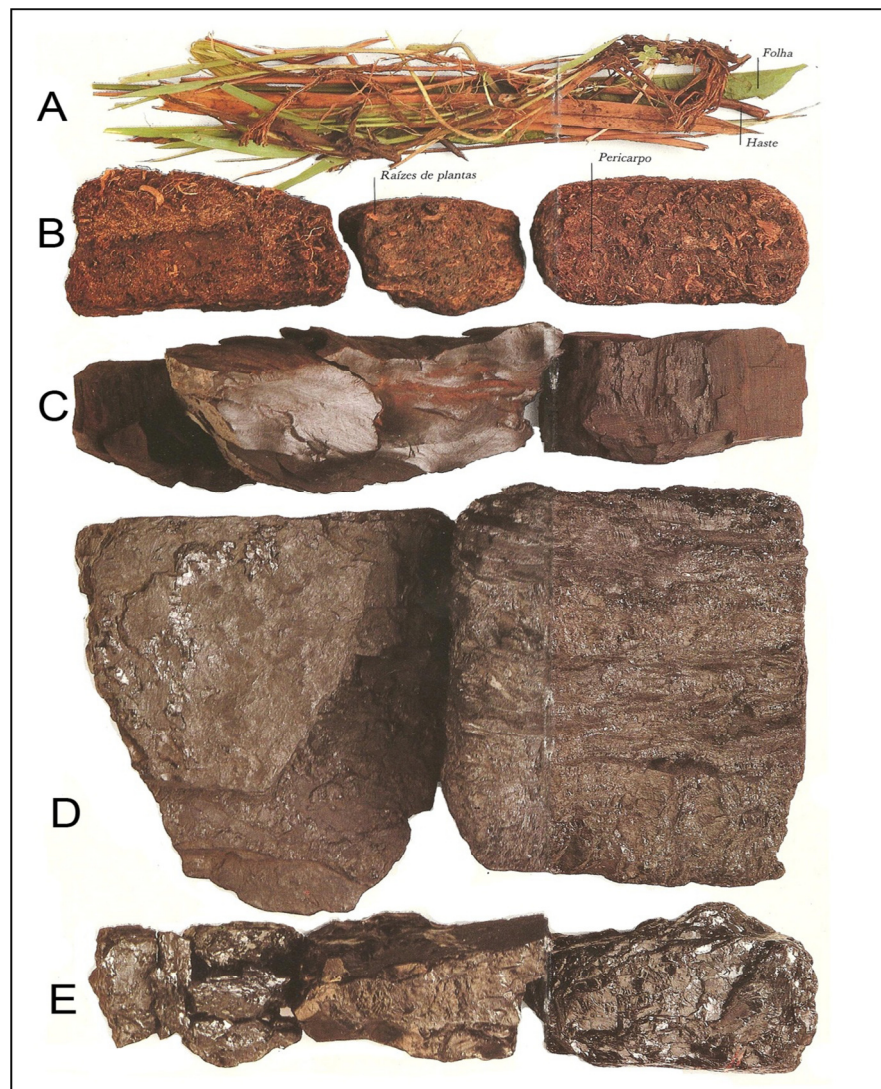
Com a compactação da turfa, durante o estágio geoquímico ou metamórfico, as mudanças progressivas que ocorrem (dentro dos carvões) são o aumento no conteúdo de carbono e uma diminuição no conteúdo de hidrogênio e oxigênio (MENDONÇA FILHO, 2010b), resultando em perda de voláteis, em decorrência com a crescente profundidade de soterramento e aumento de temperatura (MENDONÇA FILHO, 2010b). Transformando-se lentamente em **linhito** (Figura 2C), um carvão brando e marrom, o qual ainda possui vestígios identificáveis de plantas e de baixa categoria. Varia de tonalidade podendo ser castanho ou negro. Podem-se discernir os vegetais que o compõem. O linhito desintegra-se rapidamente quando exposto ao ar e queima com pouca ou nenhuma fumaça. É facilmente solúvel em álcalis. O seu teor d'água varia entre 10-30% e o poder calorífico é de 4.000 a 6.000 kcal/kg (MENDONÇA FILHO, 2010b).

Gradativamente, a compactação aumenta a temperatura dos sedimentos, assim como a pressão sobre estes (Figura 1), onde o carbono vai se modificando, tomando forma e passando de linhito para **sub-betuminoso**, carvão de baixa categoria, de cor pretão qual desintegra-se em contato com o ar, e produz fumaça ao queimar. Não é coqueificável, mas é uma importante fonte de hidrocarbonetos aromáticos que são muito utilizados na indústria química.

Caso o processo tenha continuidade, é formado o carvão **betuminoso** (Figura 2D), tipologia de categoria média a alta. Sua coloração é negra e possuem qualidades de coqueificação mais expressivas à medida que seus valores de voláteis diminuem, normalmente produzem fumaça ao serem queimados. Ao evoluírem na escala de carbonificação passam a carvões de alta categoria com uma textura densa, é semelhante a uma rocha, e tornam-se coqueificáveis (MENDONÇA FILHO, 2010b). Também utilizado na produção de energia e na indústria por ter um bom potencial calorífico. Porém, para se atingir a tipologia de carvão com maior concentração carbonosa, consecutivamente de poder calorífico e menor teor de cinzas que o betuminoso, é necessário um aumento da temperatura entre 100 - 200 °C, para que todos os materiais voláteis presentes no carvão sejam eliminados, sendo que posteriormente, pelo mesmo processo se origina o **antracito** (Figura 2), que apresenta um conteúdo carbonífero superior a 90% e com textura densa, semelhante a uma rocha (Mendonça Filho, 2010b). Geralmente é preto brilhante usado principalmente para o aquecimento residencial e comercial (MENDONÇA FILHO, 2010b).

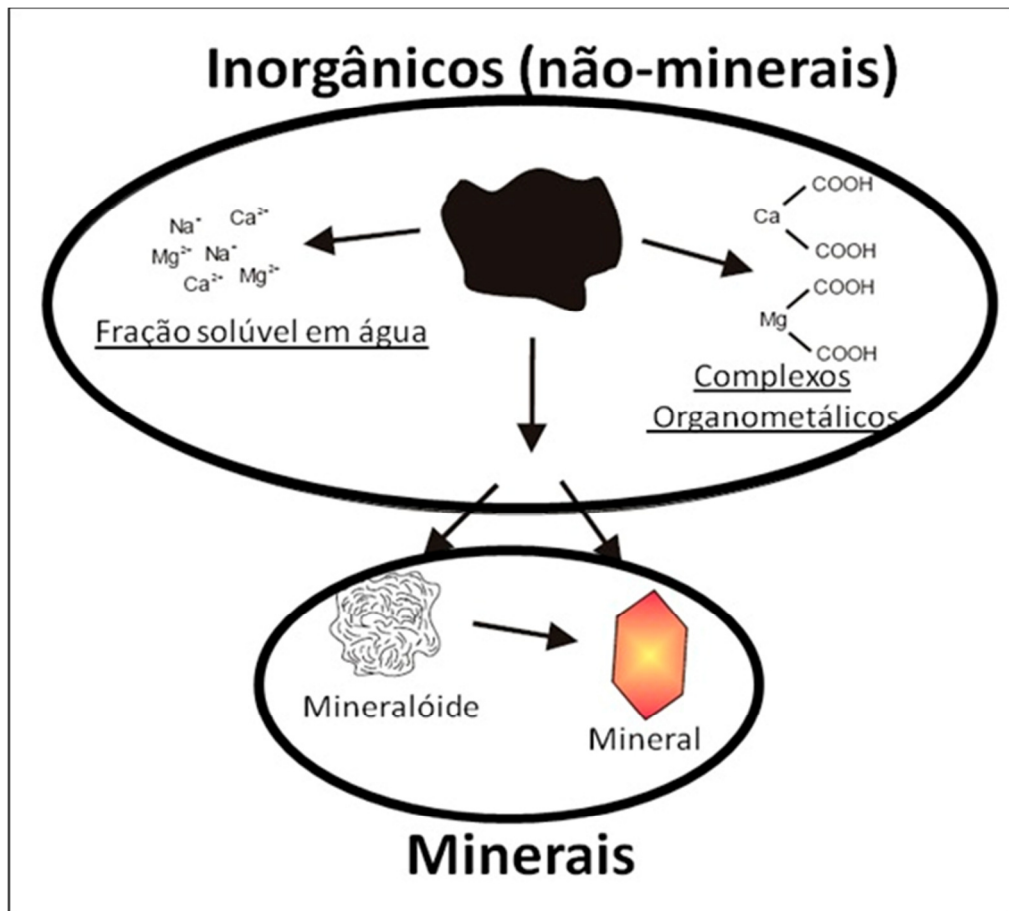
A formação geológica dos carvões influencia diretamente na sua composição e *rank*, onde o grau de carbonificação refere-se ao nível de maturação do carvão. Neste processo ocorrem diferentes concentrações de sais dissolvidos e outras substâncias inorgânicas na água contida neste (nas fases iniciais), além de elementos inorgânicos incorporados dentro dos compostos orgânicos (macerais) e partículas inorgânicas discretas (cristalinas ou não cristalinas) que representam componentes minerais verdadeiros (Figura 3).

Figura 2: Formação do carvão mineral.



Fonte: Symes, 1995.

Figura 3: Natureza dos materiais inorgânicos presentes em carvões.



Fonte: Ward, 2007.

No Brasil os jazimentos de carvão conhecidos localizam-se, especificamente, nos sedimentos gondwânicos da borda leste da Bacia Sedimentar do Paraná (Figura 4), que afloram segundo uma faixa estreita e contínua que bordeja o Escudo gaúcho nas porções oeste e norte e os Escudos Catarinense, Paranaense e Paulista na porção oeste, atravessando os estados sulinos com direção próxima a norte-sul (Mendonça Filho, 2010b).

Os principais horizontes carboníferos do Brasil Meridional ocorrem na Formação Rio Bonito. Esta formação, que apresenta seu desenvolvimento mais completo em Santa Catarina, é constituída de uma seção arenosa basal (Membro Triunfo); de uma seção média essencialmente argilosa (Membro Paraguaçu); e de uma seção superior areno-argilosa (Membro Siderópolis) que contém as principais camadas de carvão exploradas neste Estado. A espessura da Unidade varia entre 80 e 270 metros.

Esta Formação datada do Permiano é constituída por uma sucessão sedimentar cíclica de pacotes de arenitos, siltitos e folhelhos, depositados num ambiente costeiro, formado por rios, deltas, baías e estuários com planícies de marés, ilhas de barreira e plataforma marinha

rasa, numa época em que a Bacia do Paraná era um grande golfo do antigo supercontinente Gondwana. Golfo este, aberto à sudoeste, para o antigo oceano Panthalassa.

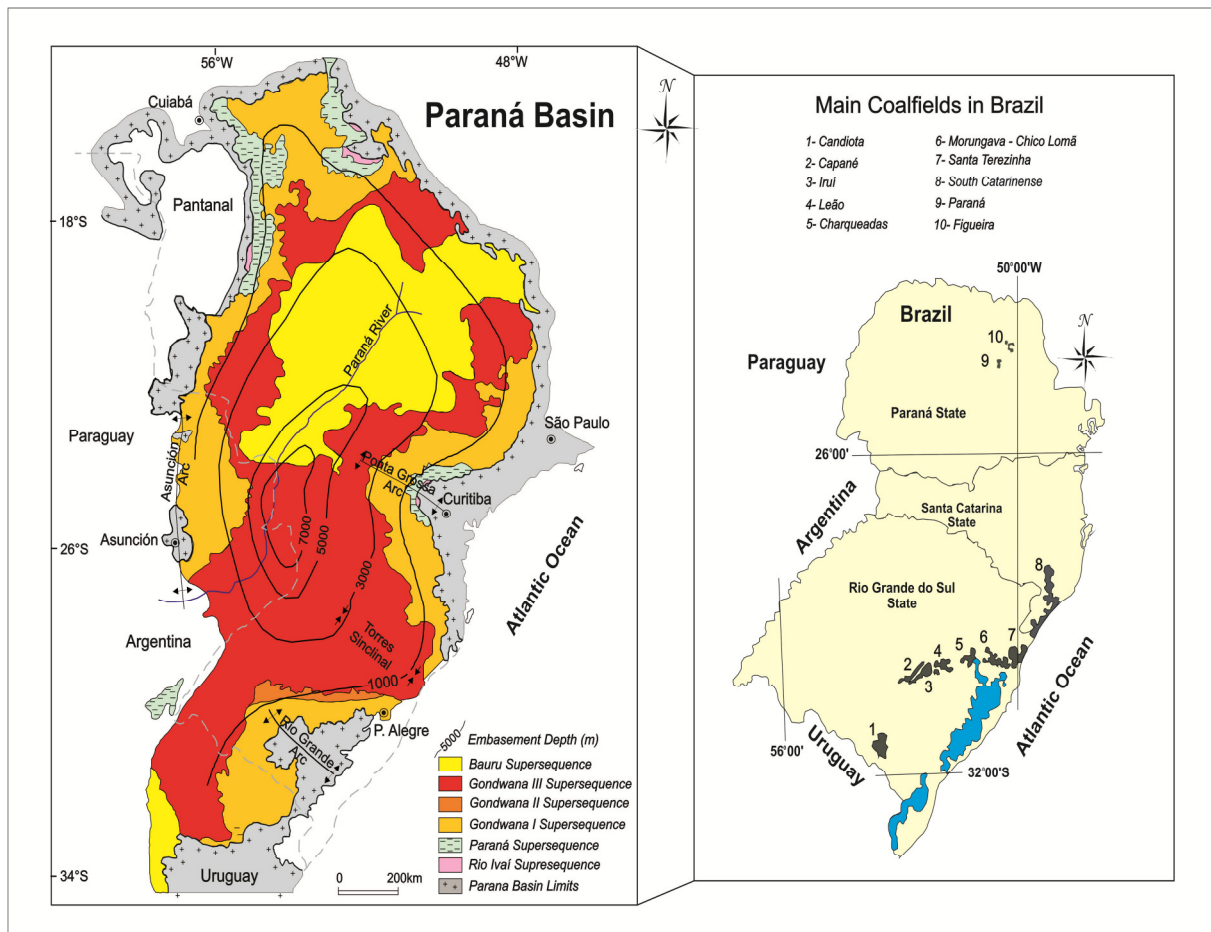
A grande fonte de conhecimentos da Formação Rio Bonito provém de sondagens profundas da PETROBRAS e rasas do Serviço Geológico do Brasil - CPRM/DNPM (MENDONÇA FILHO, 2010b), sondagens estas que alcançam centenas de metros de profundidade e executadas ao longo de toda borda leste da Bacia do Paraná, objetivando a pesquisa de carvão.

Os primeiros estudos realizados para avaliação do potencial dos carvões da Formação Rio Bonito datam de 1841, quando a presença de "carvão de pedra" foi constatada por técnicos e cientistas brasileiros e estrangeiros em missão do Governo Imperial Brasileiro (MENDONÇA FILHO, 2010b). Em 1908 foi publicado o Relatório White, por Israel Charles White, chefe da Comissão de Estudos das Minas de Carvão de Pedra do Brasil (Mendonça Filho, 2010b), cujo objetivo era identificar a potencialidade dos carvões brasileiros.

Sob a visão da estratigrafia de seqüências, Milani (1997) reorganiza todo o arcabouço geológico da bacia e analisa individualmente cada seqüência, concluindo que as três seqüências mais antigas materializam grandes ciclos transgressivos-regressivos paleozóicos, enquanto que as seqüências mais jovens formam pacotes sedimentares continentais e extensos pacotes de rochas ígneas.

As deposições das diferentes seqüências foram condicionadas tectonicamente pelas estruturas do embasamento e pelos eventos orogênicos paleozóicos que atingiram a borda oeste do continente. Segundo Milani (1997), o arcabouço estratigráfico da Bacia do Paraná é constituído por seis unidades aloestratigráficas de segunda ordem, ou Superseqüências denominadas: Rio Ivaí (Idade Caradoniano-Landoveriano), Paraná (Lockoviano-Frasniano), Gondwana I (Westfaliano-Scythiano), Gondwana II (Anisiano-Noriano), Gondwana III (Neojurássico-Berriasiano) e Bauru (Aptiano-Maestrichtiano) (Figura 4).

Figura 4: Geologia da Bacia do Paraná com os dez maiores depósitos de carvão do Brasil



Fonte: Adaptado de Milani (1997).

METODOLOGIA

Foram coletadas amostras de três usinas de beneficiamento, de diferentes áreas de mineração na região sul do Brasil. As amostras foram coletadas das empresas Copelmi Mineração Ltda., localizada entre as cidades de Minas do Leão e Butiá, Rio Grande do Sul; Carbonífera Criciúma S.A., localizada no município de Lauro Müller, Santa Catarina; Carbonífera do Cambuí Ltda., localizada no município de Figueira, Paraná. O programa de coleta das amostras representativas foi planejado conforme a produção de cada empresa, pois esta pesquisa não tem como objetivo caracterizar as amostras conforme a sua formação geológica, e sim, compreender os impactos ambientais e a composição físico-geoquímica dos sub-produtos do carvão após o processo de beneficiamento. Podendo assim providenciar uma base de dados consistente para futuros planos de recuperação da área.

Cabe ressaltar que todas as amostras foram homogeneizadas conforme o regulamentado pelas normativas da ASTM D2797 (1991). Todas as amostras foram armazenadas em tubos de ensaio plásticos hermeticamente selados e envolvidas com plásticos de polietileno selados.

No laboratório (UNILASALLE – Campus II) as amostras foram secas em estufa a 40°C durante 24 h, para evitar a volatilização dos elementos como mercúrio, selênio, bromo entre outros altamente voláteis ou a degradação da matéria orgânica. Após foram divididas, sendo guardada uma parcela de cada para se houver a necessidade de para experimentos adicionais ou contraprova. Em seguida foram trituradas e peneiradas com peneira mesh 8 e posteriormente foram homogeneizadas e quarteadas, sendo separado os volumes para cada análise específica e contra-provas.

Análises Petrográficas

Análise de macerais

Baseia-se na identificação e quantificação dos diferentes macerais e material contidos nas amostras, seguido da nomenclatura do ICCP (1998, 2001), sendo de fundamental importância para a caracterização do carvão, permite avaliar as condições paleoambientais de formação das turfeiras através da determinação e avaliação das variações compostionais (LEVANDOWSKI, 2009). A análise petrográfica é expressa em Vol% e foi determinada com um microscópio Leitz Orthoplan.

A contagem dos pontos é feita através de um contador de pontos semi-automático (SWIFT F 415C) o qual é acoplado ao microscópio e é realizada em linhas regulares e

espaços pré-definidos (distância aproximadamente igual a metade do tamanho da partícula) para evitar que seja contado mais de um ponto na mesma partícula.

Reflectância da vitrinita

Segundo a literatura, Pross (2007) o método óptico de avaliação de maturação mais proeminente é a medida de reflectância da vitrinita (e.g. Tissot & Welte, 1984; Teichmüller et al, 1998). De acordo com Teichmüller & Durand, (1983) a composição química e o percentual de luz branca refletida aumenta de acordo com o grau de carbonificação devido as estruturas dos anéis aromáticos que sofrem um reordenamento à medida que aumenta o grau de carbonificação. A idéia do método é por comparação determinar a cor da vitrinita da amostra analisada comparando com padrões de reflectâncias conhecidas e assim estabelecer o nível de maturação da rocha analisada. Para tal exame microscópico foi empregado o microscópio Leitz Orthoplan usando reflectedlight óptica e uma foto 50 × objetivo óleo de imersão, no Center for Applied Energy Research da University of Kentucky (US).

A determinação do poder reflector foi realizado através da medições de 50 partes de colotelinita, com leituras ortogonais para ser calculada a média para a reflectância aleatória e uma leitura da reflectância máxima em uma rotação da fase, com luz polarizada a 45 graus e um filtro passa banda 546-nm, seguindo ISO 7404/5 (1984). Para calibrar o sistema utilizou-se 0,94% R padrão de vidro, para posteriormente os dados serem inseridos em uma planilha do Excel a fim de aplicar as fórmulas necessárias para o cálculo das médias e desvios-padrão para os pontos de dados. Durante o trabalho, a calibração é realizada a cada intervalo de leitura entre cada seção analisada à fim de manter a precisão das medidas.

Determinação química

Análise Elementar

A Análise Elementar, determinação do percentual em massa do carbono, bem como do enxofre, nitrogênio, hidrogênio e oxigênio, foi determinada por LECO, modelo TruSpec CHNS, realizada nas dependências da Rede de Infraestruturas de Apoio á Investigación e ao Desenvolvimento Tecnolóxico (RIAIDT), Universidad de Santiago de Compostela – Espanha. Com essa técnica é possível determinar a porcentagem de material orgânico presente nas amostras, podendo assim, determinar as características principais das amostras de acordo com sua origem.

Fluorescência de Raios- X

Para determinação dos elementos majoritários foi aplicada a técnica de fluorescência de Raios X (XRF). As amostras foram secas a 815°C para posteriormente serem trituradas a fim de determinar os elementos (Si, Al, Fe, Ca, Na, K, Mg, Ti e P). A escolha desta técnica se deve à relativa facilidade de preparação da amostra (pastilha prensada ou moldada após fusão) e caráter multielementar que permite a fácil comparação dos resultados químicos e mineralógicos. A calibração do aparelho foi feita a partir de padrões sintéticos sólidos, preparados a partir de mistura de grafite e celulose (representando a parte orgânica do carvão) e cinza de rocha (representando os constituintes inorgânicos do carvão) que foi também prensada. A amostra foi analisada sob a forma de pastilha prensada de borosilicato conforme descrito por Norrish e Hutton (1969). O método foi validado mediante análise de amostras certificadas de carvão, com a utilização de um equipamento de XRF da marca Philips PW2400 (SILVA et al., 2010a), na University of New South Wales (Austrália).

ICP Óptico e de Massas

Estudos anteriores (KALKREUTH et al., 2006; SILVA et al., 2009a) descrevem a determinação de diversos elementos por ICP OES e ICP-MS, para carvões brasileiros, que foram decompostos pelo método “sinter”. Este método consiste em misturar 0,1 g de amostra e 0,5 g de Na₂O₂, em um cadinho de grafite, queimar a mistura por 35 minutos a 445 °C. Na cinza obtida são adicionados 20 mL de H₂O e 20 mL de HNO₃ 20% (v/v) para posterior determinação dos elementos majoritários. No entanto, no presente estudo optou-se pela determinação de elementos minoritários e elementos traço das amostras utilizando uma extração com HNO₃ seguida de uma digestão ácida com HF-HNO₃-HClO₄ tal como descrito por (QUEROL et al., 1997), evitando assim a volatilização dos elementos como As, Cd, Mo, Se, Pb, entre muitos outros relativamente voláteis a 445°C (OLIVEIRA et al., 2012a). As soluções resultantes foram analisadas por ICP OES e ICP-MS. Como gás carregador do vapor de mercúrio foi utilizado argônio comercial da White Martins - Praxair, sendo este também utilizado para a geração e manutenção do plasma, como gás de nebulização e auxiliar nos equipamentos de ICP-MS e ICP OES do Institute of Environmental Assessment and Water Research (IDAEA-CSIC, Barcelona-Espanha). Como gás de purga do sistema óptico do equipamento de ICP OES foi utilizado nitrogênio com pureza de 99,998%, da White Martins -

Praxair. Uma amostra de carvão certificado (SARM-19) e um branco foram igualmente digeridas para certificar os resultados analíticos. Os erros analíticos foram estimados em 10% para Cd, Mo, e P (QUEROL et al., 1997). As análises de mercúrio foram medidas diretamente sem prévio tratamento utilizando uma espectrometria de absorção atômica LECO AMA 254. Almejando evitar erros resultantes de contaminação, os frascos utilizados para conter as amostras foram descontaminados mediante contato com solução de HNO₃ 10% (v/v) durante 48 horas e após isto, lavados com água destilada e deionizada. Os frascos de teflon utilizados para a decomposição das amostras foram descontaminados pela adição de mistura contendo 7 mL de HNO₃ destilado e 2 mL de HF e aquecimento a 160°C durante 4 horas. A vidraria empregada foi descontaminada pelo contato com solução de HNO₃ 10% (v/v) durante 24 h e posteriormente lavada com água destilada e enxaguada com água deionizada para então ser utilizada.

Ensaios de lixiviação

Para avaliar a mobilidade geoquímica dos elementos presentes nas amostras de carvão, aplicou-se o teste padrão, desenvolvido pela União Européia (EN 12457-2:2002), sendo realizado no Institute of Environmental Assessment and Water Research (IDAEA-CSIC, Barcelona - Espanha). Isto é um simples “batch” onde são utilizados uma proporção (L/S) de 10 L/kg durante 24h de agitação via lixiviador com água deionizada. O teste foi aplicado em triplicata, afim de garantir a confiabilidade dos resultados dos elementos determinados por ICP OES, ICP-MS. O pH de cada lixiviado também foi aferido, com um pHmetro DM-2P da Digimed, para traçar a relações entre este parâmetro e os elementos lixiviáveis.

Determinação mineralógica

Microscopia Eletrônica de Varredura

As análises de Microscopia Eletrônica de Varredura com detector de Raios-X (SEM/EDS), permite a observação da superfície dos minerais, obtendo imagens aumentadas 290.000 vezes e uma resolução de até 4 nanômetros em condições de 6nm a pressão variável. O funcionamento baseia-se na incidência de um feixe eletrônico sobre uma amostra condutora. O feixe eletrônico fixa um ponto e escaneia a superfície. Como resultado da interação do feixe eletrônico com a amostra produz-se a emissão de sinais: elétrons reto dispersados, elétrons secundários, raios X e outros. Estes sinais são captados por detectores

que os processam. Em seguida são amplificados e transformados em sinais elétricos como pixeles a um monitor. Esta técnica foi desenvolvida nas dependências da Rede de Infraestruturas de Apoio á Investigación e ao Desenvolvimento Tecnolóxico (RIAIDT), Universidad de Santiago de Compostela – Espanha, para estudar os minerais que tenham entre 2-500 μm , com um SEM da LEO Model-435VP com Oxford EDS de resolução > 133eV, tal como publicado em anteriores estudos (Silva et al., 2010a; Silva et al, 2011a,b,c,d; Oliveira et al., 2011a,b) e voltagem de 20 kV.

Microscopia Eletrônica de Transmissão

A Microscopia Eletrônica de Transmissão de alta resolução com detector de raios-X (HR-TEM/EDS), utiliza como fonte de iluminação um feixe eletrônico que é dirigido e focalizado mediante lentes eletromagnéticas. Este processo é realizado no interior de uma coluna, em condições de alto baleiro, de modo que os elétrons acelerados sigam trajetórias retas, salvo que se interrelacionam com os átomos presentes na amostra. O choque dos elétrons com os átomos da amostra faz com que estes percam velocidade e variem a sua trajetória. Os elétrons que não chocam com a amostra projetam-se sobre uma tela fluorescente. Ao formar-se a imagem, as áreas que mais desviam os elétrons apareceram mais escuras, se comparado com as que desviam menos. Com o emprego desta analítica, visou-se estudar nanominerais e estruturas menores que 0,1 μm de elevada importância ambiental e para a saúde humana, podendo assim, diagnosticar um melhor panorama dos impactos ambientais gerados pela utilização de carvão, a qual foi desdoblada no Centro de Apoio Científico e Tecnológico á Investigación – CACTI da Universidad de Vigo.

Difração de Raios-X e low-temperature ash (LTA)

A Cristalografía de Raios-X é o estudo da estrutura cristalina e molecular dos sólidos estruturados fixos e vem sendo uma ferramenta de grande interesse por parte da comunidade científica, nestes últimos anos, devido o desenvolvimento de uma grande quantidade de acessórios que permite aplicar ao difratômetro uma grande versatilidade. Portanto, representativas porções dos carvões coletados foram trituradas (<212 μm) e subsequentemente sujeitas a baixa temperatura de incineração de oxigênio no plasma-LTA (GLUSKOTER, 1965; StandardsAustrália, 2000), com porcentagem em peso de low-temperature ash - LTA, para então serem estudadas por difração de raios-X (DRX), via um

difratômetro Phillips PW1830 com radiação Cu K- α e um escâner de 2 a 60° 2θ, na University of New South Wales (Austrália). O método LTA foi empregado por se tratar de um procedimento de incineração eficaz, sem mudanças significativas na composição da amostra, a fim de se obter uma melhor amostra representativa e avaliação dos minerais presentes no carvão.

As análises mineralógicas quantitativas foram desenvolvidas com Siroquant™, um software comercial de interpretação (TAYLOR, 1998), baseado em técnicas de análises para DRX de Rietveld (1974). Para estimar a porcentagem das fases pobremente cristalinas nas amostras de carvões, foi adicionado separadamente, nas amostras, fases de sílica amorfa tal como descrito por Ward e French (2006). Posteriormente a essas etapas, os elementos majoritários (como óxidos), as amostras de carvões foram calcinadas a 815°C. A cinza resultante foi prensada em pastilha de borosilicato, conforme descrita por Norrish e Hutton (1969), na University of New South Wales (Austrália) por fluorescência de raios-X utilizando um espectrômetro Philips PW2400.

REFERÊNCIAS

- ABCM, Associação Brasileira de Carvão Mineral. Disponível em:
http://www.carvaomineral.com.br/interna_conteudo.php?i_subarea=8&i_area=4
 Acesso dia 10 de abril de 2014.
- ANEEL, Agência Nacional de Energia Elétrica. Brasil, 2012. Relatório ANEEL 2011. Brasília, p. 108
- ASTM, American Society for Testing and Materials, 1991. Standard practice for preparing coal samples for microscopical analysis by reflected light. ASTM Standard D 2797-91, American Society for Testing and Materials, West Conshohocken, PA, p. 3.
- ASTM, American Society for Testing and Materials, 1996. Standard test methods for collection of a gross sample of coal. ASTM Standard D2234-89. American Society for Testing and Materials, West Conshohocken, PA, p.10.
- BATES, R.L., JACKSON, J.A. (editors). 1987. Glossary of geology. Third edition. American Geological Intitute. Alexandria, VA.
- BOHOR, B.P., GLUSKOTER, H.J., 1973. Boron in illite as a paleosalinity indicator of Illinois coals. *Journal of Sedimentary Petrology*, v. 43, p. 945-956.
- BOYD, R.J., 2002. The partitioning behaviour of boron from tourmaline during ashing of coal. *International Journal of Coal Geology*, v. 53, p. 43-54.
- BRYERS, R.W., 1996. Fireside slagging, fouling, and high-temperature corrosion of heat-transfer surface due to impurities in steam-raising fuels. *Progress in Energy and Combustion Science*, v. 22, p. 29-120.
- CLARKE, L.B., SLOSS, L.L., 1992. Trace element emissions from coal combustion and gasification. IEA Coal Research, Series IEACR/49, IEA Clean Coal Centre, London.
- DAI, S. et al, 2005. Mineralogy and geochemistry of a late Permian coal in the Dafang Coalfield, Guizhou, China: influence from siliceous and iron-rich calcic hydrothermal fluids. *International Journal of Coal Geology* v. 61, p. 241-258.
- DAI, S. et al, 2012. Petrology, mineralogy, and geochemistry of the Ge-rich coal from the Wulantuga Ge ore deposit, Inner Mongolia, China: New data and genetic implications. *International Journal of Coal Geology*, v. 90-91, p.72-99.
- DAI, S. et al, 2013. Factors controlling geochemical and mineralogical compositions of coals preserved within marine carbonate successions: A case study from the Heshan Coalfield, southern China. *International Journal of Coal Geology*, v. 109-110, p. 77-100.
- DNPM, DEPARTAMENTO NACIONAL DE PRODUÇÃO MINERAL, 2010. Anuário Mineral Brasileiro 2010, Vol. 1. Brasília, p. 871.
- DE SOUZA, K.F., SAMPAIO, C.H., KUSSLER, J.A.T., 2012. Washability curves for the lower coal seams in Candiota Mine – Brazil. *Fuel Processing Technology*, v. 96, p. 140-149.

- DIEHL, S.F. et al, 2012. Distribution of arsenic, selenium, and other trace elements in high pyrite Appalachian coals: Evidence for multiple episodes of pyrite formation. International Journal of Coal Geology, v.94, p. 238-249.
- FEIL, N., SAMPAIO, C.H., WOTRUBA, H., 2012. Influence of jig frequency on the separation of coal from the Bonito seam – Santa Catarina, Brazil. Fuel Processing Technology, v. 96, p. 22-26.
- FINKELMAN, R.B., 1981. Modes of occurrence of trace elements in coal. US Geological Survey Open File Report, v. 81-99, p. 301.
- FINKELMAN, R.B., 1994. Modes of occurrence of potentially hazardous elements in coal: Levels of confidence. Fuel Processing Technology, v. 39, p. 21–34
- FRAZER, F.W., BELCHER, C.B., 1973. Quantitative determination of the mineral matter content of coal by a radio-frequency oxidation technique. Fuel, v. 52, p. 41-46.
- GLUSKOTER, H.J., 1965. Electronic low temperature ashing of bituminous coal. Fuel, v. 44, p. 285-291.
- GLUSKOTER, H.J . et al, 1977. Trace elements in coal: Occurrence and distribution. Illinois State Geological Survey Circular, 499, 154 pp.
- GOODARZI, F., SWAINE, D.J., 1994. Paleoenvironmental and environmental implications of the boron content of coals. Geological Survey of Canada Bulletin 471, 1–46.
- GOODARZI, F., SWAINE, D.J., 1995. Environmental Aspects of Trace Elements in Coal. Kluwer Academic Publishers, Dordrecht, 312 pp.
- HOLZ, M., ADE, M.B., KALKREUTH, W., 1999. Coal seam petrology analyzed within a sequence stratigraphy framework: Preliminary results from the Early Permian Rio Bonito Formation of southernmost Brazilian Gondwanaland. In: Lemos de Souza, M.J., Marques, M.M., Fernandes, J.P. (Eds), Proceedings and Papers, 2nd Symposium on Gondwana Coals, Porto, 1998, Faculdade de Ciências do Porto, Departamento de Geologia, Memória 5, 25-36.
- HOWER, J.C., BLANCHARD, L.J., ROBERTSON, J.D., 1998. Magnitude of minor element reduction through beneficiation of Central Appalachian coals. Coal Preparation 19, 213–229.
- HUGGINS, F.E. et al, 2009. Elemental modes of occurrence in an Illinois #6 coal and fractions prepared by physical separation techniques at a coal preparation plant. International Journal of Coal Geology 78, 65-76.
- KALKREUTH, W., . et al, 2006. Petrology and chemistry of Permian coals from the Paraná Basin: 1. Santa Terezinha, Leão-Butiá and Candiota Coalfields, Rio Grande do Sul, Brazil. International Journal of Coal Geology 68, 79–116.
- KALKREUTH, W. et al, 2004. The application of FAMM (Fluorescence Alteration of Multiple Macerals) analyses for evaluating rank of Parana' Basin coals, Brazil. International Journal of Coal Geology 57, 167–185.

- KLEPZIG, M.C., 2001. Palinologia aplicada à reconstituição das unidades de paisagem e dinâmica das turfeiras formadoras dos carvões permianos do Rio Grande do Sul, Brasil, Tese Doutorado, Inst. Geociências, UFRGS.
- KOLKER, A., 2012. Minor element distribution in iron disulfides in coal: A geochemical review. International Journal of Coal Geology 94, 32-43.
- KOUKOUZAS, N. et al, 2010. Mineralogy of lignites and associated strata in the Mavropigi field of the Ptolemais Basin, northern Greece. International Journal of Coal Geology 81, 182-190.
- LEVANDOWSKI, J.H., 2009. Petrologia e geoquímica das camadas de carvão e sua relação com gás natural determinado no poço CBM 001-ST-RS, Bacia do Paraná. Dissertação (Mestrado, Inst. Geociências, UFRGS) Porto Alegre p. 92
- MARCELLO, R.R. et al, 2008. Inorganic pigments made from the recycling of coal mine drainage treatment sludge. Journal of Environmental Management 88, 1280-1284.
- MASTALERZ, M., DROBNIAK, A., 2012. Gallium and germanium in selected Indiana coals. International Journal of Coal Geology 94, 302-313.
- MASTALERZ, M., PADGETT, P.L., 1999. From in situ coal to the final coal product: a case study of the Danville Coal Member (Indiana). International Journal of Coal Geology 41, 107-123.
- MATJIE, R.H. et al, 2008. Chemical composition of glass and crystalline phases in coarse gasification ash. Fuel 87, 857-869.
- MATJIE, R.H. et al, 2012a. Mineralogical transformations in coal feedstocks during carbon conversion, based on packed bed combustor tests, Part 1: Bulk coal ash studies. Coal Combustion and Gasification Products 4, 45-54.
- MATJIE, R.H., WARD, C.R., LI, Z., 2012b. Mineralogical transformations in coal feedstocks during carbon conversion, based on packed bed combustor tests, Part 2: Behaviour of individual particles. Coal Combustion and Gasification Products 4, 55-67.
- MEDONÇA FILHO, J.G. et al, 2010. Organic Facies Characterization of a Sedimentary Section from the Santa Catarina Coalfield. T.S.O.P Annual Meeting, Denver, Colorado, USA, Abstracts, p. 42.
- MENDONÇA FILHO, J.G.; KERN, M. L., 2010b, Introdução a Geologia do Carvão: aspectos econômicos, Mercado Mundial, Petrologia e Produção de Metano. Workshop Geologia e mineralogia do Carvão. Universidade Federal do Rio de Janeiro.
- MILANI, E. J. 1997. Evolução tectono-estratigráfica da Bacia do Paraná e seu relacionamento com a geodinâmica fanerozóica do Gondwana Sul-Oeste. 1997.
- MILANI, E.J., FRANÇA, A.B., SCHNEIDER, R.L., 1994. Bacia do Paraná. In: Feijó, F.J. (Ed.), Cartas estratigráficas das bacias sedimentares brasileiras. Rio de Janeiro, Boletim de Geociências da Petrobras, vol. 8 (1), pp. 69-82.

MINEROPAR.1989. Oportunidades empresariais para exploração de recursos minerais do Paraná. Governo do Estado do Paraná, Secretaria da Industria e Comércio, Minerais do Paraná, S/A, 278P.

MOORE, F., Esmaeili, A., 2012. Mineralogy and geochemistry of the coals from the Karmozd and Kiasar coal mines, Mazandaran province, Iran. International Journal of Coal Geology 96-97, 9-21.

NORRISH, K.; HUTTON, J.T., 1969. An accurate X-ray spectrographic method for the analysis of a wide range of geological samples. *Geochimica et Cosmochimica Acta* 33, 431–453.

OLIVEIRA, M.L.S. et al, 2012. Mineralogy and leaching characteristics of beneficiated coal products from Santa Catarina, Brazil. International Journal of Coal Geology 94, 314-325.

OLIVEIRA, M.L.S. et al, 2013. Partitioning of Mineralogical and Inorganic Geochemical Components of Coals from Santa Catarina, Brazil, by Industrial Beneficiation Processes. International Journal of Coal Geology, 116, 75-92.

PIRES, M., QUEROL, X., 2004. Characterization of Candiota (south Brazil) coal and combustion by-products. International Journal of Coal Geology, 60, 57–72.

QUEROL, X., WHATELEY, M. K. G., Fernandez-Turiel, J. L., Tuncali, E., 1997. Geological controls on the mineralogy and geochemistry of the Beypazari lignite, central Anatolia, Turkey. International Journal of Coal Geology 33, 255-271.

QUEROL, X., FERNANDEZ-TURIEL, J.L., Lopez-Soler, A., 1995. Trace elements in coal and their behaviour during combustion in a large power station. Fuel 74, 331-343.

QUEROL X. et al, 1997. Geological controls on the mineralogy and geochemistry of the Beypazari lignite, central Anatolia, Turkey. International Journal of Coal Geology 33, 255–271.

QUEROL, X. et al, 2001. Determination of element affinities by density fractionation of bulk coal samples. Fuel 80, 83–96.

QUEROL, X. et al, 2008. Environmental characterization of burnt coal gangue banks at Yangquan, Shanxi Province, China. International Journal of Coal Geology 75, 93-104.

QUICK, W.J., IRONS, R., 2002. Trace element partitioning during the firing of washed and untreated power station coals. Fuel 81, 665–672.

QUISPE, D. et al, 2012. Changes in mobility of hazardous elements during coal combustion in Santa Catarina power plant (Brazil). Fuel 94, 495-503.

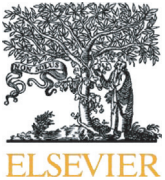
RAO, C.P., GLUSKOTER, H.J., 1973. Occurrence and distribution of minerals in Illinois coals. Illinois State Geological Survey Circular 476, 56 pp.

- REIFENSTEIN, A.P. et al, 1999. Behaviour of selected minerals in an improved ash fusion test: quartz, potassium feldspar, sodium feldspar, kaolinite, illite, calcite, dolomite, siderite, pyrite and apatite. *Fuel* 78, 1449-1461.
- RIBEIRO, J. et al, 2013a. Extensive FE-SEM/EDS, HR-TEM/EDS and ToF-SIMS studies of micron- to nano-particles in anthracite fly ash. *Science of the Total Environment* 452-453, 98-107.
- RIBEIRO, J. et al, 2013b. Mineral speciation and fate of some hazardous contaminants in coal waste pile from anthracite mining in Portugal. *International Journal of Coal Geology* 109-110, 15-23.
- RIETVELD, H.M., 1969. A profile refinement method for nuclear and magnetic structures. *Journal of Applied Crystallography* 2, 65-71.
- RILEY, K.W. et al, 2012. Modes of occurrence of trace and minor elements in some Australian coals. *International Journal of Coal Geology* 94, 214-224.
- SAMPAIO, C. H., TAVARES, L.M.M., 2005. Beneficiamento Gravimétrico: Uma introdução aos processos de concentração mineral e reciclagem de materiais por densidade. 1. ed., Porto Alegre, Editora UFRGS, vol. 1. 603 pp.
- SAMPAIO, C.H. et al, 2008. Coal beneficiation of Candiota mine by dry jiggling. *Fuel Processing Technology* 89, 198-202.
- SAMPAIO, C.H., DUARTE, C., MILTZAREK, G.L., 2011. Characterization and uses of a southern Brazilian coal. *Proceedings of XIV Balkan Mineral Processing Congress*, Tuzla, Library Dervis Susic Tuzla, 2011, vol. 2, pp. 652-655.
- SENIOR, C.L. et al, 2000. Distribution of trace elements in selected pulverized coals as a function of particle size and density. *Fuel Processing Technology* 63, 215-241.
- SILVA, L.F.O. et al, 2010. Mineralogy and leaching characteristics of coal ash from a major Brazilian power plant. *Coal Combustion and Gasification Products* 2, 51-65.
- SILVA, L.F.O. et al, 2012. Multianalytical approaches to the characterisation of minerals associated with coals and the diagnosis of their potential risk by using combined instrumental microspectroscopic techniques and thermodynamic speciation. *Fuel* 94, 52-63.
- STANDARDS AUSTRALIA, 2000. Higher rank coal - mineral matter and water of constitution. Australian Standard 1038 Part 22, 20 pp.
- SUÁREZ-RUIZ, I., WARD, C. R., 2008. Basic factors controlling coal quality and technological behavior of coal. In: Suárez-Ruiz, I., Crelling, J. C. (eds.), *Applied Coal Petrology*, Academic Press, Burlington, MA, pp. 19-59.
- SWAINE, D.J., 1990. *Trace Elements in Coal*. Butterworth, London, 278 pp.
- TAYLOR, J. C., 1991. Computer programs for standardless quantitative analysis of minerals using the full powder diffraction profile. *Powder Diffraction* 6, 2-9.

- THOMAS, L., 2002. Coal Geology (2nd Edition). John Wiley and Sons, Chichester, UK, p.384
- VAMVUKA, D. et al, 2001. Ash quality of a beneficiated lignite from Ptolemais Basin, northern Greece. *Energy & Fuels* 15, 1181-1185.
- VASSILEV, S.V., ESKENAZY, G.M., VASSILEVA, C.G., 2001. Behaviour of elements and minerals during preparation and combustion of the Pernik coal, Bulgaria. *Fuel Processing Technology* 72, 103-129.
- WAGNER, N.J., TLOTLENG, M.T., 2012. Distribution of selected trace elements in density fractionated Waterberg coals from South Africa. *International Journal of Coal Geology* 94, 225-237.
- WANG,W. et al, 2006. Partitioning of elements and macerals during preparation of Antaibao coal. *International Journal of Coal Geology* 68, 223–232.
- WARD, C.R., 1980. Mode of occurrence of trace elements in some Australian coals. *Coal Geology*, 2, 77-98.
- WARD, C.R. et al, 2011. Element leachability from a coal stockpile and associated coastal sand deposits. *Fuel Processing Technology* 92, 817-824.
- WARD, C.R. et al, 1999. Mineral matter and trace elements in coals of the Gunnedah Basin, New South Wales, Australia. *International Journal of Coal Geology* 40, 281-308.
- YOSSIFOVA, M.G., 2014. Petrology, mineralogy and geochemistry of Balkan coals and their waste products, *International Journal of Coal Geology* 122, 1-20.
- ZHUANG, X. et al, 2000. Mineralogy and geochemistry of coal from the Liupanshui mining district, Guizhou, south China. *International Journal of Coal Geology* 45, 21-37.
- ZHUANG, X. et al, 2006. Geochemistry and mineralogy of the Cretaceous Wulantuga high-germanium coal deposit in Shengli coal field, Inner Mongolia, northeastern China. *International Journal of Coal Geology* 66, 119-136.
- ZOCCHE, J.J. et al, 2014. Heavy-Metal Content and Oxidative Damage in *Hypsiboas faber*: The Impact of Coal-Mining Pollutants on Amphibians. *Archives of Environmental Contamination and Toxicology*, v. 66, p. 69-77.
- ZOCCHE, J.J. et al, 2013. Assessment of heavy metal content and DNA damage in *Hypsiboas faber* (anuran amphibian) in coal open-casting mine. *Environmental Toxicology and Pharmacology*, v 36, p. 194-201.
- .

CAPITULO II

RESULTADOS NA
FORMA DE ARTIGO
CIENTÍFICO
PUBLICADO.



A mineralogical and geochemical study of three Brazilian coal cleaning rejects: Demonstration of electron beam applications



César M.N.L. Cutruneo ^a, Marcos L.S. Oliveira ^{a,b}, Colin R. Ward ^c, James C. Hower ^d, Irineu A.S. de Brum ^e, Carlos H. Sampaio ^e, Rubens M. Kautzmann ^a, Silvio R. Taffarel ^a, Elba C. Teixeira ^{f,g}, Luis F.O. Silva ^{a,b,*}

^a Laboratory of Environmental Researches and Nanotechnology Development, Centro Universitário La Salle, Mestrado em Avaliação de Impactos Ambientais em Mineração, Victor Barreto, 2288 Centro, 92010-000 Canoas, RS, Brazil

^b Environmental Science and Nanotechnology Department, Catarinense Institute of Environmental Research and Human Development, IPADHC, Capivari de Baixo, Santa Catarina, Brazil

^c School of Biological, Earth and Environmental Sciences, University of New South Wales, Sydney, NSW 2052, Australia

^d University of Kentucky Center for Applied Energy Research, 2540 Research Park Drive, Lexington, KY 40511, USA

^e Universidade Federal do Rio Grande do Sul, Escola de Engenharia, Departamento de Metalurgia, Centro de Tecnologia, Av. Bento Gonçalves, 9500. Bairro Agronomia. CEP: 91501-970, Porto Alegre, RS, Brazil

^f Programa de Pós-Graduação em Sensoriamento Remoto e Meteorologia (UFRGS), Porto Alegre, RS, Brazil

^g Fundação Estadual de Proteção Ambiental Henrique Luis Roessler, Porto Alegre, RS, Brazil

ARTICLE INFO

Article history:

Received 6 February 2014

Received in revised form 22 May 2014

Accepted 22 May 2014

Available online 29 May 2014

Keywords:

Coal preparation

Coal petrology

Mineral matter

X-ray diffraction

Electron microscopy

Trace element geochemistry

ABSTRACT

The background and anthropogenic levels of hazardous elements in the surface soil of a coal mining area depend on the geological setting of the region and the underlying soil material, but may also be influenced by water-borne or aeolian transport of sediment from adjacent coal-related waste piles. Very few studies have focused on the chemical and mineralogical composition of Brazilian coal cleaning rejects (CCRs), which may represent significant sources of soil or water contamination. In this study, we have investigated the quantitative distribution of minerals and potentially hazardous elements in CCRs and a run-of-mine coal from the Brazilian states of Rio Grande do Sul and Santa Catarina. The major minerals, identified by X-ray diffraction (XRD), high-resolution transmission electron microscopy (HR-TEM), and field-emission scanning electron microscopy/energy dispersive X-ray analysis techniques (FE-SEM/EDS) are kaolinite, quartz, mixed-layer illite-smectite, pyrite, jarosite, melanterite, gypsum, rutile, and calcite, while minor minerals include barite, hematite, siderite, sphalerite, and goethite. Galena, magnetite, zircon, and many other species may also occur as accessory/trace minerals. Pyrite and jarosite are relatively abundant in some cases, making up to around 4% or 5% of the mineral matter, with jarosite, melanterite, and gypsum probably formed by complex interaction of oxidation products from Fe-sulfides and clay or carbonate components, initiated by exposure and storage of the host material. Such atmospheric exposure promotes sulfide oxidation that releases substantial sulfate loads as well as Ca^{2+} , K^+ , Mg^{2+} , Cl^- , and Al^{3+} . Metals with the most severe discharges were Zn, Cu, Mn, Co, Ni, and Cd. Most of the trace pollutants in the CCRs displayed a pH-dependent solubility, being immobile in near-neutral samples but mobile under the low-pH conditions associated with oxidized material. The results highlight the complex interactions among mineral matter components of the CCRs during storage, and the potential for release of potentially hazardous elements in association with longer-term exposure and storage.

© 2014 Elsevier B.V. All rights reserved.

1. Introduction

Brazil is the largest consumer of coal in the South America (Oliveira et al., 2012, 2013). However, with the increasing use of coal there is growing concern about the environmental and human health impacts from potentially hazardous trace elements released in the course of coal mining, cleaning, transportation, and combustion.

According to the Santa Catarina State Coal Industry Syndicate the average run-of-mine (ROM) coal production is 6 Mt/year, from which 3.5 Mt/year are rejected and disposed of in landfills (Marcello et al., 2008). The Rio Grande do Sul and Santa Catarina coal mining region (Fig. 1) was classified as a national environmental endangered area by a 1980 Federal Decree. Accordingly, the area obtained special government assistance to address polluted soil and water quality concerns. This assistance allowed the mining sector to meet Brazilian demands for steam coal while protecting the environment. In response to a court ruling by the Federal Prosecution following a public lawsuit, and in accordance with associated agreements, the coal mining companies and the federal government are devoting special attention to

* Corresponding author.

E-mail addresses: luis.oliveira@unilasalle.edu.br (M.L.S. Oliveira), felipeqma@hotmail.com (L.F.O. Silva).



Fig. 1. Location of coal mines from which the samples were obtained and used in this study. **1.a:** Cambuí. **1.b:** Criciúma. **1.c:** Fine Copelmi and Coarse Copelmi.

environmental projects in areas degraded by past coal mining operations. For this reason, the need for research on the behavior and potential use of coal cleaning rejects (CCRs) has become more economically and environmentally relevant.

The impacts on human health and regional environment caused by coal use are mainly related to the type and abundance of the minerals present in the coals and, especially, to the levels of potentially toxic elements contained within the minerals (Dai et al., 2004a; Finkelman, 1993; Finkelman et al., 2002). Coal cleaning processes are designed to remove the minerals occurring in the coal prior to use. An understanding of the mode of association of minerals with the coal matrix is important before application of coal cleaning technology. Large amounts of coal-derived minerals become concentrated in the residues from these coal-cleaning processes, especially from high-ash coals such as Brazilian coals. Knowledge of the mineral characteristics is also very important in understanding the formation of ultrafine and nanoparticles during coal cleaning, and to develop the necessary control steps. Brazilian CCRs are

often disposed of, however, with few attempts to understand their potential impacts on the environment.

Brazilian coal mining companies have valid environmental operating licenses for mine exploitation and preparation plants, and substantial efforts are taking place to meet environmental regulations regarding site reclamation. A number of measures are applied to reduce the environmental impact of coal mining and coal cleaning activities, such as restricting truck traffic at night, watering roads to reduce dust formation, and covering trucks to prevent spilling. However, these measures have proven to be insufficient to prevent damage caused by mining activity in the Santa Catarina coal mines.

With the exception of secondary products associated with pyrite oxidation, the minerals in coal cleaning residues are usually similar to those found in coals (Dai et al., 2008a,b; Depoi et al., 2008; Kalkreuth et al., 2006, 2010; Oliveira et al., 2012; Querol et al., 2008; Ribeiro et al., 2013a,b; Silva et al., 2009; Suárez-Ruiz and Ward, 2008; Yossifova, 2014). Most of the minerals themselves do not present

environmental or human health concerns (unless inhaled, e.g. fine quartz and several clays). However, an abundance of coal-derived ultrafine Fe-sulfides and nanoparticulates (e.g. anatase, quartz, Fe-sulfates, Fe-oxides, and siderite containing hazardous elements) may present some concerns (e.g. Dai et al., 2012, 2013; Huggins et al., 2012; Oliveira et al., 2012; Yossifova, 2014). For example, crystalline silica is correlated with the incidence of lung cancer (Tian et al., 2008) and, in 1997, the World Health Organization's International Agency for Research on Cancer (IARC) reclassified quartz and crystalline silica from a Class 2 (1987 evaluation) carcinogen to a Class 1 carcinogen, stating that sufficient evidence existed for carcinogenicity of quartz in both humans and experimental animals. However, amorphous silica may also be beneficial, with positive effects on production of grasses (Schaller et al., 2012), as well as on pathogen and herbivore defense (Fawe et al., 1998) and amelioration of abiotic stress (Ma, 2004).

Evaluating/assessing the elemental and mineralogical composition of coal and coal by-products or wastes is important in assessing their potential environmental human health impact (Finkelman, 1994, 1995; Finkelman et al., 2002). Some miners and people living around Brazilian coal mines have suffered serious lung disease caused by inhaling coal dust. Ren et al. (2004), in a study of Chinese mines, reported some autopsies showing that the lungs of miners contain higher Cr than those of non-miners. Some Brazilian coals are highly enriched in potentially hazardous trace elements (e.g. Ti from nanometric anatase and rutile; Fe-oxides containing Cd, Pb, and V), which may be related to lung cancer. However human health studies are in development and excessive speculation with respect to these aspects would be premature.

The modes of occurrence of potentially hazardous elements are particularly important for populations exposed to their influence, as is the case in the area near CCR emplacements. Brazilian CCRs, derived from coals deposited in fluvial to marine-influenced environments, are generally enriched in some elements (e.g., Cr, V, Rb, Sr), not only because seawater contains higher concentrations of those elements than freshwater (Oliveira et al., 2012), but also because plankton in marine water are enriched in those elements and can also change the pH, Eh, and H₂S content, leading to a favorable environment for enrichment of trace element components (Wang et al., 2007, 2008). Similar observations have been reported for Chinese coals (Dai et al., 2013; Wang et al., 2007, 2008).

Hazardous element concentrations are not the only factor that needs to be considered in assessing the behavior of elements in coals and CCRs. The mode of occurrence (e.g. whether the element forms a specific mineral, whether it is dispersed within a particular host mineral or in the residual macerals) may control to a large extent the potential hazard posed by the element. Such information has, however, been largely ignored in proposed environmental regulations regarding hazardous elements in coals and CCRs.

The objective of the present research was to evaluate the modes of hazardous elements and mineral matter occurrence in typical Brazilian CCRs, using a combination of chemical and mineralogical analyses. It is hoped that the results will provide new data to develop a technical basis of further rehabilitation plans in the coal mining areas concerned.

2. Santa Catarina coal basin

The Santa Catarina and Rio Grande do Sul coal basin (Fig. 1), located in the southeastern portion of the state and covering a polygonal area of approximately 1200 km², is about 80-km long in a north–south direction. The coal-bearing sequence in that area is represented by shales, sandstones, conglomerates, and clay layers of the Rio Bonito Formation within the Early Permian Guata Group (Kalkreuth et al., 2010).

The coals mined in this and other parts of Brazil are, in general, poor in quality owing to their high-mineral matter and sulfur contents (Depoi-

et al., 2008; Kalkreuth et al., 2006; Levandowski and Kalkreuth, 2009; Oliveira et al., 2013, 2014; Silva et al., 2009). Run-of-mine products, therefore, require beneficiation prior to combustion. Coal cleaning processes are receiving increasingly greater attention in Brazil, due to the increasing amounts of coal that need to be handled as well as the low washability of the mineral-matter rich Brazilian coals (Oliveira et al., 2013; Silva et al., 2010).

3. Methods

3.1. Sampling and sample preparation

Three CCR samples from coal beneficiation plants and a run-of-mine (ROM) sample were collected from three different coal mining areas of southern Brazil. Two of the CCRs, the Fine Copelmi and Coarse Copelmi samples, were taken from the Copelmi Mining's Recreio mine, located between the towns of Minas do Leão and Butiá, Rio Grande do Sul state (latitude: 30°9' S and longitude: 52°1' W). The third CCR sample (Criciúma) was from the Carbonifera Criciúma S.A., and was obtained from a unit located in the county of Lauro Müller (latitude: 28°23'34" S and longitude: 49°23'48" W), in Santa Catarina state. The run-of-mine coal, the Cambuí sample, was from the Carbonifera do Cambuí Ltda. mine, located in the county of Figueira (latitude: 23°50'57" S and longitude: 50°24'11" W), in Paraná state.

The Coarse Copelmi sample represents the reject stream produced by a jig from the ROM product. The Fine Copelmi sample represents the tailings produced after the fine fraction of the clean coal from the jig has been further treated by a spiral concentrator system. The Criciúma CCR sample represents a blend of reject streams from a number of different beneficiation processes, taken from a tailings dam, and was collected as part of an investigation into the potential for further coal recovery from the reject material.

The samples were collected, using stainless steel spatulas, according to the Associação Brasileira de Normas Técnicas and American Society for Testing and Materials (ASTM D2234-89, 1996) procedures. After collection each sample was homogenized according to ASTM D2797-91 (1991) and split for the various analyses. In addition, separate subsamples of the homogenized materials were prepared for some purposes by sieving, magnetic separation, and handpicking under a binocular microscope, to concentrate particular mineral components. An agate mortar and pestle was used for manual grinding of the samples. The samples were stored in paper and plastic bags, which were carefully placed and arranged in cardboard boxes and stored at room temperature.

3.2. Analytical procedures

3.2.1. Petrology

Petrographic examination of the coals was conducted at the University of Kentucky Center for Applied Energy Research using a Leitz Orthoplan microscope equipped with a reflected (polarized) light, oil-immersion objective (50×). Samples were prepared as epoxy-bound 2.54-cm-diameter pellets and were ground and polished to a final 0.5-μm-alumina finish (Hower et al., 1999, 2005).

3.2.2. Mineralogy

The mineralogy of each powdered sample was analyzed by X-ray powder diffraction in the Mark Wainwright Analytical Centre at the University of New South Wales using a Phillips PW-1830 diffractometer with Cu Kα radiation, and the minerals identified by reference to the ICDD Powder Diffraction File. Because of the high mineral content, low-temperature oxygen-plasma ashing was not included in the analysis program. Quantitative analyses of mineral phases in each sample were made using SIROQUANT™, commercial interpretation software (Taylor, 1991) based on the Rietveld XRD analysis technique.

The samples and selected concentrates were studied using Raman spectroscopy, field emission scanning electron microscopy (FE-SEM), high-resolution transmission electron microscope (HR-TEM) with selected area electron diffraction (SAED) and/or microbeam diffraction (MBD), Fast Fourier transform (FFT), scanning transmission electron microscopy (STEM), and energy-dispersive X-ray spectrometer (EDS) analysis, using techniques described in previous studies (Quispe et al., 2012; Silva et al., 2011a,b,c,d,e). These instrumental techniques provide fast (e.g. XRD), non-destructive (e.g. electron beam), and highly-selective analysis (e.g. Raman spectroscopy) of both the whole coal and CCR ultrafine/nano-particle surfaces.

3.2.3. Chemistry

A representative portion of each sample was calcined at 1050 °C, and then fused with lithium metaborate and cast into a disc, following the method of Norrish and Hutton (1969). The disc was analyzed by X-ray fluorescence (XRF) spectrometry at the University of New South Wales using a Philips PW 2400 spectrometer and SuperQ software.

Sample digestion for minor and trace element determinations was performed by accurately weighing 0.100 ± 0.01 g of size-reduced sample into a vial and adding concentrated HNO_3 before heating at 80 °C overnight, with the aim of digesting reactive organic phases (Querol et al., 1997). This suspension was then centrifuged; the supernatant was transferred to a volumetric flask and the solid residue was placed back in the vial, where it was digested by adding HF, HNO_3 , and HClO_4 , heated overnight, concentrated and evaporated, to digest the silicate and oxide phases. The dry residue was re-constituted with HNO_3 and MQ water to 100 mL of 5% v/v HNO_3 and stored in HDPE bottles. Reference materials (SARM 19, NIST SRM 1633b), duplicated samples and blanks were all prepared in a similar manner to check the accuracy of the analytical and digestion methods. The resulting solutions were then analyzed for trace elements by inductively coupled plasma-mass spectroscopy (ICP-MS, Perkin Elmer Elan 6000) at the Institute of Environmental Assessment and Water Research, Barcelona. Arsenic and Se were determined by ICP-MS with collision cell technology (Li et al., 2014).

In order to study the potential for leaching of potentially toxic elements from the samples, the EN 12457–2 compliance leaching test (European Committee for Standardisation, 2002) was applied. This is a single batch leaching test performed at a liquid to solid ratio (L/S) of 10 L/kg, with deionized water as the leachant and 24 h of agitation time. The analyses in all cases were performed in duplicate. Major, minor, and trace element concentrations in the leachates were determined by ICP-MS, ICP-AES, and high-performance liquid chromatography techniques.

4. Results and discussion

For all of the samples, we note that although several national and international standards classify coal as having >50 wt.% organics, those classifications refer to coal in place, not to mined materials that can contain rock from the roof, floor, and partings thicker than the 0.375-inch (0.95-cm) thickness commonly excluded in coal chemistry analyses. A coal refuse is the mixture of coal and rock that did not report to the clean coal product. The coal particles in the refuse are still coal, no matter how many rock fragments surround them.

4.1. Petrology

The maceral assemblages are dominated by vitrinite and fusinite (Table 1; Fig. 2A), with minor to trace amounts of sporinite and cutinite. The mineral assemblages visible under the microscope are dominated by clay (Fig. 2B), sulfides, quartz, and carbonates. Natural coke associated with fusinite is an important constituent of the Cricúma rejects (Fig. 2C and D). Vitrodetrinite is present as small vitrinite fragments of varying shapes surrounded by clay minerals. Inertinite is present as

Table 1

Petrology (volume %) of samples studied. The first column for each sample is on the mineral-included basis, the second column is the mineral-free calculation of the first column.

Maceral/Mineral	Cambuá	Cricúma	Fine Copelmi	Coarse Copelmi
Telinite	2.6	6.5	0.6	4.7
Collotelinite	24.6	61.5	4.8	37.5
Vitrodetrinite	2.4	6.0	3.0	23.4
Collodetrinite	0.0	0.0	0.0	0.0
Corpogelinite	0.6	1.5	0.0	0.0
Gelinite	0.0	0.0	0.0	0.0
Total vitrinite	30.2	75.5	8.4	65.6
Fusinite	7.4	18.5	1.0	7.8
Semifusinite	0.8	2.0	0.6	4.7
Micrinite	0.2	0.5	0.0	0.0
Macrinite	0.8	2.0	0.0	0.0
Secretinitite	0.6	1.5	0.0	0.0
Funginite	t	t	0.0	0.0
Inertodetrinite	0.0	0.0	0.0	0.0
Total inertinite	9.8	24.5	1.6	12.5
Sporinite	t	t	0.8	6.3
Cutinite	0.0	0.0	0.2	1.6
Resinite	0.0	0.0	0.0	0.0
Alginite	0.0	0.0	0.0	0.0
Liptodetrinite	0.0	0.0	0.0	0.0
Suberinitite	0.0	0.0	0.0	0.0
Exudatinite	0.0	0.0	0.0	0.0
Total liptinite	0.0	0.0	1.0	7.8
Silicate	46.8		62.0	63.8
Sulfide	5.6		8.4	6.8
Carbonate	0.0		0.6	4.2
Quartz	7.6		16.2	7.8
Total minerals	60.0		87.2	82.6
Natural coke	0.0	0.0	1.8	14.1
			0.0	0.0
			0.0	0.0

t = trace.

the macerals funginite, semifusinite, fusinite, macrinite, micrinite, and inertodetrinite. Similar data were previously reported by Oliveira et al. (2012, 2013).

4.2. Mineral compositions

X-ray diffraction analysis indicates that the major minerals in the samples are kaolinite, quartz, illite, interstratified illite/smectite, gypsum, jarosite, pyrite, rutile, calcite, and melanterite (Table 2). Kaolinite is the dominant clay mineral in the crystalline fraction of the two Copelmi samples, with lesser but still significant proportions of quartz and interstratified illite/smectite (I/S). Illite and I/S are more abundant in the mineral fraction of the Cricúma and Cambuá samples, along with similar proportions of quartz but lesser proportions of kaolinite than those found in the Copelmi materials. Significant proportions of calcite and ankerite are also present in the mineral matter of the Fine Copelmi sample; feldspar (probably Na-rich plagioclase) occurs in all samples except the Fine Copelmi material.

Significant proportions of pyrite and, except for the Fine Copelmi material, pyrite oxidation products, jarosite and melanterite, were identified in the mineral matter of the samples by XRD techniques. A trace of sphalerite is also indicated in the Cambuá ROM sample. Gypsum, possibly derived from the interaction of sulfuric acid from pyrite oxidation with associated carbonate minerals (Rao and Gluskoter, 1973), is also present in all cases as a minor but significant component.

The minerals detected by electron beam and Raman techniques are also shown in Table 2. Most of these are at concentrations below the limit of detection by the XRD study. Many of these minerals occur in intimate association with the coal matrix at the particle size under consideration (Oliveira et al., 2013, 2014). Some of them, mainly sulfate (e.g. jarosite, gypsum, melanterite) and ferrite minerals, may have been generated in situ through weathering or dissolution of the original compounds (e.g. pyrite) in the coals and subsequent precipitation of

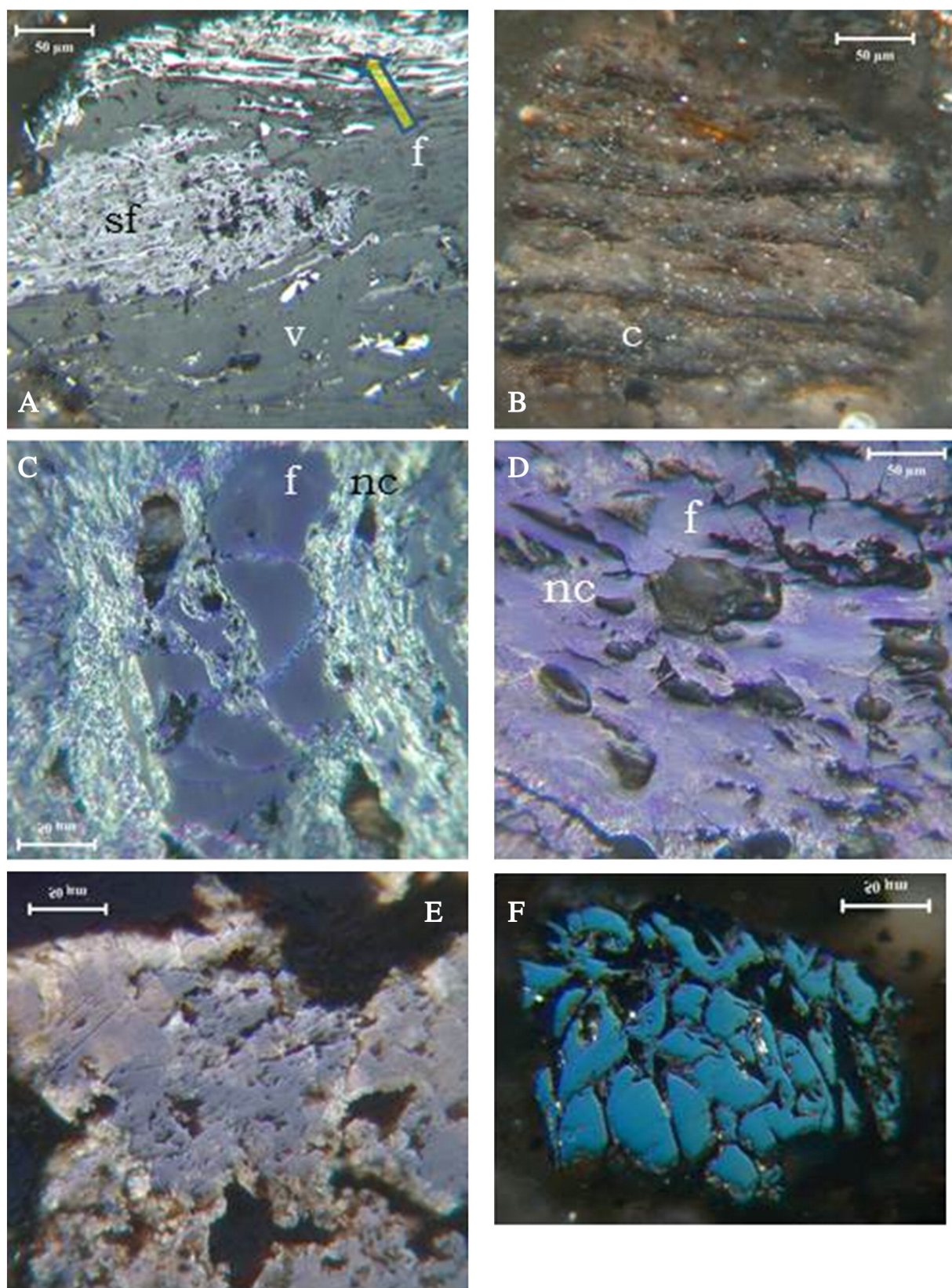


Fig. 2. Examples of petrographic assemblages in the coal cleaning rejects. A, fusinite (f), semifusinite (sf), and vitrinite (v) (Cambuí); B, clay (c) with thin organic layers (Fine Copelmi); C, fusinite (f) with natural coke (nc) (Criciuma, crossed polars with wavelength plate); D, fusinite (f) with natural coke (nc) (Criciuma, crossed polars with wavelength plate); E, sphalerite (Cambuí, crossed polars with wavelength plate); F, pyrite in fusinite lumens (Fine Copelmi, crossed polars with wavelength plate).

new thermodynamically stable solid phases from dissolved cations and anions. Some of these new mineral phases may contain toxic metals (e.g. Hg, Cd, Cr, and Pb) that can be released as free cationic species

and consequently produce bioavailable metal species when dust or leachates are transported outside the coal mining facilities (Quispe et al., 2012; Silva et al., 2010).

Table 2

Minerals and amorphous phases identified in samples studied.

	Fine Copelmi	Coarse Copelmi	Criciúma	Cambuí
<i>XRD quantification (%)</i>				
Quartz	24.8	23.5	16.7	26.6
Kaolinite	50.6	55.0	31.2	17.3
Illite	n. d.	n. d.	11.2	11.7
Illite-smectite	9.1	7.2	25.9	21.1
Feldspar (albite)	n. d.	3.9	4.2	10.2
Calcite	7.1	n. d.	n. d.	n. d.
Ankerite	1.4	n. d.	n. d.	n. d.
Pyrite	3.1	0.9	1.9	3.5
Sphalerite	n. d.	n. d.	n. d.	0.4
Jarosite	n. d.	1.5	4.1	4.8
Melanterite	n. d.	4.9	n. d.	n. d.
Gypsum	2.3	2.9	4.7	3.5
Rutile	1.6	0.3	n. d.	0.9
<i>Minor detected phases</i>				
Carbonates				
Calcite, CaCO ₃	c	c	n.d.	a
Siderite, FeCO ₃	a,c	c	a	a,b,c
Oxides and hydroxides				
Anatase, TiO ₂	a,c	b,c	c	c
Brucite, Mg(OH) ₃	n.d.	b	n.d.	b,c
Chromite FeCr ₂ O ₄	a	b,c	n.d.	a
Goethite, Fe(OH) ₃	a,c	a,b,c	c	a,c
Gibbsite, Al(OH) ₃	a,c	a,b,c	c	a
Hematite, Fe ₂ O ₃	a, c	a,b,c	a,c	a,c
Quartz, SiO ₂	a,b,c	a,b,c	a,b,c	a,b,c
Rutile, TiO ₂	c	c	n.d.	n.d.
Phosphates				
Monazite, (Ce, La, Th, Nd, Y)PO ₄	a	a,c	a	a
Xenotime, YPO ₄	a	a	n.d.	n.d.
Salt				
Halite, NaCl	n.d.	n.d.	n.d.	a,b,c
Silicates				
Albite, NaAlSi ₃ O ₈	a,c	a,b,c	a	a,b,c
Chlorite, (Fe, Mg, Al) ₆ (Si, Al) ₄ O ₁₀ (OH) ₈	c	n.d.	n.d.	c
Illite, K _{1.5} Al ₄ (Si _{6.5} Al _{1.5})O ₂₀ (OH) ₄	n.d.	n.d.	a,b	a,c
Kaolinite, Al ₂ Si ₂ O ₅ (OH) ₄	a,b,c	a,b,c	a,b,c	a,b,c
Zircon, ZrSiO ₄	a,c	a	a	a
Sulfates				
Aluminite, Al ₂ (SO ₄) ₂ (OH) ₄ ·7H ₂ O	a,c	c	a,c	a,c
Anhydrite, CaSO ₄	s	a,b	a	a
Barite, BaSO ₄	a,c	a	a	n.d.
Epsomite, MgSO ₄ ·7H ₂ O	a,c	a,b	a,c	a,b
Gypsum, CaSO ₄ ·2H ₂ O	a,b,c	a	a	a
Halotrichite, FeAl ₂ (SO ₄) ₄ ·22H ₂ O	a,b	a,b	a,b	a,b
Hexahydrite, MgSO ₄ ·6H ₂ O	a,b,c	a,b	n.d.	n.d.
Jarosite, KFe ³⁺ ₃ (SO ₄) ₂ (OH) ₆	a	a	a,b	n.d.
Melanterite FeSO ₄ ·7H ₂ O	a,b,c	a,c	a,b,c	a,b,c
Natrojarosite, NaFe ₃ (SO ₄) ₂ (OH) ₆	c	a,b	n.d.	n.d.
Pickeringite, MgAl ₂ (SO ₄) ₄ ·22H ₂ O	c	n.d.	n.d.	c
Schwertmannite, Fe ₁₆ O ₁₆ (OH) ₁₂ (SO ₄) ₂	a,b,c	a	a	a
Zircon, ZrSiO ₄	c	a,c	c	c
Sulfides				
Galena, PbS	a,c	a	a	n.d.
Marcasite, FeS ₂	a,b,c	a,b,c	a,b,c	a,b,c
Pyrite, FeS ₂	a,c	a,b,c	a,b,c	a,b,c
Sphalerite, ZnS	n.d.	c	n.d.	a,c
Amorphous	a,b,c	a,b,c	a,b,c	a,b,c

Analytical methods for minor phases: a = FE-SEM/EDS, b = Raman, c = HR-TEM/STEM/MBD/SAED/EDS.

n.d. = not detected.

thus either of authigenic or epigenetic origin in the original coal sources. Illite commonly occurs as a mixture of micro and ultrafine particles, probably of detrital origin. The clay minerals also occur as individual aggregates or as intimate mixtures with pyrite and calcite. Fine-grained mineral masses, representing mixtures of quartz and kaolinite, with illite and/or pyrite in some cases, are often interblended with the residual organic matter present in the CCRs, especially, but not only, infilling the lumens of the inertinite components.

Common minor elements in the illite are Ti and Fe. Elements such as Cl, Na, Mg, Ca, and S were also detected by FE-SEM and HR-TEM coupled with EDS in the other clay mineral components.

Accessory silicate minerals (Table 2) include feldspar grains (20–50 µm) or elongated feldspar-clay agglomerates (~3 × 12 µm). Sub-angular zircon crystals are a common accessory mineral in the coal and CCR samples.

4.3.2. Oxides and hydroxides

Apart from the abundant quartz indicated by X-ray diffraction (Table 2), oxide species detected by Raman, FE-SEM/EDS and HR-TEM/EDS/MBD/STEM techniques include hematite, goethite (α -FeOOH), gibbsite (α -AlOOH), brucite ($Mg(OH)_2$), anatase, and rutile (Table 2).

All of the samples analyzed by HR-TEM/SAED/FFT/EDS contain abundant hematite (Table 2), mixed with a carbonaceous matrix (Fig. 3A). FE-SEM and HR-TEM/SAED/MBD images and supporting EDS data indicate the presence of additional fine crystalline phases, such as Fe-rich oxide. Fast Fourier transform (FFT) and spectroscopic techniques (e.g. electron energy-loss spectroscopy and EDS), used to support identification of the nanohematite, clarified important results with for example, Fig. 3A showing a complex assemblage of angular nanohematite identified in the Criciúma sample with residual amorphous silicate.

Hematite, in places enriched in Cr, is also a common nanoparticle in the CCRs, occurring as spherical and highly aggregated particles (Fig. 3A). Cr-spinel is also present as grains associated with clay minerals. Hematite is often seen to be closely mixed with quartz, feldspar, jarosite, goethite, ferrihydrite, amorphous phases, and rutile by FE-SEM/EDS techniques. The other non-quartz oxides occur in all samples, but in smaller proportions than the hematite. Some of these phases (e.g. goethite and ferrihydrite) may be products formed by oxidation of pyrite and reactions of the produced acid with calcite or ankerite. The hematite, and also the gibbsite, may represent precipitates formed from highly acidic solutions (in which Fe and/or Al are soluble) as the pH is increased, reducing the relevant cation solubility (cf. Ward, 2002).

Gibbsite forms 1 × 10 µm aggregates of kidney-shaped grains, with impurities of K, Fe, Ni, and Si. From an environmental perspective, one of the important features of the insoluble mineral nanoparticles (e.g. hematite) is their high surface area, which facilitates their role as powerful sequestrates of potentially hazardous elements.

The presence of spherical nanoquartz particles (Fig. 3B) in the Copelmi coal was also confirmed by HR-TEM/EDS/FFT/STEM. The particle diameter (~37 nm) was estimated from the HR image, and the elemental composition determined by EDS. The crystallinity of nanoquartz particles was easily analyzed by FFT. This nanoquartz detection is important because of the link between crystalline silica exposure and lung cancer risk. The nanoquartz embedded in the coal particles in this work setting may be a particular case; whether this occurrence of quartz occurs in other ambient air settings should be investigated in order to protect the Brazilian general population.

4.3.3. Carbonates

Although only identified by XRD in one sample (Fine Copelmi), small amounts of calcite are commonly seen in the Coarse Copelmi and Cambuí CCR samples by other techniques (Table 2). The calcite is mostly associated with the residual coal macerals, occurring especially in

4.3. Modes of mineral occurrence

4.3.1. Silicates

The kaolinite in the samples occurs primarily in plant cell cavities of the maceral components, often as pseudohexagonal crystals, and was

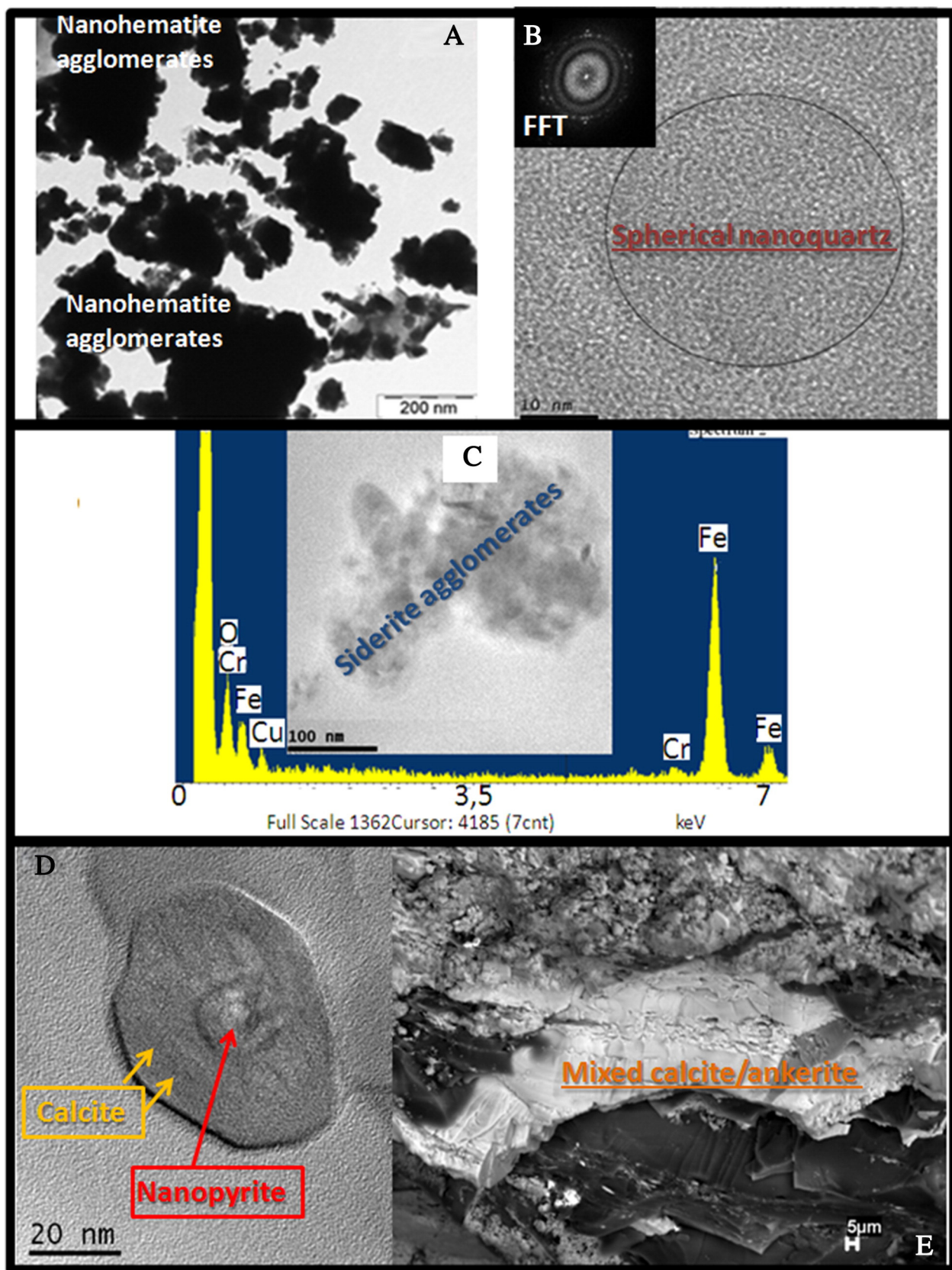


Fig. 3. (A) Bright-field HR-TEM image of nanohematite agglomerates containing quartz and clay minerals; (B) spherical nanoquartz including Fast Fourier transform. (C) nanosiderite crystal agglomerates containing Cr; (D) nanopyrite in calcite (in fusinite of Fine Copelmi sample); (E) mixed calcite/ankerite (Coarse Copelmi).

association with vitrinite. Massive syngenetic calcite occurs separately or in association with massive Fe-sulfides (eg. pyrite), filling cell lumens, and encrusting cellular walls. Other carbonate minerals include

ankerite, detected by XRD in the Fine Copelmi sample, and siderite, detected by HR-TEM (Fig. 3C), FE-SEM, and Raman techniques (Table 2). The calcite and ankerite mainly occur as infillings of micro-cleats in

the residual coal (in association with vitrinite), filling fractures that were opened up after burial and rank advance, and as cell-fillings in the inertinite (Fig. 3D).

The greater abundance of carbonates, especially ankerite, in the Fine Copelmi sample suggests that coal particles containing calcite and ankerite as cleat infillings in vitrinite may have been incorporated in the clean coal product from the jig plant, but then rejected when small particles of carbonate-bearing macerals in the fine fraction of that coal were subsequently passed through the spiral concentrator

system. Greater abundance of similar carbonate minerals (calcite and dolomite) in the fine fraction compared to the coarse fraction of a South African coal was also noted by Matjie et al. (2008).

4.3.4. Sulfides

Pyrite (Figs. 2E, F, 3D, 4, and 5), sphalerite, and marcasite are the most abundant sulfide minerals (Table 2). Galena was also detected by Raman, FE-SEM, and HR-TEM analyses. Authigenic marcasite is present as tubular (~25–70 μm) and bi-pyramidal (12 μm) crystals,

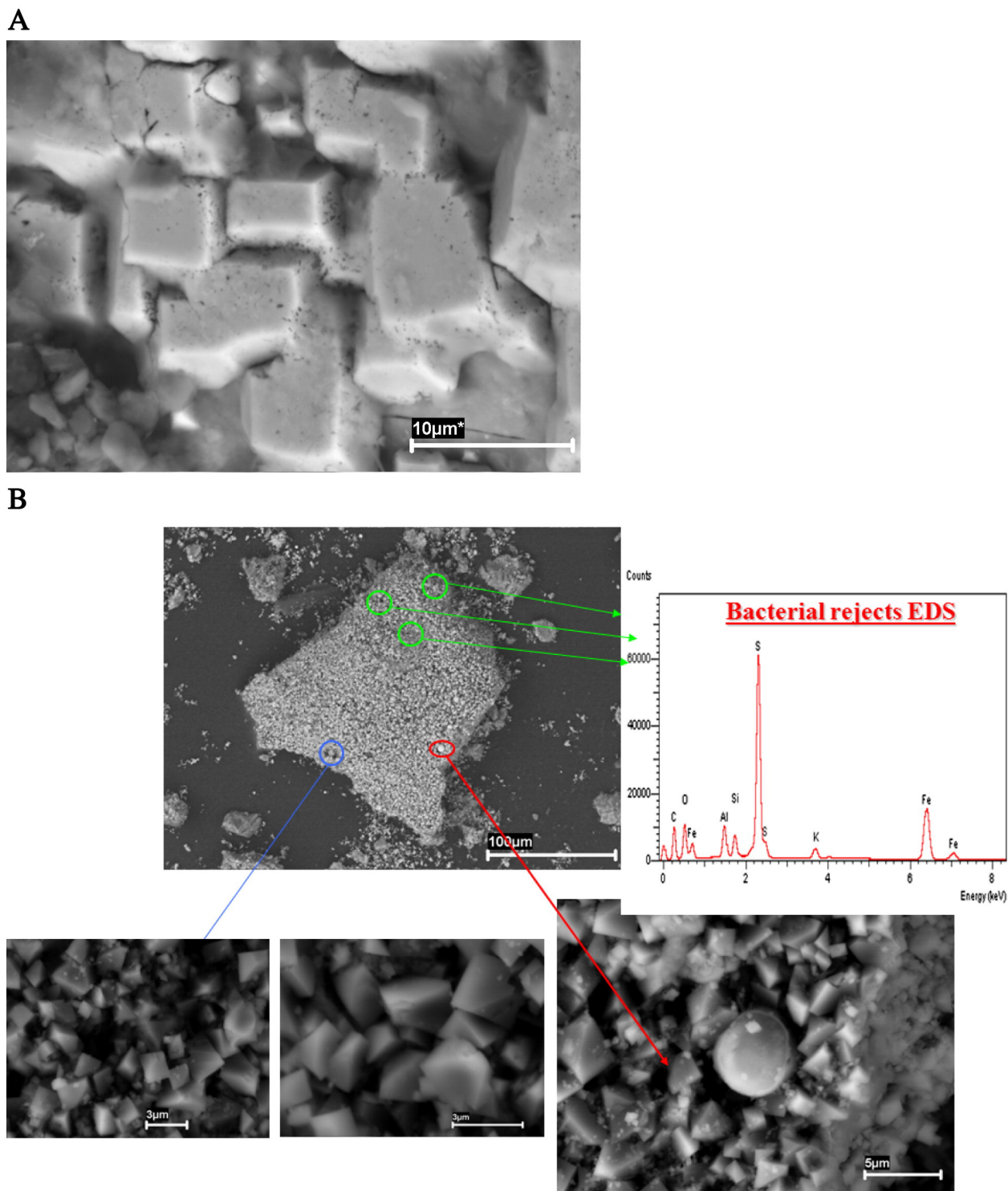


Fig. 4. SEM secondary electron images. (A) Typical cubic pyrite from Santa Catarina Coal Zone (Cambuí sample); (B) Lens of epigenetic frambooidal pyrite, showing fruiting bodies in the process of formation (Cambuí sample). EDS from spherical particle in the lower right image.

and as poly-crystalline aggregates associated principally with calcite. Discrete individual crystals and aggregates, commonly of pyrite, are also seen dispersed within the residual macerals present in the CCRs, especially in the vitrinite bands. Other pyrite forms include 0.5- to 50- μm syngenetic pyrite frambooids, with octahedral habits of the micro-crystals present as individual bodies or their clusters; euhedral crystals present as cubic and octahedral crystals or their aggregates; and massive grains present as infillings of cell lumens (Fig. 5), multi-lumen sclerotia, encrustations on cellular walls, and as discrete grains. In many cases, massive grains of pyrite are also present in association with frambooidal and euhedral pyrite. The euhedral and massive pyrite was originally formed in close association with organic matter. In addition, the syngenetic pyrite may be associated with amorphous clay and with calcite.

Frambooidal pyrite forms spherical aggregates of octahedral micro-crystals, and is present as lenses covering and filling cracks in the organic matter (Fig. 4B). This type of formation may have been due to successive changes in environmental conditions as a result of orogenesis and a renewal of microorganism activity (Yossifova, 2014). Previous authors have postulated a bacterial origin for frambooidal pyrite, or possibly a fungal origin (Chou, 2012; Wiese and Fyfe, 1986; Yossifova et al., 2011).

The composition of the pyrite surfaces and the tendency of metal ions to be adsorbed on to them from aqueous solution may, to a considerable extent, also influence the rate of pyrite oxidation. This is consistent with the fact that some metals, such as Na, K, Ca, Mg, Al, Ni, Cu, Ag, Pb, Zn, Cd, and As, are known to occur on natural pyrite surfaces (Al et al., 1997). More detailed investigations of such minerals as hosts for the trace elements in the coals were conducted to evaluate this possibility further.

Hand-picked fractions enriched in certain minerals (e.g. pyrite, gypsum, jarosite, and hematite) were separated under a binocular microscope and analyzed using FE-SEM/EDS and HR-TEM/SAED/MBD/FFT/EDS techniques. The EDS spectra of the samples studied confirmed the presence of several hazardous elements in the sulfide, carbonate, and mixed-mineral fractions, indicating encapsulation by adsorption, and/or precipitation of those elements. The potential contributions of such element impurities to the sorption behavior of sulfides and/or carbonates should be considered in any discussion of the underlying sorption mechanisms, especially due to their potential toxicity to human health. The enriched elements detected by SEM and TEM coupled with EDS in the mineral fractions with equal or higher concentrations relative to those in the analyzed samples are listed below:

- Calcite and dolomite: Ba, Be, Fe, Mn, Mo, P, Pb, Si, and Sr;
- Siderite: Al, Cr, Cu, and Mn;
- Pyrite (as euhedral crystals forming lenses) and calcite + dolomite: Ba, Hg, Mn, Mo, Ni, Pb, Se, Sr, and Ti;
- Quartz, pyrite, dolomite + calcite + K-feldspar: Ba, Be, Cr, Mo, Mn, Pb, Sn, Ti, V, and Yb;
- Pyrite as massive epigenetic plates: Ba, Be, Co, Cd, Mn, Mo, Ni, Pb, Se, Sr, and Zn; and
- Pyrite as massive syngenetic concretions: As, Ag, Ba, Co, Ga, Mn, Mo, Ni, Pb, Sb, Se, Sn, Tl, and Yb,

4.3.5. Sulfates

The major sulfate constituents of the coal and CCR samples (Table 2) are gypsum (Fig. 6) and jarosite (Fig. 7). Other sulfates detected by FE-SEM/HR-TEM/Raman techniques include aluminite, anhydrite, barite, epsomite, hexahydrite, melanterite, natrojarosite, pickeringite, and

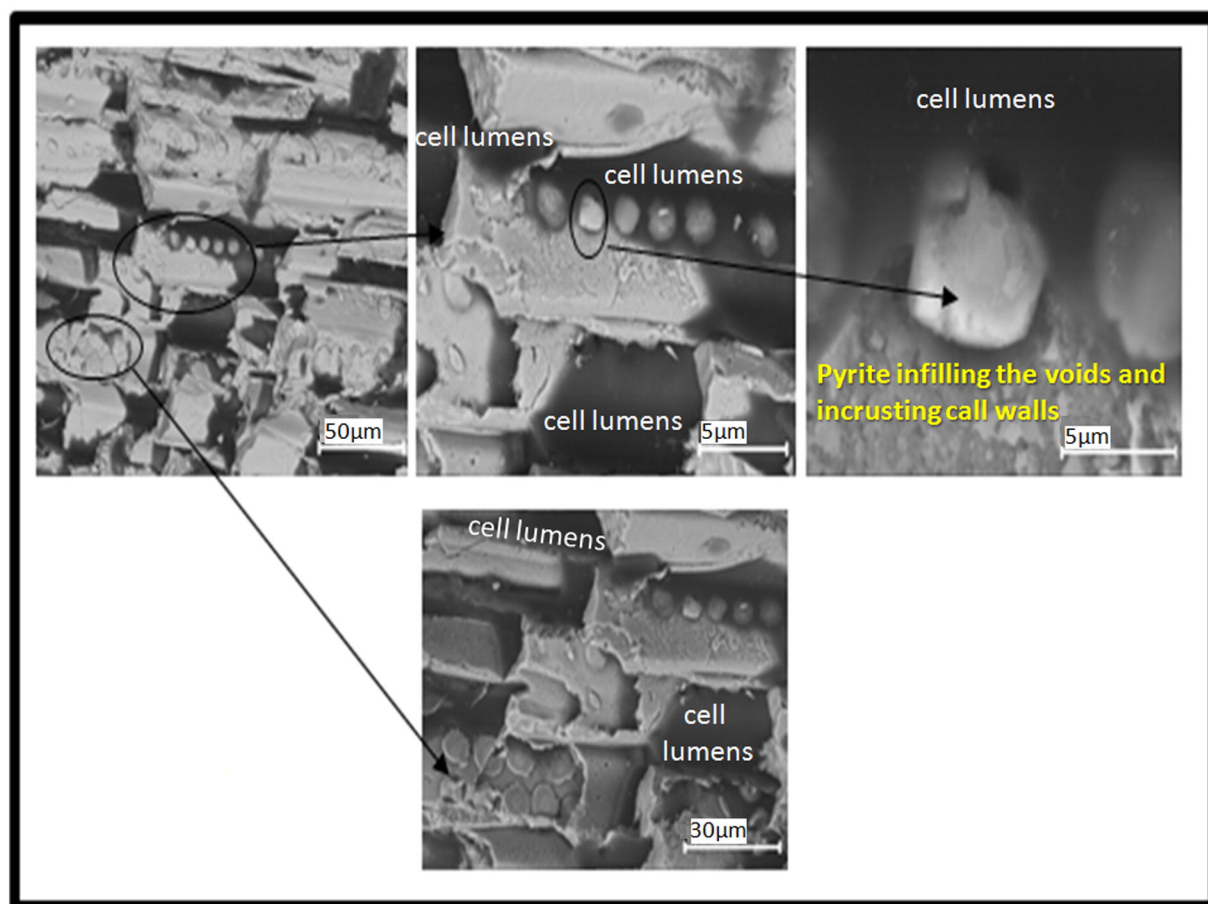


Fig. 5. SEM secondary electron image. Pyrite infilling the voids (cell lumens) and incrusting cell walls (Cambuí sample).

schwertmannite. Based on a geochemical model (Silva et al., 2011e), some of these minerals are probably the products of sulfide oxidation. Gypsum is present as: (1) cryptocrystalline concretions and crusts on the surfaces of frambooidal pyrite; (2) platy crystals around 20 µm across; (3) prismatic crystals; and (4) lenses, veins, and fine crusts in cracks. The gypsum and jarosite in the pyrite were probably derived from interactions between calcite in the samples and sulfuric acid produced by pyrite oxidation, forming Fe-sulfate minerals such as szomolnokite ($\text{FeSO}_4 \cdot \text{H}_2\text{O}$) and coquimbite ($\text{Fe}_2(\text{SO}_4)_3 \cdot 9\text{H}_2\text{O}$), together with a significant proportion of gypsum. Rao and Gluskoter (1973) have described coquimbite and szomolnokite as oxidation products of pyrite in coals from the Illinois Basin, developed after exposure to the atmosphere with storage. A similar process probably occurred in the sulfide concentrates of the present study.

In these samples, barite is present as aggregates of tabular crystals as rosettes with lengths of 30–65 µm. The mineral probably has a hydrothermal origin. The chemistry, morphology, and size of this sulfate are similar to the hydrothermal barite described by Paytan et al. (2002) for oceanic settings. However, the chemistry, morphology, and size of the fine crystals and elliptic grains of barite observed surrounding the above aggregates accord with the authigenic (sedimentary) type observed by Paytan et al. (2002). The chemical composition of the crusts surrounding the barite aggregates (fluxing minerals) includes impurities such as Ca, Fe, P, S, Sr, Al, and Si.

4.3.6. Phosphates

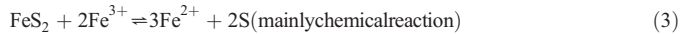
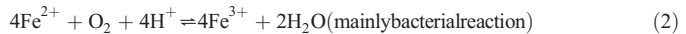
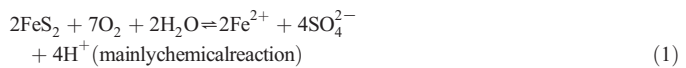
No phosphate minerals were detected by XRD, however, monazite and xenotime were observed by both FE-SEM/EDS (Figs. 8, 9D) and HR-TEM/SAED/EDS. The results of element mapping for a typical monazite (Fig. 8), indicate that P, La, Th, and Ce are all distributed evenly across the particle, further confirming the element association.

4.4. Mineral interactions

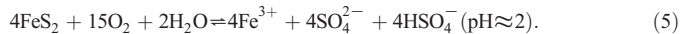
Oxidation of sulfides, primarily pyrite, during mining, coal cleaning and/or storage has resulted in the formation of a large number of sulfate, oxide, and hydroxide mineral phases in the samples of the present study. Since pyrite in Brazilian and other coals is commonly a host for potentially toxic trace elements (e.g. As, Pb, Hg, Se; Dai et al., 2005;

Finkelman, 1993; Silva et al., 2009; Oliveira et al., 2012), pyrite oxidation may also release these elements into the surrounding environment.

Pyrite is known to react with water and dissolved molecular oxygen to form sulfate ions and cationic Fe^{3+} or Fe oxy/hydroxides (Cravotta, 2008). The regeneration of Fe^{3+} (which is reduced to Fe^{2+} on reaction with pyrite) is the key reaction in promoting ongoing oxidation of the mineral. At pH values above 4, this may be mediated chemically or biologically (by Fe-oxidizing bacteria such as *Gallionella ferruginea*) (Cravotta, 2008). Below pH 4, abiotic Fe oxidation is negligible, and the activities of moderately and extremely acidophilic Fe-oxidizing bacteria have a pivotal role in the genesis of acid mine waters (Silva et al., 2010, 2011a,c,e). The following partial reactions, spectroscopically demonstrated by Raman monitoring on parallel experiments conducted with and without the presence of iron-oxidizing bacteria (Sasaki, 1997), are responsible for pyrite oxidation:



Thus, the overall oxidation of pyrite (Rimstidt and Vaughan, 2003) that is kinetically enhanced by the presence of anaerobic microorganisms is:



The sulfate mineral that dominates in the CCRs of the present study is rhombohedral jarosite (Figs. 6 and 7). Its formation is thought to require a wet, oxidizing, acidic environment (Gasharova et al., 2005). This phase is important environmentally because its structure readily

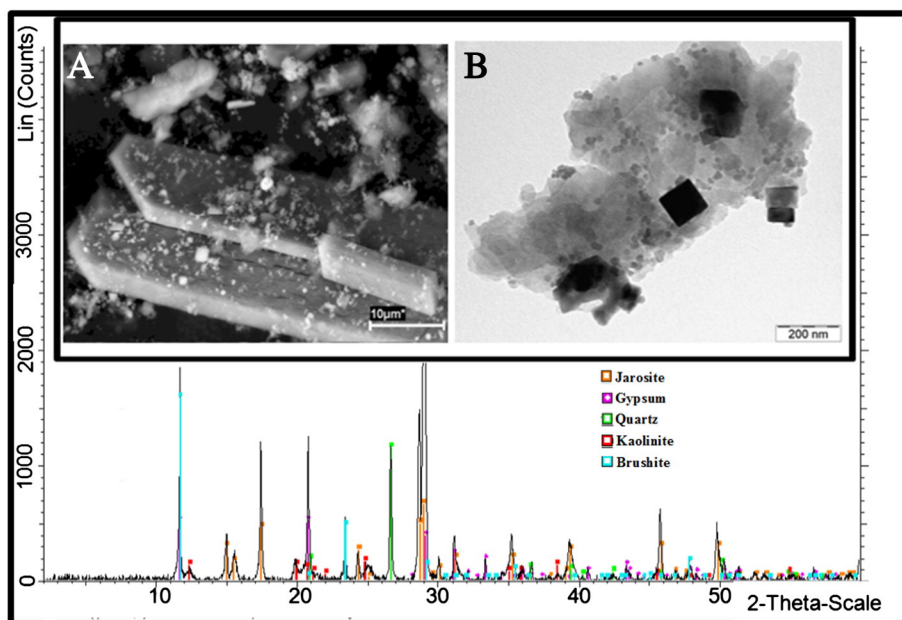


Fig. 6. X-ray diffractogram showing jarosite, gypsum, quartz, kaolinite, and brushite in Criciúma sample. Inset: (A) SEM image of gypsum crystals in an association with rhombohedral jarosite (secondary electron image); (B) TEM image of rhombohedral jarosite in association with goethite, and alteration of iron hydroxides to nanospherules of hematite.

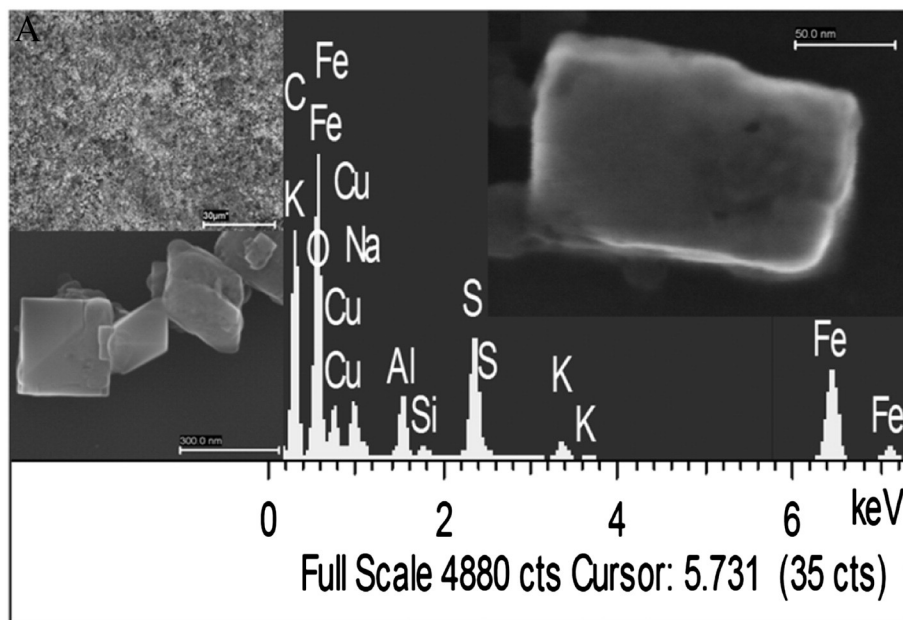
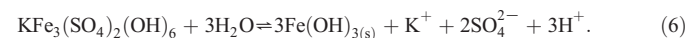


Fig. 7. SEM secondary electron images. (A) General view of jarosite aggregates and magnification of ultra-fine jarosite grains containing clay minerals plus typical SEM/EDS pattern (Cu is from Cu grid).

takes up Pb (Stoffregen et al., 2000) and Cr (Silva et al., 2009). Laboratory bulk-dissolution experiments (shaking in pure water) using synthetic H_3O^- , Na-, and K-dominant jarosite, and a partly Cr^{3+} -substituted jarosite, have shown that the stability increases in the same sequence (Gasharova, 2000; Göttlicher and Gasharova, 2000). The natural ascent of the rainwater and groundwater table or flooding can change the pH and Eh conditions of the environment in waste emplacements at the Brazilian coal mining sites. With increasing pH, jarosite becomes unstable and hydrolyzes, releasing sulfate anions and toxic elements into surface contaminated soils. The stability of jarosite is generally limited to a

relatively narrow range of acidic conditions. As pH increases, jarosite is transformed to ferric oxyhydroxide, represented in the following discussion as $\text{Fe(OH)}_{3(s)}$. The reaction between these two phases (Silva et al., 2011e) is as follows:



The transition pH between jarosite and aged, more crystalline ferric oxyhydroxide (hematite and goethite) would, therefore, be correspondingly lower (Welch et al., 2007). For example, in the presence of rain,

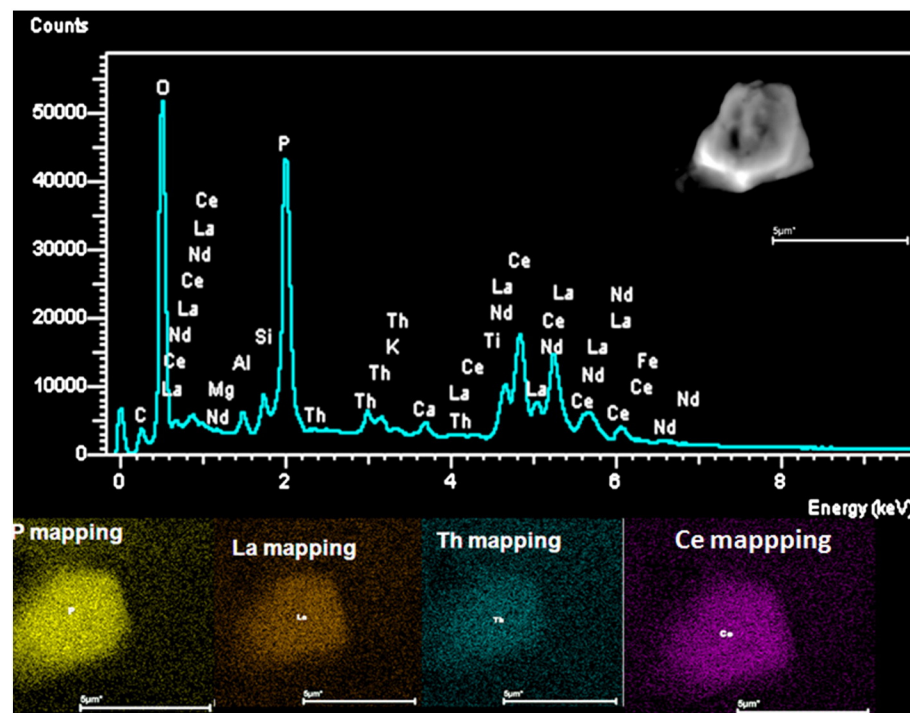


Fig. 8. SEM secondary electron image. SEM/EDS pattern of a typical monazite particle detected as a minor constituent in all CCRs. Image of pattern shown in upper left, and element mapping patterns for P, La, Th and Ce shown in lower part.

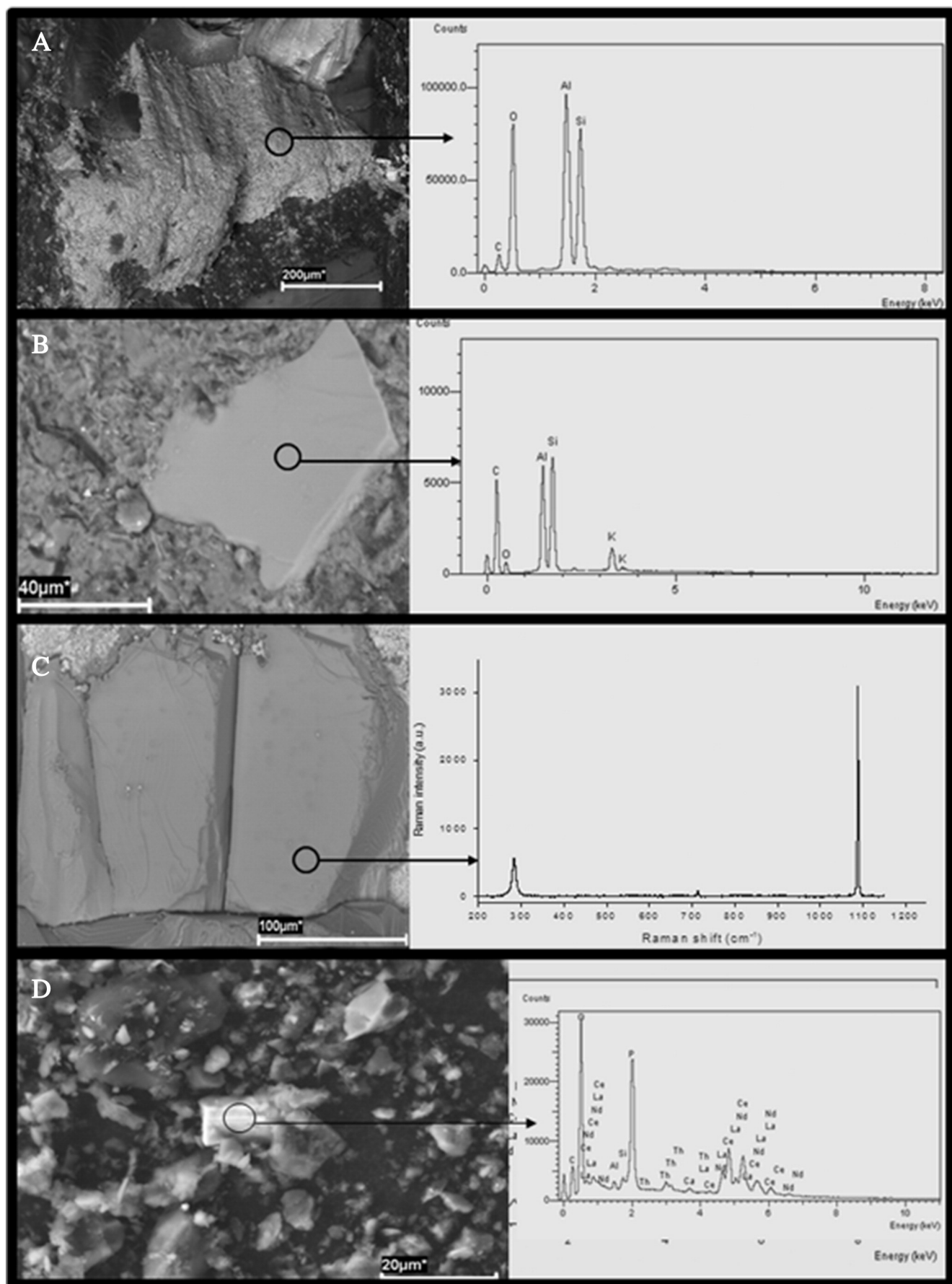


Fig. 9. SEM secondary electron images. SEM images and EDS spectra of (A) kaolinite and (B) illite (Cambuí sample). (C) SEM image of calcite and Raman spectroscopy identification (Coarse Copelmi sample). (D) Monazite showing a SEM image of natural surface and its EDS spectrum for elemental composition (Coarse Copelmi sample).

they dissolve incongruently, acidifying the water and leaving ferric oxide behind.

Fine oxide/hydroxide grains with compositions of Cr > Fe and Fe > Cr were also found in jarosite aggregates in the CCRs of the present study. Under most conditions (e.g. under acidic conditions at low temperature, without intermediate ferric oxyhydroxide phases) the jarosite is also accompanied by kaolinite, schwertmannite, goethite, hematite, ferrihydrite, brushite, and gypsum (Silva et al., 2011a,c,d,e). Detailed geochemical modeling of acidic evaporative processes for the CCR materials predicts that jarosite will transform to goethite and/or hematite during fluid recharge events (Fig. 6B). In addition, it is possible that the jarosite was not completely transformed to hematite because the aqueous phase became highly saline and gypsum was formed due to evaporation.

Carbonates can be beneficial by providing buffering capacity to help neutralize the acid formed by the oxidation of sulfides. Sulfates of Ca, Fe, Ba, Mg, and Na were identified and may be weathering products of pyrite and reaction of the resultant acids with other minerals such as carbonates and phosphates.

Melanterite [$\text{Fe}^{2+}\text{SO}_4 \cdot 7\text{H}_2\text{O}$] is one of the most common soluble sulfate minerals found in nature (Silva et al., 2011d,e). Melanterite dehydrates to rozenite [$\text{Fe}^{2+}\text{SO}_4 \cdot 4\text{H}_2\text{O}$] or to szomolnokite [$\text{Fe}^{2+}\text{SO}_4 \cdot \text{H}_2\text{O}$]. In this study, melanterite typically forms blocky, equant crystals with prominent growth zones, and generally includes minor concentrations of Cu or Zn.

5. Major and trace element compositions

5.1. Major elements

The percentages of the major element oxides in the samples studied are given in Table 3. As might be expected from the mineralogy indicated by XRD analysis (Table 2), the materials are dominated by SiO_2 and Al_2O_3 (from clays, e.g. Fig. 9A and B) with lesser but still significant proportions of Fe_2O_3 , CaO , K_2O , and SO_3 . The CCR samples produced loss-on-ignition (LOI) values of 17.82 to 27.86%; if this is made up mainly of carbonaceous material (residual organic matter), such values would indicate ash percentages for the rejects of around 70 to 80%. The run-of-mine Cambuí sample has an LOI of around 33%, indicating a 67% ash yield. The residuals from the LOI percentages (i.e. 100% minus the LOI values) are also consistent with the total percentages of visible minerals in the respective samples indicated by microscopic analysis (Table 1), especially for the CCR materials.

If the chemical compositions are recalculated to an LOI-free basis (Table 4), the major element chemistry for most elements is similar to the average major-element ash chemistry for a range of ROM coals from the Santa Catarina Basin reported by Oliveira et al. (2013). However, the LOI-free proportions of Fe_2O_3 and SO_3 are higher for the samples in the present study, including both the ROM coal (Cambuí sample) and the three CCR materials. As shown by Oliveira et al. (2013), beneficiation of Santa Catarina coals reduces the proportion of pyrite in the mineral matter of the clean coals compared to that of the equivalent ROM material, and hence the reject fractions of the same coals would be expected to have higher pyrite contents. The higher percentage of Fe_2O_3 in the samples studied is thus consistent with a higher proportion of pyrite and pyrite oxidation products (e.g. jarosite, melanterite) in the rejects from Santa Catarina beneficiation plants compared to typical clean coal materials. The ROM coal of the present study also has a higher than average percentage of Fe_2O_3 , presumably reflecting a higher than average pyrite content for that particular coal source.

5.2. Trace elements

The concentrations of trace elements in the samples, as determined by ICP-MS techniques, are listed in Table 3, along with world average concentrations for the same trace elements in coals as estimated by

Table 3
Inorganic chemistry of samples studied.
World average after Ketris and Yudovich (2009).

Element/oxide	Fine Copelmi	Coarse Copelmi	Criciúma	Cambuí	World average
SiO_2	40.94	39.16	44.57	36.56	nd
Al_2O_3	17.26	18.07	18.06	10.31	nd
Fe_2O_3	7.2	6.54	7.4	7.87	nd
MnO	0.03	0.02	0.03	0.04	nd
TiO_2	0.69	0.72	0.84	0.57	nd
CaO	2.82	1.08	1.3	1.41	nd
MgO	0.45	0.39	0.55	0.91	nd
Na_2O	0.42	0.38	0.62	1.24	nd
K_2O	1.21	1.14	1.87	1.83	nd
SO_3	6.21	5.68	6.21	5.77	nd
P_2O_5	0.05	0.04	0.08	0.07	nd
LOI	20.76	27.86	17.82	33.14	nd
Total	98.04	101.08	99.35	99.72	nd
Li	55	96	112	40	12
Be	3	6	5	3	1.6
B	120	123	320	205	52
Sc	5	9	8	7	3.9
Ti	3573	4614	4543	4300	800
V	87	72	71	83	25
Cr	52	43	41	52	16
Mn	284	253	83	268	86
Co	9	8	8	11	5.1
Ni	21	18	15	23	13
Cu	26	26	20	26	16
Zn	908	721	74	239	23
Ga	6	14	14	13	5.8
Ge	6	6	2	2	2.2
As	365	55	21	38	8.3
Se	4	7	6	6	1.3
Rb	68	64	59	128	14
Sr	70	73	62	93	110
Y	30	64	39	22	8.4
Zr	203	166	133	124	36
Nb	79	120	94	131	3.7
Mo	22	6	4	5	2.2
Cd	4	1	<0.01	<0.01	0.22
Sn	3	6	5	5	1.1
Sb	3	2	3	2	0.92
Cs	4	16	19	21	1
Ba	377	3246	239	291	150
La	33	50	44	37	11
Ce	71	114	98	79	23
Pr	8	13	11	9	3.5
Nd	30	52	42	33	12
Sm	6	12	9	7	2
Eu	<0.01	2	1	0.47	
Gd	6	12	8	6	2.7
Tb	<0.01	2	1	0.32	
Dy	6	11	7	5	2.1
Ho	1	2	1	0.54	
Er	3	6	4	3	0.93
Tm	<0.01	<0.01	<0.01	<0.01	0.31
Yb	3	5	3	3	1
Lu	<0.01	<0.01	<0.01	<0.01	0.2
Hf	5	6	5	4	1.2
Ta	7	12	12	11	0.28
W	6	12	12	12	1.1
Tl	5	6	3	4	0.63
Pb	146	64	53	73	7.8
Bi	<0.01	<0.01	<0.01	<0.01	0.97
Th	11	17	16	16	3.3
U	62	7	6	5	2.4

Major-element oxides in wt.%; trace elements in mg/kg. LOI = loss on ignition at 1050 °C. nd = no data.

Ketris and Yudovich (2009). Partly because the materials contain quite high proportions of mineral matter, almost all element concentrations in the four samples studied are significantly higher than the average values for the world coals. Elements of environmental significance with concentrations over 10 times the world average values include Zn, As, Cd, and Pb. These are generally regarded as siderophile elements,

Table 4

Inorganic chemistry of samples studied (wt.%), expressed to an LOI-free basis.

	Fine Copelmi	Coarse Copelmi	Criciúma	Cambuí	Average ROM*
SiO ₂	52.98	53.48	54.67	54.91	57.32
Al ₂ O ₃	22.33	24.68	22.15	15.49	26.53
Fe ₂ O ₃	9.32	8.93	9.08	11.82	6.68
MnO	0.04	0.03	0.04	0.06	0.04
TiO ₂	0.89	0.98	1.03	0.86	1.22
CaO	3.65	1.48	1.59	2.12	1.98
MgO	0.58	0.53	0.67	1.37	1.02
Na ₂ O	0.54	0.52	0.76	1.86	0.88
K ₂ O	1.57	1.56	2.29	2.75	2.76
SO ₃	8.04	7.76	7.62	8.67	2.39
P ₂ O ₅	0.06	0.05	0.10	0.11	0.11
Total	100.00	100.00	100.00	100.00	100.93

Comparison to average ash of Santa Catarina ROM coals (*) from Oliveira et al. (2013) is also indicated.

and may be associated with the relatively high proportions of pyrite and pyrite oxidation products in the ROM and CCR materials.

5.3. Modes of trace hazardous element occurrence

Knowledge of the mode of occurrence of an element enables the prediction of its distribution in a coal deposit, and its possible behavior during coal preparation. The concentrations and modes of occurrence of elements in coal are influenced by a number of factors, such as depositional environment, nature of country rocks, hydrothermal fluids, volcanic ashes, and igneous intrusion effects (Dai et al., 2012, 2013; Goodarzi, 1995; Oliveira et al., 2013).

5.3.1. Antimony

In the present study, HR-TEM/EDS/SAED data indicate that Sb occurs in the pyrite and minor accessory sulfides and sulfates (e.g. marcasite, jarosite, and natrojarosite), sparsely dispersed through the organic matrix. Due to its low overall concentration in the CCR and ROM samples, Sb is unlikely to be of health or environmental concern. However, taking into account its high volatility and its preferential accumulation in Brazilian coal fly ash (Oliveira et al., 2012, 2013), the concentration and mobility of this element may still need to be monitored.

5.3.2. Arsenic

The occurrence of arsenic detected by HR-TEM/SAED/EDS in the coals of the present study is thought to be associated with sulfide minerals, specifically pyrite and marcasite, although a small proportion may also be organically associated. Similar observations have been previously reported by other authors (Finkelman, 1994; Goodarzi, 2002; Hower et al., 2008; Ketris and Yudovich, 2009).

5.3.3. Barium

Barium is an alkaline metal naturally present in some coals at relatively high concentrations (Finkelman, 1994; Ketris and Yudovich, 2009). Barium in the CCRs and ROM coal of the present study mostly occurs as barite, with an overall concentration below the limit of detection by XRD techniques. Both Sr and Ca were found as impurities in this mineral. FE-SEM/EDS analysis shows that the outer portion of the barite includes impurities such as Fe, P, S, Al, and Si, which may indicate the occurrence of several other phases as well. Some of the Ba was removed by acid water (see Table 5) during the leaching process. The concentration of free Ba in natural water is very low, because its dissolution is limited by equilibrium with barite (BaSO₄) and witherite (BaCO₃). Silva et al. (2011d) have documented an overall symmetrical behavior between Ba and SO₄²⁻, suggesting that the Ba content in sediment-water systems is controlled by equilibrium with BaSO₄.

5.3.4. Chromium

The concentrations of Cr in the samples of the present study (Table 5) are high when compared to the average values of the world coals (Ketris and Yudovich, 2009). Electron beam studies coupled with EDS indicate that the Cr in the Fine Copelmi, Coarse Copelmi and Cambuí samples has several associations (e.g. organic, siderite, illite, chlorite, and crocoite). Goodarzi (2002) also indicates that Cr is mostly associated with clay minerals and possibly with pyrite and carbonates in high-S coals.

5.3.5. Lead

In the ROM and CCR samples analyzed for the present study, Pb is generally associated with the mineral matter, primarily with sulfides and carbonates (e.g. pyrite, calcite and dolomite; see Table 5, Fig. 3D, E), including phases such as galena (PbS), clausthalite (PbSe), pyrite, siderite and secondary minerals (e.g. hematite, melanterite, and jarosite). Similar results have also been obtained in studies by Finkelman (1994), Goodarzi (2002), Ketris and Yudovich (2009), and Oliveira et al. (2012).

5.3.6. Manganese

Except for the Criciúma sample, Mn concentrations for the CCR and ROM samples of the present study (Table 3) are higher in comparison to the average values in world coals (Ketris and Yudovich, 2009). They are also slightly higher than for average values of Santa Catarina ROM coals (Silva et al., 2009; Oliveira et al., 2012), probably because of the higher overall mineral matter contents in the samples of the present study. Our interpretation for the high concentrations of Mn in the CCRs is that, during coal beneficiation, Mn-bearing minerals were removed from the raw coals and concentrated in the CCRs.

5.3.7. Nickel

Nickel is one of the more mobile and bioavailable heavy metal ions that may be present in Brazilian coals (Oliveira et al., 2012). Data from

Table 5

Concentrations (mg/L) of a number of elements released from the studied samples by leaching tests.

	Fine Copelmi	Coarse Copelmi	Criciúma	Cambuí
pH	7.94	3.82	3.84	7.88
Conductivity ($\mu\text{S}/\text{cm}$)	1910	3365	2895	1313
Al		91.185	107.5	
Ca	435.9	598.8	441.1	254.8
Fe		377.7	137.8	
K	4.4			9.3
Mg	22.3	28.8	103.1	17.2
Na	2.6			19.8
S	370.1	935.4	809.6	234.8
Si	1.0	1.8	2.5	1.4
Li	0.098	0.386	0.367	0.044
Be		0.065		0.024
B	0.109	0.022		
Sc		0.135	0.029	
Cr		0.020	0.013	
Mn	0.687	8.171	15.160	1.598
Co	0.058	0.598	0.746	0.114
Ni	0.096	0.720	1.168	0.145
Cu		0.064	0.385	0.000
Zn	0.003	3.044	56.001	0.004
As		0.003	0.013	
Se	0.013	0.018	0.013	0.006
Rb	0.030	0.005	0.001	0.021
Sr	1.415	2.757	0.427	2.465
Y		0.527	0.264	
Zr	0.003	0.0004	0.004	
Cd		0.004	0.289	
Cs	0.007	0.006		0.001
Ba	0.015	0.022	0.013	0.025
U	0.002	0.007	0.5	0.002

Blanks indicate values below detection limits.

the FE-SEM/EDS and HR-TEM/EDS/SAED analyses suggest that the Ni in the samples of the present study is associated with sulfides, such as millerite (NiS), and also with the organic matter.

5.3.8. Selenium

Analysis of the CCR and ROM samples by FE-SEM/EDS, and especially by HR-TEM/SAED/EDS, indicate that the Se in the materials is most commonly associated with pyrite. Previous studies, however, have suggested many other associations in coal, including selenides such as clausthalite (PbSe) (Dai et al., 2006), organic associations, other sulfides and selenides, and as ions absorbed on clay components (Finkelman, 1994, 1995; Hower and Robertson, 2003).

5.3.9. Transition metals

Iron is abundant in the mineral matter of the CCR and ROM samples (Table 2). Although XRD analysis shows that pyrite and its oxidation products are also abundant in the mineral matter of the samples studied, the total proportion of Fe₂O₃ indicated by those components accounts for less than half of the total Fe₂O₃ observed by direct chemical analysis of the respective ash residues. The electron beam studies also indicate that the Fe occurs mainly as Fe-sulfides (e.g. pyrite, marcasite), as well as in the sphalerite structure. Other Fe-bearing phases include carbonates (e.g. siderite, Fig. 3C), Fe-sulfates (e.g. jarosite and natrojarosite), Fe-oxides (e.g. magnesioferrite, hematite, magnetite, and maghemite), and Fe-Al silicate (e.g. illite and I/S clay minerals). Ankerite is also present, often containing traces of potentially hazardous (Mn, Pb, and Cd) elements in the mineral structure.

Titanium is detected in the samples by the electron beam studies, often in association with illite (Fig. 10A) and I/S. However, discrete particles of rutile (Fig. 10B) and anatase (Fig. 10C) are also present.

Vanadium has a dual association in coal, and may occur both with clay minerals and with the organic matter (Finkelman, 1995). Vanadium-bearing coals can be a significant environmental hazard because of the high toxicity of the metal. Although the V concentration in the all samples of the present study is higher than the average for world coals (Ketris and Yudovich, 2009), it is less than that found in some other coal deposits. For example, much higher V concentrations occur in the Dong mine, Heshan coalfield, Guangxi Province, China (0.14% on a whole coal basis and 0.5% in the ash; Zheng et al., 2005); the Zhijin deposit, Guizhou Province, China (0.06% on a whole coal basis and 0.2% in the ash; Dai et al., 2004b); and in the uppermost lithotype of the Western Kentucky No. 9 coal, Kentucky, USA (exceeding 1% on the ash basis; 11.67% ash; Hower et al., 2000).

The Zn concentration in all samples of the present study is significantly higher than the average for world coals (Table 3), especially in the two Copelmi CCR materials. Sphalerite is present in the Coarse Copelmi and Cambuí samples, and in one case is in sufficient concentration to be identified by XRD (Table 2). Zinc occurring as a minor component in pyrite, or alternatively in some of the clay minerals, may also be involved.

Zirconium is a relatively abundant trace element in Brazilian and other Gondwana coals (Oliveira et al., 2012; Ward et al., 1999), with concentrations ranging from 70 to almost 800 mg/kg (Oliveira et al., 2012, 2013). The Zr concentrations in the samples of the present study are significantly higher than world average values (Table 5), but are slightly less than the average values for ROM and clean coals from Santa Catarina indicated by Oliveira et al. (2013). The occurrence of Zr in Brazilian coals and coal by-products is usually ascribed to the presence of discrete zircon particles; however, as indicated by Oliveira et al. (2013), these may include small zircon crystals occurring in the micro-pores of some of the maceral components. Zircon has been identified by HR-TEM/STEM/MBD/SAED/EDS and FE-SEM/EDS techniques (Table 2) in all samples of the present study.

5.3.10. Rare-earth and radioactive elements

The rare earth elements (REEs) in coal may provide useful information on the source of the different mineral-matter components (e.g. Dai et al., 2012, 2013; Wang et al., 2005); some coals may also contain sufficient REE concentrations to represent potential economic sources of these valuable elements for industry (Seredin and Dai, 2012). The REEs in the CCR and ROM samples of the present study are mostly associated with clays and other detrital minerals (e.g. Figs. 8, 9), although the acidity of the coal-forming environment may also have had some influence on their concentration.

Humic and ulmic acids can strongly adsorb U and other metal ions, forming uranyl organic complexes in the environment (Ren et al., 2004). The presence and behavior of radioactive elements (e.g. Th) and P in CCRs have been a source of increasing concern in recent years, despite their low concentrations in most coals, because of their potential to cause contamination of natural systems. In the present study, the radioactive elements may occur in phosphate minerals such as monazite and xenotime (Table 2), although they may also have a possible affinity to kaolinite (Fig. 9) and neo-formed amorphous Al–Si–K–Mg–Na-phases. Oliveira et al. (2013) found an association between U and Zr.

5.3.11. Gold

Sulfur, apparently as S₀ and occurring with Au (Fig. 11), has been identified in some samples studied by FE-SEM and HR-TEM/SAED/EDS. The Au grains are associated with mixed-layer clay minerals and amorphous Al–Cr–Fe–Ni–O–S–Si-phases, and likely have a terrigenous/hydrothermal origin. Similar observations have been reported from other coals by Seredin and Dai (2014) and Yossifova (2014). The irregular S grains occur as transparent monoclinic crystals and are associated with euhedral pyrite.

5.4. Leaching of elements

As reported in previous work on Brazilian coal products (Oliveira et al., 2012), the element mobility from such materials depends very much on the pH that is developed in the leaching solution. Leaching tests carried out for the present study (Table 5) show that the Coarse Copelmi and the Criciuma samples have low pH values and the Fine Copelmi and Cambuí samples have high pH values when exposed to water under the EN 12457–2 conditions. The electrical conductivity (an indicator of total salinity, e.g. Fig. 12) and also the mobility of several elements, such as Al, Fe, K, Mn, Na, and Zn, are higher in the low-pH samples. The fact that Ba in the samples mostly occurs as (highly insoluble) barite crystals (e.g. Fig. 13, detected after the leaching procedure) probably accounts for the very low Ba leaching characteristics (extractable proportions <0.2%) observed in the study.

The low pH is probably due to the fact that the pyrite in the relevant samples had been oxidized, and that residual sulfuric acid or acidic products became active when water was added. Such oxidation is typically also indicated by the presence of jarosite and similar phases in the mineral matter of low-pH samples (Oliveira et al., 2012).

The XRD data in Table 2 show that the Fine Copelmi sample does not contain jarosite (or melanterite), but that the other three samples all have significant jarosite contents. The leaching test data on the Fine Copelmi sample (high pH; Table 5) are thus consistent with the presence of fresh, un-oxidized pyrite, together with abundant carbonate minerals (calcite, ankerite). The Coarse Copelmi and Criciuma samples (low-pH), by contrast, have relatively abundant jarosite, suggesting that the pyrite in those samples has been oxidized, either before sample collection or between collection and analysis.

In contrast, the data in Table 2 show that the Cambuí sample contained a similar proportion of jarosite to the Coarse Copelmi and Criciuma materials when subjected to XRD analysis. On the basis of its mineralogy it would thus have been expected to have a low pH, rather

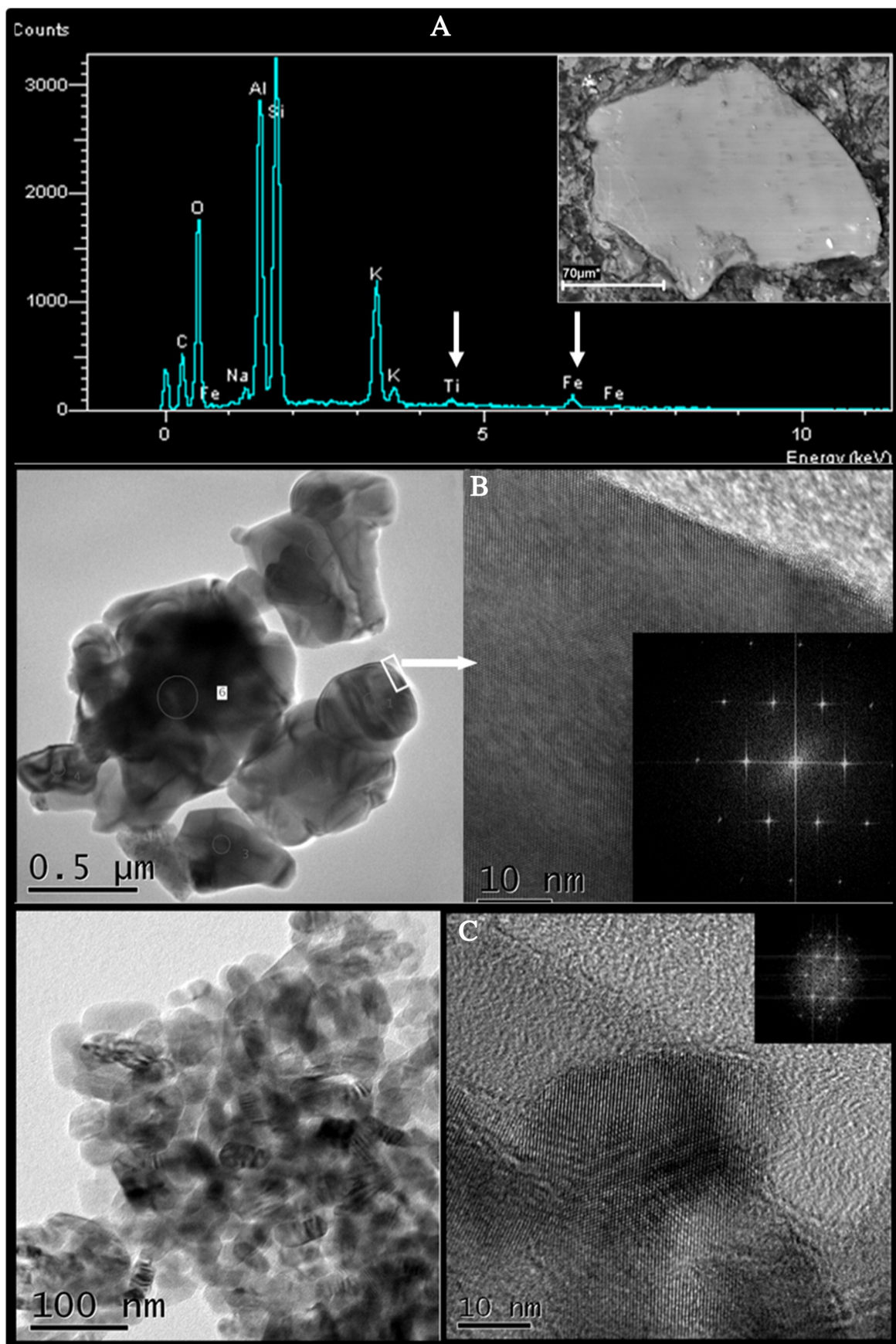


Fig. 10. SEM secondary electron images of (A) illite, together with EDS data showing presence of Ti and Fe; (B) Massive rutile and (C) anatase agglomerate, with crystalline detail from HR-TEM image after Fast Fourier transform in each case.

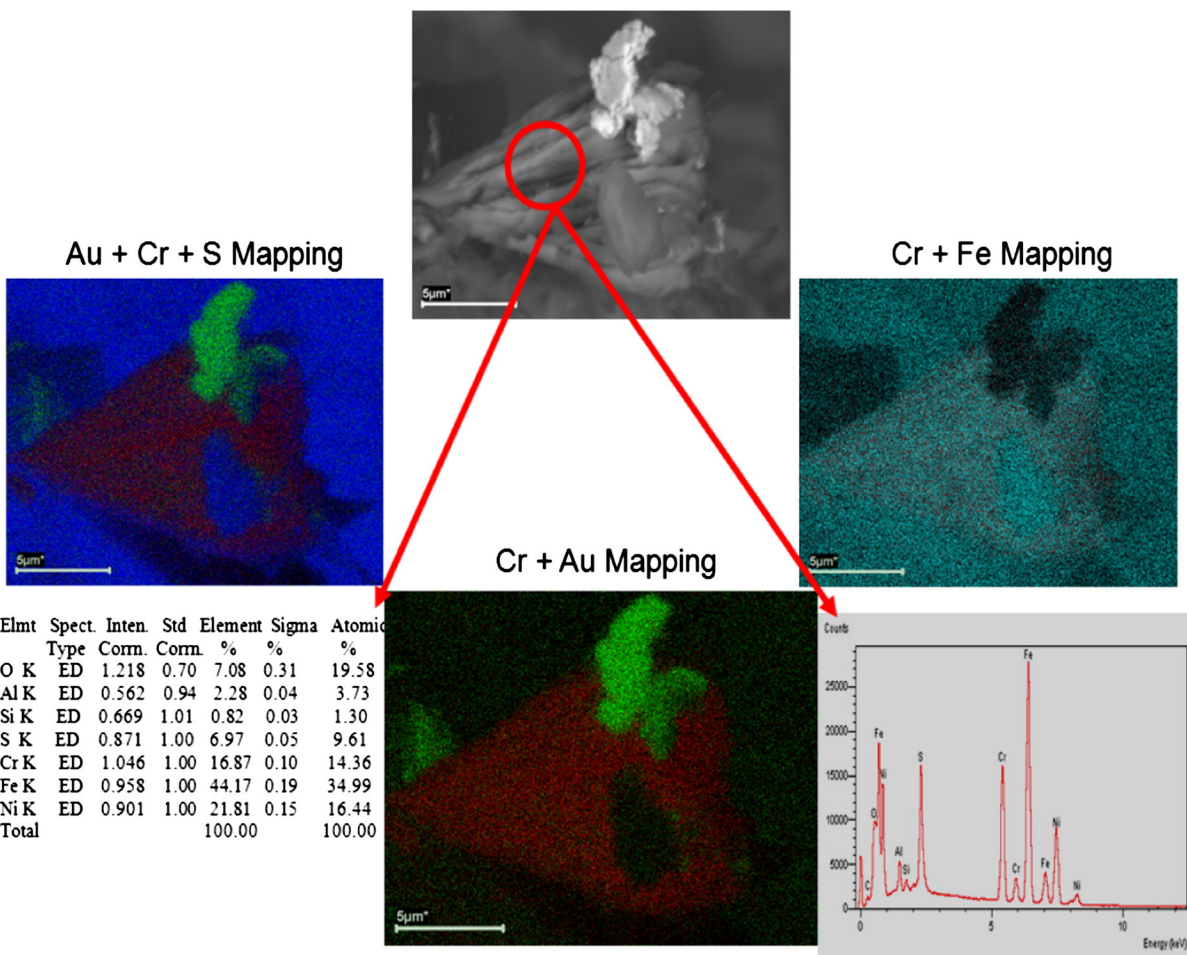


Fig. 11. SEM, secondary electron images of detrital Au grain associated with clay minerals (in this case Cambuí sample). FFT data confirm the mineral identity. The gold grains contain Ni and are associated with clay minerals containing Cr, amorphous sulfides, and quartz grains.

than a high pH (Table 5), in the leaching tests. The reasons for this inconsistency are still under investigation, but may reflect oxidation of the sample during storage, after leaching but before the XRD study was carried out.

6. Conclusions

The CCR and ROM samples studied are all relatively rich in mineral matter, with the major minerals being quartz, kaolinite, illite, I/S and pyrite, plus minor phases that include jarosite, melanerite, gypsum, calcite, and ankerite. Small amounts of a much wider range of minerals, including hematite, barite, sphalerite and siderite, can also be identified by SEM, TEM and Raman techniques.

Pyrite is relatively abundant in most samples, making up up to 5% of the mineral matter. The principal sulfate minerals, jarosite, melanerite, probably represent oxidation products of pyrite, formed due to exposure of the material, while the gypsum represents a product of reaction between pyrite-derived acids and calcite or ankerite in the relevant materials. Because the sulfates would probably have been washed away from the materials during the coal-cleaning processes, the necessary exposure for the CCRs probably occurred after the coals were passed through the relevant preparation plant.

Trace element concentrations in the studied samples are significantly higher than the average values for world coals. This probably reflects the greater abundance of mineral matter in the materials, and suggests that most of the elements involved have a mineral rather than an organic affinity. Some components traditionally regarded as

siderophile elements, such as As, Cd, Pb, and Zn, are particularly abundant in relation to world averages, and are probably associated with the pyrite and its oxidation products. Mobilization of these elements as the pyrite (and other sulfides) breaks down during storage may represent a source of adverse environmental impact around such CCR emplacement sites.

In general the trace metals with the greatest concentrations expected in leachates from the CCRs are Zn, Cu, Mn, Co, Ni, and Cd. Metal dissolution is enhanced under the acidic conditions associated with pyrite oxidation. In these low-pH samples, the water extractable fractions of some metals increased by up to 80%, and the overall level of leaching was higher. Milder leaching conditions associated with near-neutral pH conditions and less-oxidized samples produce substantially less metal leaching. Most environmentally relevant elements were highly immobile, which could be linked to coprecipitation and/or adsorption on to Fe and Mn oxyhydroxides. These observations underline the critical influence of the mode of occurrence and the pH on metal mobility in the CCR materials.

Acknowledgments

The authors acknowledge the logistical support from the coal mining companies (access to samples). The authors thank the CNPq, FAPERGS, UNILASALLE, and the Electron Microscopy Center of the Federal University of Rio Grande do Sul for the analyses. Editor Shifeng Dai and the anonymous referees are thanked for their constructive comments on the manuscript.

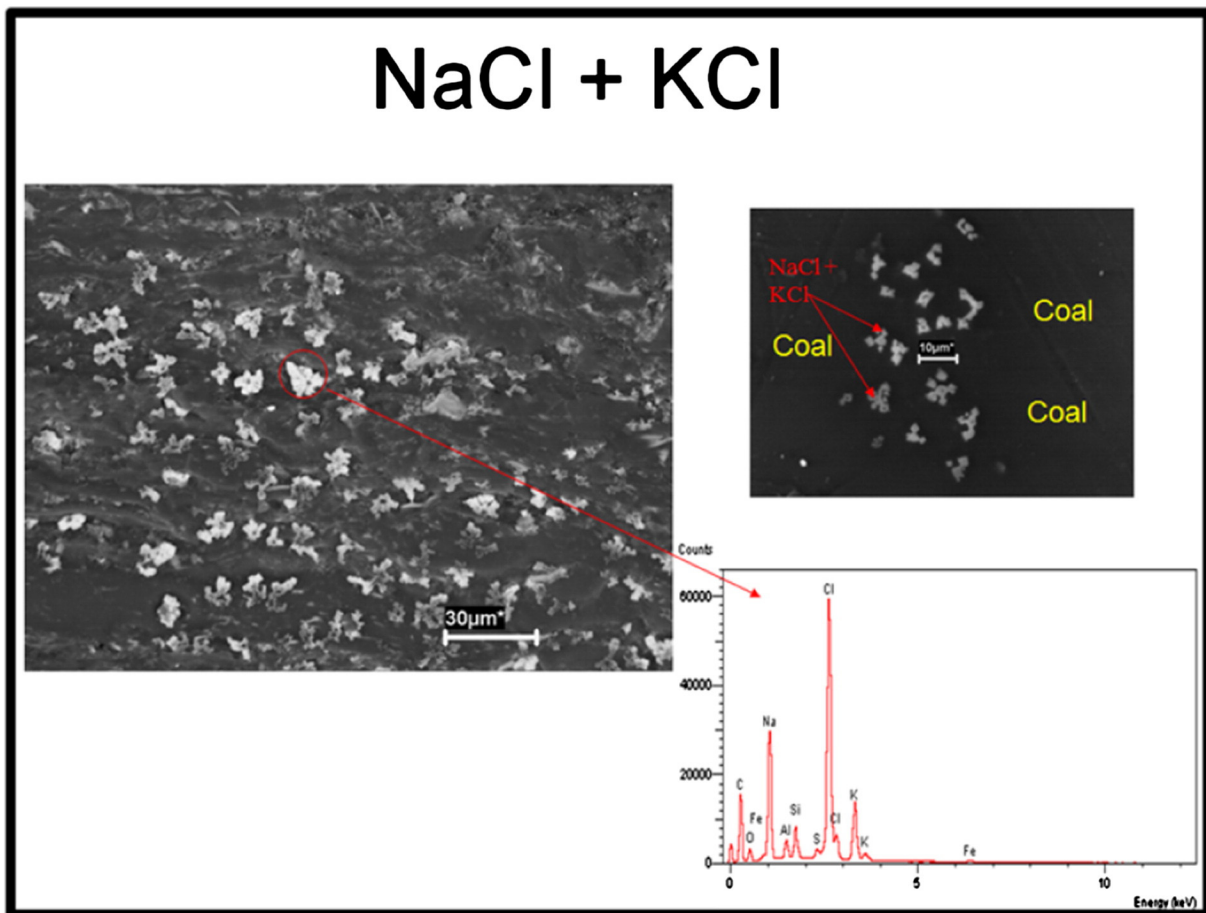


Fig. 12. SEM secondary electron images of typical salts identified in the CCR and ROM samples (Fine Copelmi, Coarse Copelmi, and Cambuí samples).

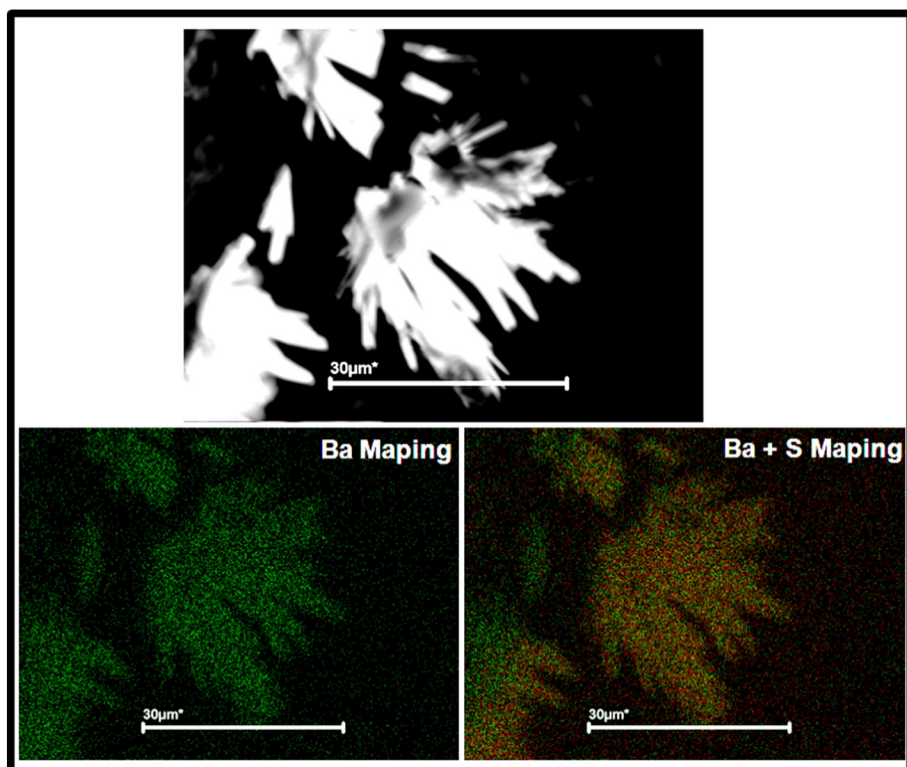


Fig. 13. SEM secondary electron images of typical barite (showing Ba and S mapping) associated with the organic matter after leaching procedure (Coarse Copelmi sample).

References

- Al, T.A., Blowes, D.W., Martin, C.J., Cabri, L.J., Jambor, J.L., 1997. Aqueous geochemistry and analysis of pyrite surfaces in sulfide-rich mine tailings. *Geochim. Cosmochim. Acta* 61, 2353–2366.
- American Society for Testing, Materials (ASTM), 1991. Standard Practice for Preparing Coal Samples for Microscopical Analysis by Reflected Light. ASTM Standard D 2797–91. American Society for Testing and Materials, West Conshohocken, PA, (3 pp.).
- American Society for Testing, Materials (ASTM), 1996. Standard Test Methods for Collection of a Gross Sample of Coal. ASTM Standard D2234-89. American Society for Testing and Materials, West Conshohocken, PA, (10 pp.).
- Chou, C.-L., 2012. Sulphur in coals: a review of geochemistry and origins. *Int. J. Coal Geol.* 100, 1–13.
- Cravotta III, C.A., 2008. Dissolved metals and associated constituents in abandoned coal-mine discharges, Pennsylvania, USA. Part 1: constituent quantities and correlations. *Appl. Geochem.* 23, 166–202.
- Dai, S., Ren, D., Ma, S., 2004a. The cause of endemic fluorosis in western Guizhou Province, Southwest China. *Fuel* 83, 2095–2098.
- Dai, S., Li, D., Ren, D., Tang, Y., Shao, L., Song, H., 2004b. Geochemistry of the late Permian No. 30 coal seam, Zijin Coalfield of Southwest China: influence of a siliceous low-temperature hydrothermal fluid. *Appl. Geochem.* 19, 1315–1330.
- Dai, S., Ren, D., Tang, Y., Yue, M., Hao, L., 2005. Concentration and distribution of elements in Late Permian coals from western Guizhou Province, China. *Int. J. Coal Geol.* 61, 119–137.
- Dai, S., Ren, D., Chou, C.-L., Li, S., Jiang, Y., 2006. Mineralogy and geochemistry of the No. 6 coal (Pennsylvanian) in the Jungar Coalfield, Ordos Basin, China. *Int. J. Coal Geol.* 66, 253–270.
- Dai, S., Li, D., Chou, C.-L., Zhao, L., Zhang, Y., Ren, D., Ma, Y., Sun, Y., 2008a. Mineralogy and geochemistry of boehmite-rich coals: new insights from the Haerwusu Surface Mine, Jungar Coalfield, Inner Mongolia, China. *Int. J. Coal Geol.* 74, 185–202.
- Dai, S., Ren, D., Zhou, Y., Chou, C.-L., Wang, X., Zhao, L., Zhu, X., 2008b. Mineralogy and geochemistry of a superhigh-organic-sulfur coal, Yanshan Coalfield, Yunnan, China: evidence for a volcanic ash component and influence by submarine exhalation. *Chem. Geol.* 255, 182–194.
- Dai, S., Ren, D., Chou, C.-L., Finkelman, R.B., Seredin, V.V., Zhou, Y., 2012. Geochemistry of trace elements in Chinese coals: a review of abundances, genetic types, impacts on human health, and industrial utilization. *Int. J. Coal Geol.* 94, 3–21.
- Dai, S., Zhang, W., Ward, C.R., Seredin, V.V., Hower, J.C., Li, X., Song, W., Wang, X., Kang, H., Zheng, L., Wang, P., Zhou, D., 2013. Mineralogical and geochemical anomalies of late Permian coals from the Fusui Coalfield, Guangxi Province, southern China: influences of terrigenous materials and hydrothermal fluids. *Int. J. Coal Geol.* 105, 60–84.
- Depoi, F.S., Pozebon, D., Kalkreuth, W., 2008. Chemical characterization of feed coals and combustion-by-products from Brazilian power plants. *Int. J. Coal Geol.* 76, 227–236.
- European Committee for Standardisation, 2002. Characterisation of Waste—Leaching—Compliance Test for Leaching of Granular Waste Materials and Sludges—Part 2: One Stage Batch Test at a Liquid to Solid Ratio of 10 L/kg for Materials With Particle Size Below 4 mm, (EN 12457-2).
- Fawcett, A., Abou-Zaid, M., Menzies, J.G., Belanger, R.R., 1998. Silicon-mediated accumulation of flavonoid phytoalexins in cucumber. *Phytopathology* 88, 396–401.
- Finkelman, R.B., 1993. Trace and Minor Elements in Coal. In: Macko, S.A. (Ed.), Engel, M. H. *Organic Geochemistry*, New York, pp. 593–607.
- Finkelman, R.B., 1994. Modes of occurrence of potentially hazardous elements in coal: levels of confidence. *Fuel Process. Technol.* 39, 21–34.
- Finkelman, R.B., 1995. Modes of occurrence of environmentally sensitive trace elements in coal. In: Swaine, D.J., Goodarzi, F. (Eds.), *Environmental Aspects of Trace Elements in Coal*. Kluwer, Dordrecht, pp. 24–50 (Chap. 3).
- Finkelman, R.B., Orem, W., Castranova, V., Tat, C.A., Belkin, H.E., Zheng, B., Lerch, H.E., Maharaj, S.V., Bates, A.L., 2002. Health impacts of coal and coal use: possible solutions. *Int. J. Coal Geol.* 50, 425–443.
- Gasharova, B., 2000. Jarosite $\text{AFe}_3(\text{SO}_4)_2(\text{OH})_6$: Kristallchemische Charakterisierung und aquatische Reaktionen. (PhD Thesis) Univ. Heidelberg, Germany..
- Gasharova, B., Göttlicher, J., Becker, U., 2005. Dissolution at the surface of jarosite: an in situ AFM study. *Chem. Geol.* 215, 499–516.
- Goodarzi, F., 1995. Geology of trace elements in coal. In: Swaine, D.J., Goodarzi, F. (Eds.), *Environmental Aspects of Trace Elements in Coal*. Kluwer Academic Publishers, Dordrecht, Netherlands.
- Goodarzi, F., 2002. Mineralogy, elemental composition and modes of occurrence of elements in Canadian feed-coals. *Fuel* 81, 1199–1213.
- Göttlicher, J., Gasharova, B., 2000. Interactions of iron and sulfur bearing solid phases with water in surface coal mining pits and acidic mining lakes. In: Rammlmaier, D., Mederer, J., Oberthür, Th., Heiman, R.B., Pentinghaus, H. (Eds.), *Applied Mineralogy in Research, Economy Technology, Ecology and Culture*, vol. 2. Balkema, Rotterdam, pp. 557–560.
- Hower, J.C., Robertson, J.D., 2003. Clausthalite in coal. *Int. J. Coal Geol.* 53, 219–225.
- Hower, J.C., Rathbone, R.F., Robertson, J.D., Peterson, G., Trimble, A.S., 1999. Petrology, mineralogy, and chemistry of magnetically-separated sized fly ash. *Fuel* 78, 197–203.
- Hower, J.C., Greb, S.F., Cobb, J.C., Williams, D.A., 2000. Discussion on origin of vanadium in coals: parts of the Western Kentucky (USA) No. 9 coal rich in vanadium: Special Publication No. 125, 1997, 273–286. *J. Geol. Soc.* 157, 1257–1259.
- Hower, J.C., Suárez-Ruiz, I., Mastalerz, M., 2005. An approach toward a combined scheme for the petrographic classification of fly ash: revision and clarification. *Energy and Fuels* 19, 653–655.
- Hower, J.C., Campbell, J.L., Teesdale, W.J., Nejedly, Z., Robertson, J.D., 2008. Scanning proton microprobe analysis of mercury and other trace elements in Fe-sulfides from a Kentucky coal. *Int. J. Coal Geol.* 75, 88–92.
- Huggins, F.E., Seidu, L.B.A., Shah, N., Backus, J., Huffman, G.P., Honaker, R.Q., 2012. Mobility of elements in long-term leaching tests on Illinois #6 coal rejects. *Int. J. Coal Geol.* 94, 326–336.
- Kalkreuth, W., Holz, M., Kern, M., Machado, G., Mexias, A., Silva, M., Willett, J., Finkelman, R., Burger, H., 2006. Petrology and chemistry of Permian coals from the Paraná Basin: 1. Santa Terezinha, Léo-Butiá and Candiota Coalfields, Rio Grande do Sul, Brazil. *Int. J. Coal Geol.* 68, 79–116.
- Kalkreuth, W., Holz, M., Mexias, A., Balbinot, M., Levandowski, J., Willett, J., Finkelman, R., Burger, H., 2010. Depositional setting, petrology and geochemistry of Permian coals from the Paraná Basin: 2. South Santa Catarina Coalfield, Brazil. *Int. J. Coal Geol.* 84, 213–236.
- Ketris, M.P., Yudovich, Y.E., 2009. Estimations of Clarkes for carbonaceous biolithes: world average for trace element contents in black shales and coals. *Int. J. Coal Geol.* 78, 135–148.
- Levandowski, J.H., Kalkreuth, W., 2009. Chemical and petrographical characterization of feed coal, fly ash and bottom ash from the Figueira Power Plant, Paraná, Brazil. *Int. J. Coal Geol.* 77, 269–281.
- Li, X., Dai, S., Zhang, W., Li, T., Zheng, X., Chen, W., 2014. Determination of As and Se in coal and coal combustion products using closed vessel microwave digestion and collision/reaction cell technology (CCT) of inductively coupled plasma mass spectrometry (ICP-MS). *Int. J. Coal Geol.* 124, 1–4.
- Ma, J.F., 2004. Role of silicon in enhancing the resistance of plants to biotic and abiotic stresses. *Soil Science and Plant Nutrition* 50, 11–18.
- Marcello, R.R., Galatob, S., Petersona, M., Riellac, H.G., Bernardin, A.M., 2008. Inorganic pigments made from the recycling of coal mine drainage treatment sludge. *J. Environ. Manag.* 88, 1280–1284.
- Matjie, R.H., Li, Z., Ward, C.R., French, D., 2008. Chemical composition of glass and crystalline phases in coarse gasification ash. *Fuel* 87, 857–869.
- Norrish, K., Hutton, J.T., 1969. An accurate X-ray spectrographic method for the analysis of a wide range of geological samples. *Geochim. Cosmochim. Acta* 33, 431–453.
- Oliveira, M.L.S., Ward, C.R., French, D., Hower, J.C., Querol, X., Silva, L.F.O., 2012. Mineralogy and leaching characteristics of beneficiated coal products from Santa Catarina, Brazil. *Int. J. Coal Geol.* 94, 314–325.
- Oliveira, M.L.S., Ward, C.R., Sampaio, C.H., Querol, X., Cetroneo, C.M.N.L., Taffarel, S.R., Silva, L.F.O., 2013. Partitioning of mineralogical and inorganic geochemical components of coals from Santa Catarina, Brazil, by industrial beneficiation processes. *Int. J. Coal Geol.* 116, 75–92.
- Oliveira, M.L.S., Marostega, F., Taffarel, S.R., Saikia, B.K., Waanders, F.B., DaBoit, K., Baruah, B.P., Silva, L.F.O., 2014. Nano-mineralogical investigation of coal and fly ashes from coal-based captive power plant (India): an introduction of occupational health hazards. *Sci. Total Environ.* 468–469, 1128–1137.
- Paytan, A., Mearon, S., Cobb, K., Kastner, M., 2002. Origin of marine barite deposits: Sr and S isotope characterization. *Geology* 30, 747–750.
- Querol, X., Whateley, M.K.G., Fernandez-Turiel, J.L., Tuncali, E., 1997. Geological controls on the mineralogy and geochemistry of the Beypazari lignite, central Anatolia, Turkey. *Int. J. Coal Geol.* 33, 255–271.
- Querol, X., Izquierdo, M., Monfort, E., Alvarez, E., Font, O., Moreno, T., Alastuey, A., Zhuang, X., Lud, W., Wang, Y., 2008. Environmental characterization of burnt coal gangue banks at Yangquan, Shanxi Province, China. *Int. J. Coal Geol.* 75, 93–104.
- Quispes, D., Pérez-López, R., Silva, L.F.O., Nieto, J.M., 2012. Changes in mobility of hazardous elements during coal combustion in Santa Catarina power plant (Brazil). *Fuel* 94, 495–503.
- Rao, C.P., Gluskoter, H.J., 1973. Occurrence and distribution of minerals in Illinois coals. *Illinois State Geological Survey Circular* 476 (56 pp.).
- Ren, D., Xu, D., Zhao, F., 2004. A preliminary study on the enrichment mechanism and occurrence of hazardous trace elements in the tertiary lignite from the Shenbei coal-field, China. *Int. J. Coal Geol.* 57, 187–196.
- Ribeiro, J., DaBoit, K., Flores, D., Kornbauer, M.A., Silva, L.F.O., 2013a. Extensive FE-SEM/EDS, HR-TEM/EDS and ToF-SIMS studies of micron- to nano-particles in anthracite fly ash. *Sci. Total Environ.* 452–453, 98–107.
- Ribeiro, J., Taffarel, S.R., Sampaio, C.H., Flores, D., Silva, L.F.O., 2013b. Mineral speciation and fate of some hazardous contaminants in coal waste pile from anthracite mining in Portugal. *Int. J. Coal Geol.* 109–110, 15–23.
- Rimstidt, J.D., Vaughan, D.J., 2003. Pyrite oxidation: a state-of-the-art assessment of the reaction mechanism. *Geochim. Cosmochim. Acta* 67, 873–880.
- Sasaki, K., 1997. Raman study of the microbially mediated dissolution of pyrite by *Thiobacillus ferrooxidans*. *Can. Mineral.* 35, 999–1008.
- Schaller, J., Brackhage, C., Gessner, M.O., Bäuker, E., Gert Dudel, E., 2012. Silicon supply modifies C:N:P stoichiometry and growth of *Phragmites australis*. *Plant Biol.* 14, 392–396.
- Seredin, V.V., Dai, S., 2012. Coal deposits as potential alternative sources for lanthanides and yttrium. *Int. J. Coal Geol.* 94, 67–93.
- Seredin, V.V., Dai, S., 2014. The occurrence of gold in fly ash derived from high-Ge coal. *Mineral. Deposita* 49, 1–6.
- Silva, L.F.O., Oliveira, M.L.S., da Boit, K.M., Finkelman, R.B., 2009. Characterization of Santa Catarina (Brazil) coal with respect to Human Health and Environmental Concerns. *Environ. Geochem. Health* 31, 475–485.
- Silva, L.F.O., Ward, C.R., Hower, J.C., Izquierdo, M., Waanders, F., Oliveira, M.L.O., Li, Z., Hatch, R.S., Querol, X., 2010. Mineralogy and leaching characteristics of coal ash from a major Brazilian power plant. *Coal Combustion and Gasification Products* 2, 51–65.
- Silva, L.F.O., Wollenschlager, M., Oliveira, M.L.S., 2011a. A preliminary study of coal mining drainage and environmental health in the Santa Catarina region, Brazil. *Environ. Geochem. Health* 33, 55–65.
- Silva, L.F.O., Oliveira, M.L.S., Neace, E.R., O'Keefe, J.M.K., Henke, K.R., Hower, J.C., 2011b. Nanominerals and ultrafine particles in sublimates from the Ruth Mullins coal fire, Perry County, Eastern Kentucky, USA. *Int. J. Coal Geol.* 85, 237–245.
- Silva, L.F.O., Macias, F., Oliveira, M.L.S., da Boit, K.M., Waanders, F., 2011c. Coal cleaning residues and fe-minerals implications. *Environ. Monit. Assess.* 172, 367–378.

- Silva, L.F., Izquierdo, M., Querol, X., Finkelman, R.B., Oliveira, M.L.S., Wollenschlager, M., Towler, M., Pérez-López, R., Macias, F., 2011d. Leaching of potential hazardous elements of coal cleaning rejects. *Environ. Monit. Assess.* 175, 109–126.
- Silva, L.F.O., Querol, X., da Boit, K.M., Fdez-Ortiz de, S., Vallejuelo, Madariaga, J.M., 2011e. Brazilian coal mining residues and sulphide oxidation by Fenton's reaction: an accelerated weathering procedure to evaluate possible environmental impact. *J. Hazard. Mater.* 186, 516–525.
- Stoffregen, R.E., Alpers, C.N., Jambor, J.L., 2000. Alunite–jarosite crystallography, thermodynamics, and geochronology. *Rev. Mineral.* 40, 453–479.
- Suárez-Ruiz, I., Ward, C.R., 2008. Basic factors controlling coal quality and technological behavior of coal. In: Suárez-Ruiz, I., Crelling, J.C. (Eds.), *Applied Coal Petrology*. Academic Press, Burlington, MA, pp. 19–59.
- Taylor, J.C., 1991. Computer programs for standardless quantitative analysis of minerals using the full powder diffraction profile. *Powder Diffract.* 6, 2–9.
- Tian, L., Dai, S., Wang, J., Huang, Y., Ho, S.C., Zhou, Y., Lucas, D., Koshland, C.P., 2008. Nanoquartz in Late Permian C1 coal and the high incidence of female lung cancer in the Pearl River Origin area: a retrospective cohort study. *BMC Public Health* 8, 398.
- Wang, W., Qin, Y., Song, D., Sang, S., Jiang, B., Zhu, Y., Fu, X., 2005. Element geochemistry and cleaning potential of the No. 11 coal seam from Antaibao mining district. *Science in China Ser D Earth Sciences* 48, 2142–2154.
- Wang, W., Qin, Y., Sang, S., Jiang, B., Zhu, Y., Guo, Y., 2007. Sulfur variability and element geochemistry of the No. 11 coal seam from the Antaibao mining district, China. *Fuel* 86, 777–784.
- Wang, W., Qin, Y., Sang, S., Zhu, Y., Wang, C., Weiss, D.J., 2008. Geochemistry of rare earth elements in a marine influenced coal and its organic solvent extracts from the Antaibao mining district, Shanxi, China. *Int. J. Coal Geol.* 76, 309–317.
- Ward, C.R., 2002. Analysis and significance of mineral matter in coal seams. *Int. J. Coal Geol.* 50, 135–168.
- Ward, C.R., Spears, D.A., Booth, C.A., Staton, I., Gurba, L.W., 1999. Mineral matter and trace elements in coals of the Gunnedah Basin, New South Wales, Australia. *Int. J. Coal Geol.* 40, 281–308.
- Welch, S.A., Christy, A.G., Kirste, D., Beavis, S.G., Beavis, F., 2007. Jarosite dissolution I – trace cation flux in acid sulphate soils. *Chem. Geol.* 245, 183–197.
- Wiese, R., Fyfe, W., 1986. Occurrences of iron sulfides in Ohio coals. *Int. J. Coal Geol.* 6, 251–276.
- Yossifova, M.G., 2014. Petrology, mineralogy and geochemistry of Balkan coals and their waste products. *Int. J. Coal Geol.* 122, 1–20.
- Yossifova, M.G., Valceva, D., Nikolova, S., 2011. Exogenic microbiological activity in coals. *Fuel Process. Technol.* 92, 825–835.
- Zheng, Z.M., Jiang, G.F., Liu, J.W., 2005. Six new species of Tetrigoidae (Orthoptera) from Guangxi, P. R. China. *Orient. Insects* 39, 175–185.

CAPITULO III

CONSIDERAÇÕES
FINAIS.

Diante do exposto nessa dissertação pode-se concluir que:

As amostras estudadas são relativamente concentradas em minerais, sendo os mais abundantes: quartzo, caulinita, ilita, Ilita/Smectica e pirita. Minerais menos abundantes, porém de grande importância ambiental, também puderam ser identificados, incluindo: jarosita, melanterite, gesso, calcite, ankerita, hematita, barita, esfalerita e siderita.

A pirita é relativamente abundante na maioria das amostras, sendo detectada em até 5% do total da matéria mineral, gerando produtos secundários de sua oxidação como jarosita, melanterite, formados devido à exposição do material, enquanto que o gesso representa um produto de reacção entre o ácido derivado de pirita reacionando com minerais carbonatados como calcita e ankerita.

Quanto as concentrações dos elementos-traço nas amostras estudadas, estas são significativamente mais elevadas do que os valores médios reportados por diversos autores para carvões globais. Isto provavelmente é resultado da abundância de matéria mineral nos materiais estudados.

Alguns componentes tradicionalmente considerados como elementos siderófilos, tais como o As, Cd, Pb e Zn, são particularmente abundantes em relação à média mundial e provavelmente estão associados com a pirita e seus produtos de oxidação. A mobilização destes elementos pode representar uma fonte de impacto ambiental negativo em torno das áreas de amazanamento dos resíduos do beneficiamento.

Em geral, os elementos-traço com as maiores concentrações nos lixiviados foram Zn, Cu, Mn, Co, Ni e Cd. A dissolução dos elementos químicos foi maior em condições ácidas, associadas à oxidação da pirita. Nas amostras com valores baixos de pH, as frações lixiviadas de alguns elementos representaram até 80% do total contido nas amostras. Alguns elementos de alto grau de toxicidade foram altamente imóveis, isso pode ser facilmente justificado por MEV/EDS dado que tais elementos estiveram presentes nas amostras associados via co-precipitação e/ou adsorção sobre oxihidróxidos de Al, Fe e de Mn. Tal observação demonstra a de se entender o modo de ocorrência e do pH sobre a mobilidade dos elementos constituintes das amostras.

Alguns elementos, como Ge, Li, e, possivelmente, Zr, têm maiores concentrações médias nos resíduos do beneficiamento do que no ROM estudado, sugerindo uma associação, pelo menos em parte, com a matéria orgânica especialmente com os componentes macerais.

Diante dos resultados obtidos no presente estudo, pode-se traçar como metas para posteriores estudos:

- 1- O desenvolvimento de novas técnicas de beneficiamento como ultra-som e diferentes dispersantes;
- 2- Novas metodologias de deposição dos resíduos mesclado com tecnosolos de acordo com suas propriedades geoquímicas e não apenas aterrando e compactado argilas de baixa permeabilidade;
- 3- Conscientização da população para não residir cerca das áreas de depósitos de resíduos do beneficiamento;
- 4- Desenvolver metodologias que visem avaliar o grau de toxicidade dos diferentes matérias que foram identificados na presente dissertação.

ANEXO A

TRABALHO NA FORMA DE
ARTIGO CIENTÍFICO
PUBLICADO COMO
CO-AUTOR.



Partitioning of mineralogical and inorganic geochemical components of coals from Santa Catarina, Brazil, by industrial beneficiation processes

Marcos L.S. Oliveira ^a, Colin R. Ward ^{b,*}, Carlos H. Sampaio ^c, Xavier Querol ^d, César M.N.L. Cutruneo ^e, Silvio R. Taffarel ^e, Luis F.O. Silva ^{a,e}

^a Environmental Science and Nanotechnology Department, Catarinense Institute of Environmental Research and Human Development – IPADHC, Capivari de Baixo, Santa Catarina, Brazil

^b School of Biological, Earth and Environmental Sciences, University of New South Wales, Sydney, NSW 2052, Australia

^c Universidade Federal do Rio Grande do Sul, Escola de Engenharia, Departamento de Metalurgia, Centro de Tecnologia, Av. Bento Gonçalves, 9500, Bairro Agronomia, CEP: 91501-970, Porto Alegre, RS, Brazil

^d Institute of Environmental Assessment and Water Research (IDAEA-CSIC) C/Lluís Solé y Sabaris s/n, 08028 Barcelona, Spain

^e Laboratory of Environmental Researches and Nanotechnology Development, Centro Universitário La Salle, Mestrado em Avaliação de Impactos Ambientais em Mineração, Victor Barreto, 2288 Centro, 92010-000 Canoas, RS, Brazil



CrossMark

ARTICLE INFO

Article history:

Received 3 April 2013

Received in revised form 6 July 2013

Accepted 6 July 2013

Available online 16 July 2013

Keywords:

Mineral matter

X-ray diffraction

Coal preparation

Pyrite

Trace element

ABSTRACT

Comparative studies of the mineral matter and trace elements in 12 pairs of run-of-mine (ROM) and clean-coal products from beneficiation plants in Santa Catarina, southern Brazil, have been carried out using low-temperature oxygen-plasma ashing, X-ray diffraction and chemical analysis techniques with the aim of evaluating the effect of coal preparation on the mineralogy and chemical composition of the final coal products. The results show that substantial reductions in mineral matter and ash percentages are associated with beneficiation of coals mined from the different deposits. These reductions are accompanied by changes in the percentages of Fe₂O₃ in the respective coal ashes, due to the reduction in the proportion of pyrite in the mineral matter, and also by a reduction in the percentage of Na₂O, possibly due to ion exchange within the clay minerals. The relative proportions of quartz, clay minerals, and minor phases such as calcite and feldspar (mainly albite) within the mineral matter are not, however, significantly changed by the beneficiation processes. The concentrations of most trace elements in the beneficiation products are similar to the respective concentrations in the relevant ROM materials, or are reduced to an extent similar to that of the total mineral matter percentage for the respective coal samples. This suggests an association mainly with the clay-rich mineral matter. The concentrations of As and Pb, however, are reduced to a greater extent for most samples by the beneficiation processes, consistent with a pyrite association. Concentrations of Ge, U and Zr are higher in many of the clean coals than in the respective run-of-mine materials, suggesting the possibility of preferential association, at least for some deposits, with the organic-rich fractions of the coals concerned.

© 2013 Elsevier B.V. All rights reserved.

1. Introduction

The principal coal deposits mined in Brazil are of Early Permian age, and distributed in a lenticular belt across the SE part of the country that extends from the state of Paraná in the north to the state of Rio Grande do Sul in the south (Kalkreuth et al., 2004; Thomas, 2002). Brazil's total coal resources are in the order of 32×10^9 tonnes (Kalkreuth et al., 2006), the majority of which (89%) are located in Rio Grande do Sul. Most of the remainder (a little over 10%) are located in the adjoining state of Santa Catarina (Fig. 1), and small amounts are located in Paraná and the adjacent state of São Paulo.

These resources occur within the Paraná Basin, a large intracratonic basin located in the central-eastern part of the South American Platform

(Holz et al., 1999; Kalkreuth et al., 2006), covering a total area of around 1.7×10^6 km². The sedimentary fill of the basin ranges from Ordovician-Silurian to Late Cretaceous in age, and has been divided by Milani et al. (1994) into six second-order depositional sequences. The coal-bearing interval is located within the Early Permian (Artinskian/Kungurian) Rio Bonito Formation, a fluvial to marine unit (Holz et al., 1999; Kalkreuth et al., 2006) located near the base of the third sequence, which itself is Carboniferous to Early Triassic in age. This interval is 2800 m thick at its depocentre, and represents the thickest sedimentary succession in the basin.

Petrographic and sequence stratigraphy studies (Holz et al., 1999; Kalkreuth et al., 2006) indicate that the coal seams, at least in the southern part of the basin, were formed in limno-telmatic mires, with plant material building up to produce inertinite-rich coals in back-barrier depositional settings. The peats from which the coals originated were formed in small lagoons (Kleppig, 2001), with vegetation growing and being transported inside the lagoons, and deposited along with clay-

* Corresponding author. Tel.: +61 2 9385 8718; fax: +61 2 9385 1558.

E-mail addresses: c.ward@unsw.edu.au (C.R. Ward), felipeqma@hotmail.com (L.F.O. Silva).

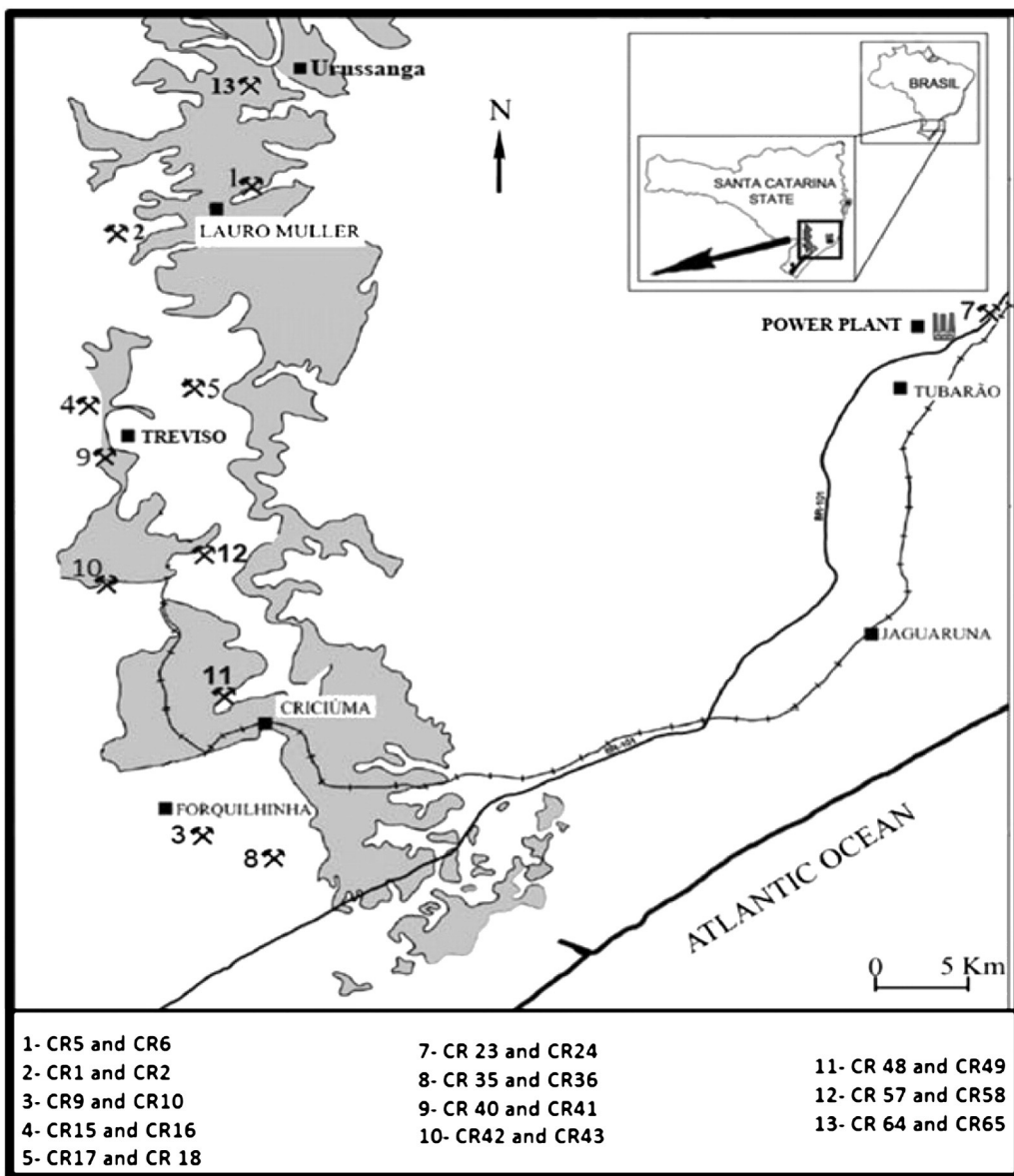


Fig. 1. Location of sample sources, and also of Jorge Lacerda (Tractebel-Suez) power station.

rich sediment. The clay-rich material thus became intimately admixed with the organic matter, resulting in coals with high ash yields (typically around 50%; Pires and Querol, 2004). The coals are commonly overlain by marine sediments, a setting that typically produces high sulphur contents (average 2.2%; Kalkreuth et al., 2006).

The coals in the southern part of Rio Grande do Sul are mainly subbituminous, but those further to the north, including the coals in Santa Catarina, are mostly high volatile bituminous in rank (Kalkreuth et al., 2004, 2006). Some coals have been locally raised to higher rank levels by igneous (diabase) intrusion effects (Kalkreuth et al., 2004). Oliveira et al. (2012) have reported mean maximum vitrinite reflectance values for Santa Catarina coals ranging from 0.44 to 1.38%, although most deposits have values between 0.7 and 1.0%. Kalkreuth et al. (2004) found that the vitrinite in Paraná Basin coals is typically perhydrous in character, and may show anomalously low (suppressed) reflectance characteristics.

Brazil's total coal production is currently around 6 Mt per annum (Departamento Nacional de Produção Mineral, 2010). Rio Grande do Sul is the largest producer in terms of tonnage, with 53.1% of the total

production; Santa Catarina produces 45.6% and Paraná 1.3%. However, because of its higher rank and calorific value, the coal from Santa Catarina currently provides 68.3% of the country's production in energy terms, with 28.5% of the coal-derived energy being produced from Rio Grande do Sul and 3.2% from the Paraná deposits.

Because of the high ash yield and high sulphur content, the run-of-mine (ROM) coals are typically beneficiated to prepare a product with lower ash and sulphur for utilisation purposes. Marcello et al. (2008) indicate that some 3.5 Mt per year, or approximately 58% of the ROM production, are rejected by this process and emplaced in landfills. Almost all of the clean coal is used for power generation, supplying five plants with a total installed capacity of about 2000 MW (Agência Nacional de Energia Elétrica, 2012). Power from these plants provides approximately 11% of Brazil's total electricity requirements (Silva et al., 2010). Three of these plants are located in Rio Grande do Sul, one in Santa Catarina, and one in Paraná.

Most of the seams mined in Santa Catarina have marginal coking properties, but current production is almost entirely used for electricity generation at the Jorge Lacerda (Tractebel Suez) Power Station

(875 MW), located near Tubarão city in the NE of the state (Fig. 1). A small amount of material, however, mainly fine coal from the preparation plants, is used in metallurgical foundry operations.

1.1. Preparation characteristics of Brazilian coals

The top sizes in Brazilian preparation plants are usually less than 40 to 50 mm (Sampaio et al., 2008, 2011). Due to the intimate admixture of vegetation and clay during peat formation, the degree of liberation of the organic matter in the crushed ROM coals is typically very low. Gravity concentration processes are widespread in the region, especially jigs and heavy medium separation for coarse coals and spirals and concentrating tables for fine coals. Despite beneficiation, clean coal products with less than 30% ash are only rarely obtained.

In order to provide products with low ash yields (about 30–35%), small top sizes should ideally be used. This would, however, cause a decrease in the efficiency of the beneficiation processes (Sampaio and Tavares, 2005), and also increase the moisture content of the products. Consequently top sizes used in the preparation plants are not over 50 mm and rarely less than 30 mm.

An example of the preparation characteristics of a Brazilian coal can be seen in Fig. 2, which shows Henry–Reinhardt liberation curves for a Candiota coal with a size range of 25.4 mm × 2 mm (de Souza et al., 2012; Feil et al., 2012). The first curve, the densimetric curve (Fig. 2A), illustrates the variation in the cumulative floats percentage as a function of separation density. In this case, for each density chosen (cut point) there is a proportion of the coal that floats (density less than the cut point) and there is a proportion of the coal that sinks (density higher than the cut point).

The second and third curves (cumulative floats and cumulative sink curves; Fig. 2B) indicate the ash yield of the coal fractions that float and sink for any given cut density. For example, if the coal in question is put into a medium of density 1.7 g cm^{-3} , 60% of the material would float and 40% would sink. The cumulative floats and cumulative sink curves indicate the ash yield of the coal that floats (60% in mass with an ash yield of 42%) and sinks (40% in mass with an ash yield of 63%).

Considering that organic matter typically has a relative density around 1.4 g cm^{-3} , clay minerals' density of around 2.2 g cm^{-3} , and middlings' (particles made up of a mixture of organic and mineral matter) density of between 1.6 g cm^{-3} and 2.0 g cm^{-3} , it is clear that large proportions of composite particles (i.e. intimate mixtures of organic and mineral material) are present in the coals subjected to beneficiation. The yield of clean coal (cumulative percent floating in Fig. 2A) may therefore vary significantly, depending on the density (cut point) at which separation is carried out.

An inverse relationship exists between clean coal yield and clean coal quality (ash percentage for cumulative floats fraction), depending on the nature of the composite particles in the crushed coal to be beneficiated. High proportions of particles with densities close to the cut point tend to make separation difficult, with small variations in cut-point density producing large variations in product yield and quality.

Beneficiation of coals in Santa Catarina provides two main classes of product:

- Coarse coals, with beneficiated size typically above 2 mm; these are sold to the Jorge Lacerda power station;
- Fine coals, with beneficiated size usually below 2 mm; these are sold to foundry coking plants or mixed with coarse coals and sent to the power station.

The Jorge Lacerda (Tractebel Suez) power plant burns medium-sulphur coal (<2% total S) with approximately 40% ash (45–50% mineral matter; Silva et al., 2010). The coal used by the power station represents a blend of material from many different suppliers; blend components are drawn not only from deposits in Santa Catarina but also from some mines in Rio Grande do Sul.

1.2. Objectives of the present study

Separation of finely crushed coal samples into different density fractions has been used in a number of studies (e.g. Gluskoter et al., 1977; Querol et al., 2001; Senior et al., 2000; Wagner and Tølteng, 2012; Ward, 1980) as a basis for assessing the modes of occurrence of different trace elements. Such an approach is generally used to indicate whether particular elements are more strongly associated with the dense, mineral-matter rich fractions of the coal (i.e. have an inorganic affinity) or with the less-dense, maceral-rich fractions (i.e. have an organic affinity). Studies are commonly carried out on samples crushed to a relatively fine particle size, with greater liberation of mineral and organic components and more efficient separation than would typically be obtained under industrial processing conditions.

Numerous studies have also been carried out on variations in coal characteristics associated with industrial-scale preparation, including variations in ash chemistry and trace element characteristics (e.g. Hower et al., 1998; Huggins et al., 2009; Mastalerz and Padgett, 1999; Moore and Esmaeili, 2012; Vamvuka et al., 2001; Vassilev et al., 2001; Wang et al., 2006). However, very few of these studies have addressed the variation in coal characteristics with preparation based on quantitative analysis of the different mineral-matter components, or focused on more than a small number of preparation plants.

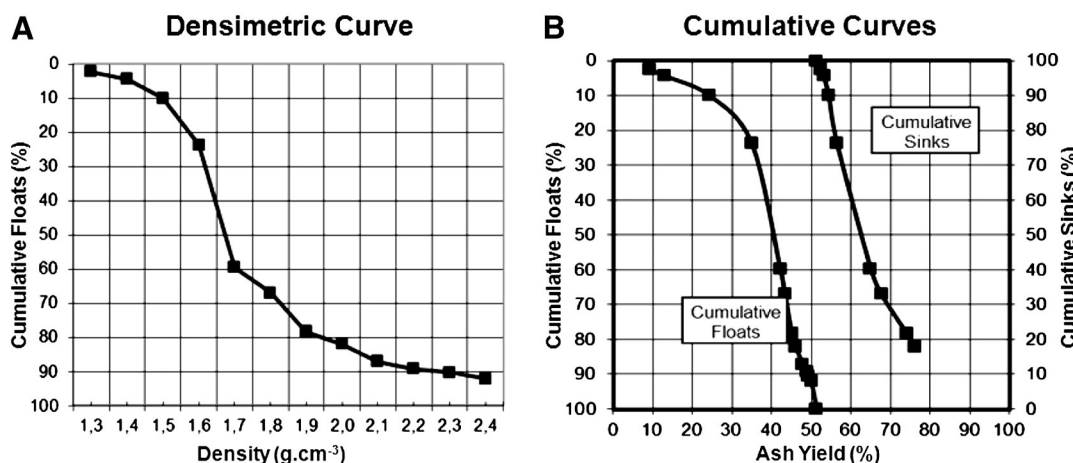


Fig. 2. Henry–Reinhardt liberation curves for a coal from Candiota, Rio Grande do Sul, with particle size range of 25.4 mm × 2 mm. A) Plot showing variation in cumulative floats percentage with separation density; B) Plot showing ash yield of cumulative floats and sink fractions for the same coal sample.

The minerals are, nevertheless, the fundamental components that affect many aspects of the coal's behaviour, including ash chemistry and associated aspects such as ash fusion and slagging (e.g. Bryers, 1996; Matjie et al., 2012a,b; Reifenstein et al., 1999), and also the occurrence and behaviour of particular trace elements, both in stockpiles (Oliveira et al., 2012; Ward et al., 2011) and during utilisation (e.g. Clarke and Sloss, 1992; Goodarzi and Swaine, 1995; Querol et al., 1995; Quick and Irons, 2002; Quispe et al., 2012).

Huggins et al. (2009) investigated the mineralogical and geochemical characteristics of the feed coal, clean coal product, rotary breaker reject and plant tailings reject for a coal from the Illinois Basin, and related variations in trace element concentrations among those fractions to variations in the relative abundance of particular mineral components. Moore and Esmaili (2012) carried out a similar study of seam channel samples, clean coal products and tailing pond materials from two underground coal mines in the Alborz Coalfield of Iran, again with a focus on variations in trace element composition. Matjie et al. (2008) evaluated partitioning of minerals among laboratory-separated float-sink fractions of a South African coal, and related the results to the modes of mineral occurrence at different particle sizes in coal crushed for industrial purposes.

The aim of the present study is to compare the mineralogical and inorganic geochemical characteristics of ROM and beneficiated coals from the principal mines and preparation plants in Santa Catarina that contribute to the blend used in the Jorge Lacerda power station, in order to evaluate the partitioning of the minerals, major elements and trace elements associated with concentration of the organic matter by the beneficiation processes that are used. As well as providing a basis for comparison to similar mineralogical studies based on other deposits, the work is intended to help in designing new preparation plants and processes, to assist the design and operation of coal-fired power stations, and to increase the level of understanding in the development and use of Brazil's high-ash coal resources.

2. Materials and methods

2.1. Sampling

A total of 24 coal samples (Table 1) were collected (12 ROM and 12 beneficiated or clean coals), from both large and small mines in the

Paraná Basin of Santa Catarina (Fig. 1). Bulk samples of 100 kg were collected over a 5-day period from each site immediately after the mining and beneficiation processes, following American Society for Testing and Materials procedures (ASTM, 1996). The samples were reduced by cone and quartering; the quartered fractions were then homogenised in the laboratory following ASTM procedures (ASTM, 1991), and split to supply subsamples for further grinding and analysis.

2.2. Analytical procedures

Powdered (<212 µm) subsamples prepared from the ROM and clean coals were oven-dried for 24 h at 40 °C. Ultimate analysis was carried out on these samples using a LECO CNHS-932 elemental analyser at the University of Rio Grande do Sul, providing data on the carbon, hydrogen, sulphur, nitrogen and oxygen contents of the dried coal samples.

Separate portions of each powdered coal were subjected to low-temperature oxygen-plasma ashing (Gluskoter, 1965; Standards Australia, 2000) at the University of New South Wales (UNSW). Three of the ROM samples, however, were grey in colour, high in mineral matter (around 80%), and did not require low-temperature ashing to provide a sample suitable for X-ray diffraction (XRD) analysis. The LTAs, including LTAs of the clean coals reported in a previous study (Oliveira et al., 2012), were evaluated by X-ray powder diffraction using a Phillips PW1830 diffractometer with CuK α radiation and a scan range from 2 to 60°·20. Quantitative analyses of the mineral phases in each LTA were made using Siroquant™, commercial interpretation software (Taylor, 1991) based on the refinement principles developed by Rietveld (1969).

Other representative portions of each powdered coal sample were ashed at 815 °C. Portions of each ash were fused with lithium metaborate and cast into discs, following the method of Norrish and Hutton (1969). Each disc was analysed by X-ray fluorescence (XRF) spectrometry using a Phillips PW 2400 spectrometer and SuperQ software, and the results expressed in oxide form. The loss-on-ignition (LOI) at 1050°C was also determined for each sample, as part of the analysis procedure.

Portions of each coal sample were acid digested following a two-step method devised to retain volatile elements (Querol et al., 1997). The process involved a hot HNO₃ extraction, followed by HF-HNO₃-HClO₄

Table 1
Source of coal samples used in this study.

Sample	Company	Mine	Coal seam	Sample type
CR 1	Carbonífera Catarinense Ltda.	3G Plano II	Barro Branco	Run-of-mine
CR 2	Carbonífera Catarinense Ltda.	3G Plano II	Barro Branco	Clean coal
CR 5	Carbonífera Catarinense Ltda.	Bonito	Bonito	Run-of-mine
CR 6	Carbonífera Catarinense Ltda.	Bonito	Bonito	Clean coal
CR 9	Carbonífera Criciúma Ltda.	Unidade Mineira II - Verdinho	Barro Branco	Run-of-mine
CR 10	Carbonífera Criciúma Ltda.	Unidade Mineira II - Verdinho	Barro Branco	Clean coal
CR 15	Carbonífera Metropolitana Ltda.	Fontanelas	Bonito	Run-of-mine
CR 16	Carbonífera Metropolitana Ltda.	Fontanelas	Bonito	Clean coal
CR 17	Carbonífera Metropolitana Ltda.	Esperança Leste	Barro Branco	Run-of-mine
CR 18	Carbonífera Metropolitana Ltda.	Esperança Leste	Barro Branco	Clean coal
CR 23	Rio Deserto Ltda.	Mina Barro Branco	Barro Branco	Run-of-mine
CR 24	Rio Deserto Ltda.	Mina Barro Branco	Barro Branco	Clean coal
CR 35	Cooperminas Ltda.	Mina 3	Barro Branco	Run-of-mine
CR 36	Cooperminas Ltda.	Mina 3	Barro Branco	Clean coal
CR 40	Carbonífera Belluno Ltda.	Morozini	Barro Branco	Run-of-mine
CR 41	Carbonífera Belluno Ltda.	Morozini	Barro Branco	Clean coal
CR 42	Carbonífera Belluno Ltda.	Cantao	Barro Branco	Run-of-mine
CR 43	Carbonífera Belluno Ltda.	Cantao	Barro Branco	Clean coal
CR 48	Carbonífera Belluno Ltda.	Morozini/Cantao	Barro Branco	Run-of-mine
CR 49	Carbonífera Belluno Ltda.	Morozini/Cantao	Barro Branco	Clean coal
CR 57	Gabriella Mineração Ltda.	Rio Fiorita	Barro Branco	Run-of-mine
CR 58	Gabriella Mineração Ltda.	Rio Fiorita	Barro Branco	Clean coal
CR 64	Carbonífera Siderópolis Ltda.	Lageado mine	Barro Branco	Run-of-mine
CR 65	Carbonífera Siderópolis Ltda.	Lageado mine	Barro Branco	Clean coal

digestion of the residue. The resulting solutions were analysed by inductively coupled plasma optical emission spectrometry (ICP-OES; Jobin Yvon Ultima 2) to determine the concentrations of major elements, and inductively coupled plasma-mass spectroscopy (ICP-MS; Perkin Elmer Elan 6000) for trace elements, at the Institute of Environmental Assessment and Water Research, Barcelona,. An international coal reference material (SARM-19) and blanks were also digested and analysed following the same procedure, to check the accuracy of the analytical and digestion methods. Analytical errors were estimated at 3% for most of the elements and around 10% for Cd, Mo, and P.

Minerals of interest in selected coals were examined on natural coal surfaces using a LEO-435VP scanning electron microscope (SEM), fitted with an Oxford energy-dispersive X-ray spectrometer (EDS) with a resolution of >133 eV (Silva et al., 2012). The accelerating voltage was 20 kV and the beam current was 10^{-10} A.

3. Results and discussion

3.1. Ash and sulphur

Table 1 shows the source and type of material (ROM or clean coal) for each sample analysed in the study. Ultimate analysis data for the ROM and clean coal samples are presented in **Table 2**. The data in **Table 2** represent values determined to a dry basis, so that the sum of the C, H, N, S and O percentages effectively represent the total proportion of organic matter. The difference between that value and 100%, also listed in **Table 2**, approximates the ash percentage (dry basis) for each sample. Ash yields range from 45 to 84% for the ROM samples (average 60.9%) and from 29 to 51% (average 40.4%) for the clean coal materials. Total sulphur ranges from 1.0 to 3.9% for the ROM coals (average 2.26%) and 0.7 to 3.2% (average 1.57%) for the clean coal samples.

Each of the clean coal samples in **Table 1** was produced from the respective ROM coal, with the ROM coal as the only source material. Comparison of the respective pairs of samples indicates that the reduction in ash percentage produced by beneficiation ranges from around 10% (CR 23 and CR 24) to over 40% (CR 48 and CR 49) in absolute terms. As indicated by Silva et al. (2010), the Tractebel-Suez power

plant typically operates with a feed coal having up to 55% ash and 2.5% total sulphur.

In one case (CR 23 and CR 24) the reduction in total sulphur was negligible, but in all other cases the reduction in ash was accompanied by a reduction in total sulphur of up to 1.6% absolute (CR 48 and CR 49, from 2.38% to 0.74%). With the exception of the high-sulphur coal in sample CR 65, all of the clean coal products listed in **Table 2** have less than 2% total sulphur, and thus are within the range used by the power plant.

3.2. Mineral matter in coal samples

Table 3 provides data on the mineralogy of the ROM and clean coal samples, based for all but three of the ROM samples on X-ray diffraction analysis of the low-temperature ash (LTA) produced by oxygen–plasma ashing. The remaining three ROM samples (CR 48, CR 57 and CR 64) had a light grey colour in powdered form, indicating a low percentage of organic matter, and the mineralogy of these samples was assessed by XRD analysis of the raw coal without an intermediate plasma-ashing process.

With the exception of the three ROM coals that were not subjected to low-temperature ashing, the percentages of LTA listed in **Table 3** range from 51 to 78% for the ROM coals and 36 to 55% for the clean coal materials. For the three ROM coals that had not been subjected to low-temperature ashing, the proportion of ash produced in preparing the material for XRF analysis is given in **Table 3** as a substitute for the LTA percentage.

Fig. 3 shows a plot of the relationship between the LTA percentages and the ash percentages indicated for the same samples by ultimate analysis (**Table 2**). The points representing the individual samples fall close to but slightly above the diagonal line on the figure indicating equality, suggesting a high level of consistency between the two parameters. The LTA percentages are slightly higher than the (inferred) ash percentages; this probably reflects inclusion of water of hydration of the clay minerals in the LTA but not in the ultimate analysis data, together with any changes at high temperature in the associated carbonate or sulphide minerals. For the three samples that were not subjected to low-temperature ashing (CR 48, CR 57 and CR 64), where higher temperatures and loss of hydration water were involved, the

Table 2
Ultimate analysis (wt. %, dry basis) of coal samples.

Sample	Company/mine	Coal	C	H	N	S	O	Total	Ash ^a
CR 1	3G Plano II	Run-of-mine	37.34	2.96	0.76	2.25	9.31	52.62	47.38
CR 2	3G Plano II	Clean coal	52.76	3.69	1.01	1.44	8.59	67.49	32.51
CR 5	Bonito	Run-of-mine	21.50	1.64	0.29	1.78	5.03	30.24	69.76
CR 6	Bonito	Clean coal	38.99	2.28	0.49	1.55	5.55	48.86	51.14
CR 9	UM II-Verdinho	Run-of-mine	26.68	1.95	0.49	2.11	5.10	36.33	63.67
CR 10	UM II-Verdinho	Clean coal	51.65	3.56	0.96	1.66	4.75	62.58	37.42
CR 15	Fontanelas	Run-of-mine	36.45	2.06	0.47	2.34	3.83	45.15	54.85
CR 16	Fontanelas	Clean coal	50.97	2.92	0.69	1.53	3.74	59.85	40.15
CR 17	Esperança Leste	Run-of-mine	36.51	2.84	0.78	2.02	5.41	47.56	52.44
CR 18	Esperança Leste	Clean coal	51.80	3.53	1.05	1.37	5.66	63.41	36.59
CR 23	Barro Branco	Run-of-mine	36.41	2.32	0.71	2.72	3.93	46.09	53.91
CR 24	Barro Branco	Clean coal	46.21	3.26	0.91	2.70	3.95	57.03	42.97
CR 35	Mina 3	Run-of-mine	45.43	3.09	0.90	1.75	3.91	55.08	44.92
CR 36	Mina 3	Clean coal	60.84	3.95	1.17	1.12	3.48	70.56	29.44
CR 40	Morozino	Run-of-mine	41.72	2.69	0.90	2.65	3.35	51.31	48.69
CR 41	Morozino	Clean coal	56.55	3.40	1.18	1.40	3.09	65.62	34.38
CR 42	Cantao	Run-of-mine	35.10	2.44	0.77	2.44	3.39	44.14	55.86
CR 43	Cantao	Clean coal	49.02	2.81	0.99	1.37	3.05	57.24	42.76
CR 48	Morozino/Cantao	Run-of-mine	12.52	1.58	0.39	2.38	2.62	19.49	80.51
CR 49	Morozino/Cantao	Clean coal	47.17	3.38	0.78	0.74	8.02	60.09	39.91
CR 57	Gabriela	Run-of-mine	8.09	1.10	0.08	0.99	5.71	15.97	84.03
CR 58	Gabriela	Clean coal	44.32	3.29	0.89	0.90	4.55	53.95	46.05
CR 64	Car. Siderópolis	Run-of-mine	11.23	1.25	0.11	3.91	6.10	22.60	77.40
CR 65	Car. Siderópolis	Clean coal	39.31	3.09	0.82	3.21	6.27	52.70	47.30
Average		Run-of-mine	29.08	2.16	0.55	2.28	4.81	38.88	61.12
Average		Clean coal	49.13	3.26	0.91	1.58	5.06	59.95	40.05

^a Ash percentage estimated by difference.

Table 3
Mineralogy of coal LTA (wt. %) by X-ray diffraction analysis.

Sample	CR01	CR02	CR05	CR06	CR09	CR10	CR15	CR16	CR17	CR18	CR23	CR24	CR35	CR36	CR40	CR41	CR42	CR43	CR48	CR49	CR57	CR58	CR64	CR65	Average	Clean %	
	ROM	Clean	ROM	Clean	ROM	Clean	ROM	Clean																			
LTA %	60.8	39.9	77.7	55.4	71.0	44.4	62.7	43.1	66.4	41.9	59.2	49.9	51.3	36.4	54.1	37.8	61.6	49.5	80.7 ^a	37.4	82.4 ^a	51.9	78.3 ^a	54.7	67.18	45.19	67.3
Quartz	16.8	15.3	22.6	24.5	16.5	12.1	23.8	26.5	13.5	11.4	19.4	26.1	18.2	15.6	17.1	15.5	17.1	20.7	20.9	22.2	19.1	17.3	16.4	18.65	10.0	10.0	
Kaolinite	40.5	30.3	13.0	13.0	30.3	20.7	3.7	5.9	35.7	27.5	14.7	8.1	33.9	29.1	27.0	17.3	30.8	20.9	38.1	43.6	33.8	29.8	36.1	26.8	28.13	22.75	80.9
Illite	15.9	19.3	18.1	14.6	11.3	11.4	16.8	24.4	13.9	13.1	18.4	22.3	7.8	28.6	10.7	20.2	11.3	15.8	14.4	13.5	10.5	14.8	21.8	14.1	14.24	17.68	124.1
Illite/smectite	20.9	30.5	35.2	38.4	30.4	45.8	38.7	28.4	22.1	31.6	36.1	33.0	32.1	21.5	35.2	43.5	32.1	41.7	3.7	9.9	24.4	31.9	13.5	33.1	27.03	32.44	120.0
Albite																											
Pyrite	2.0	1.9	1.8	1.6	3.4	1.1	3.2	1.7	3.0	2.4	4.0	3.4	1.6	1.2	3.7	0.6	0.5	0.8	0.1	0.1	0.5	0.7	1.97	1.71	86.9		
Jarosite	0.3		1.2	1.1	0.3	0.3	0.3	0.3	0.3	0.3	0.3	0.3	0.3	0.3	0.3	0.3	0.3	0.3	0.3	0.3	0.3	0.3	0.3	0.3	0.3	0.3	
Calcite																											
Dolomite	0.8		0.2																								
Siderite																											
Anatase	1.4		1.0	0.9	1.2	1.2	1.0	0.7	1.2	1.5	0.8	0.9	0.8	1.4	1.1	1.2	0.9	1.5	1.0	1.4	0.9	1.2	1.13	0.81	71.9		
Rutile	0.4		0.5		0.0	1.2	0.9	0.3	0.9	0.3	0.3	0.2	0.1	0.1	0.2	0.1	0.1	0.1	0.1	0.1	0.1	0.1	0.1	0.1	0.1	0.1	
Bassanite	1.2	2.8	1.0	1.4	1.5	1.0	2.3	3.1	1.8	2.7	1.2	0.9	0.5	1.0	1.0	1.0	0.7	1.0	2.7	0.2	0.3	0.2	1.0	1.11	1.43	239.1	
Gypsum																											
Illite + I/S	36.8	49.8	53.3	50.1	41.7	57.2	55.5	52.8	36.0	44.7	54.5	55.3	39.9	50.1	45.9	63.7	43.4	57.5	18.1	23.4	34.9	46.7	35.3	47.2	41.28	49.88	120.8
Pyrite + Jarosite	2.3	1.9	3.0	1.5	3.7	1.1	3.5	1.7	3.3	2.4	4.9	3.4	1.6	1.2	4.9	0.6	4.4	0.5	17.1	<0.8	8.4	1.7	6.8	6.0	5.33	1.90	35.7
Bassanite + Gypsum	1.2	2.8	1.0	2.3	1.5	1.0	2.3	3.1	1.8	2.7	1.2	0.0	0.9	0.5	1.0	1.0	0.7	4.3	2.7	1.1	0.3	2.7	1.0	1.67	1.51	90.5	

^a Ash yield from XRF data.

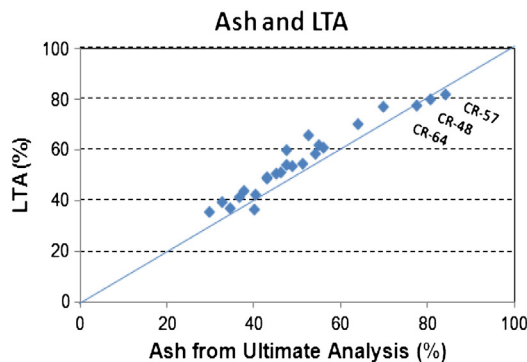


Fig. 3. Plot showing relationship between percentage of low-temperature ash (LTA) and ash percentage inferred from ultimate analysis for coal samples included in the study. Numbered points plot ash percentages determined as part of XRF analysis against ash percentages inferred from ultimate analysis data. Diagonal line represents equality of percentages from both estimates.

ash percentages determined from the XRF preparation are very close to the respective ash percentages inferred from the ultimate analysis data.

The average LTA (or in three cases high-temperature ash) percentage for the ROM samples is around 67%, and around 45% for the clean coal samples (Table 3). The average proportion of LTA for the clean coal samples is around 67% of the average proportion for the ROM materials, indicating the extent to which beneficiation has reduced the mineral matter content.

The most abundant minerals in the LTA of the ROM and clean coal samples are quartz, kaolinite, illite and interstratified illite/smectite (I/S) (Table 3). Together these components make up around 90% of the mineral matter in both sample groups. The remainder is represented by small proportions of feldspar (mainly albite), pyrite, calcite, dolomite, anatase and/or rutile, and hydrous sulphate minerals, jarosite, bassanite and gypsum.

As discussed further by Oliveira et al. (2012), the illite and I/S are primarily detrital in origin. The kaolinite, quartz and feldspar may also be mainly of detrital origin, although some of the kaolinite and quartz might also represent authigenic precipitates formed within the pores of the maceral components. The pyrite is commonly framboidal, and was probably formed mainly by bacterial reduction of sulphate in the original depositional environment; the jarosite was probably derived from oxidation of the pyrite with exposure and/or storage.

Again as discussed by Oliveira et al. (2012), the bassanite and gypsum may represent artefacts of the plasma-ashing process (cf. Frazer and Belcher, 1973), although interaction of calcite in the coals with acids produced by pyrite oxidation (cf. Rao and Gluskoter, 1973), or precipitation following evaporation of Ca-bearing pore waters in the samples (cf. Koukouzas et al., 2010), may also be involved. The occurrence of bassanite and gypsum in the ROM samples that had not been subjected to low-temperature ashing suggests that precipitation from solution was probably dominant, at least for those particular materials. Any such gypsum would, however, probably be removed from the ROM coal during preparation, so that the bassanite in the clean coal LTAs probably represents artefact material derived mainly from Ca and S in the organic matter.

3.3. Chemical composition of coal ashes

Chemical composition data for the high-temperature ashes of the coal samples are given in Table 4, expressed for consistency to an LOI-free basis. Table 4 also shows that the average ash percentage for the clean coals (taken from Table 2) is approximately 66% of the average ash percentage for the ROM materials, indicating the extent to which the ash percentage has been reduced by the beneficiation processes.

As might be expected from the mineralogy of the LTA residues, the dominant oxides in the ashes are SiO₂ and Al₂O₃. Although some

Table 4
Major element chemistry of coal ash (wt. %, LOI-free) by X-ray fluorescence analysis.

Sample	CR 01	CR 02	CR 05	CR 06	CR 09	CR 10	CR 15	CR 16	CR 17	CR 18	CR 23	CR 24	CR 35	CR 36	CR 40	CR 41	CR 42	CR 43	CR 48	CR 49	CR 57	CR 58	CR 64	CR 65				
	ROM	Clean	ROM	Average clean	Clean % of ROM																							
Ash % ^a	47.4	32.5	69.8	51.1	63.7	37.4	54.9	40.2	52.4	36.6	53.9	43.0	44.9	29.4	48.7	34.4	55.9	42.8	80.5	39.9	84.0	46.1	47.3	61.1	40.1	65.5		
SiO ₂	57.29	56.77	62.44	62.92	59.65	56.18	59.91	61.30	51.77	50.14	60.35	62.25	57.26	55.24	55.63	57.08	58.38	60.39	52.49	59.58	59.06	60.98	53.62	56.76	57.32	58.30	101.71	
Al ₂ O ₃	29.70	29.63	23.45	22.42	28.28	25.91	21.84	20.49	28.72	28.49	25.12	20.70	27.81	27.78	27.37	28.10	29.28	28.50	23.53	25.91	26.50	29.44	26.77	27.69	26.53	100.22		
Fe ₂ O ₃	5.21	5.51	5.06	4.77	5.25	5.18	6.43	3.96	8.05	4.83	5.86	7.15	5.53	5.90	8.58	3.94	5.51	2.75	10.05	3.35	6.47	3.90	8.15	8.68	6.68	4.99	74.76	
MnO	0.04	0.02	0.02	0.03	0.07	0.04	0.10	0.15	0.21	0.02	0.02	0.06	0.02	0.06	0.04	0.03	0.04	0.02	0.03	0.01	0.01	0.02	0.01	0.01	0.02	0.04	0.05	109.78
TiO ₂	1.36	1.56	0.94	0.89	1.25	1.48	0.88	0.85	1.38	1.70	0.97	0.94	1.39	1.55	1.47	1.62	1.42	1.46	1.14	1.06	1.22	1.17	1.41	1.22	1.33	1.33	109.53	
CaO	1.08	1.02	1.10	1.67	2.55	1.55	4.30	3.77	4.24	5.00	1.05	1.24	3.08	2.20	2.32	1.75	1.38	1.32	1.36	4.01	0.32	0.14	0.94	0.40	1.98	2.01	101.52	
MgO	1.09	0.67	1.37	0.93	0.91	0.65	1.24	0.86	0.67	0.89	1.35	0.93	0.86	0.67	0.82	0.73	0.80	0.55	0.52	0.89	0.62	0.51	0.63	0.55	1.02	0.82	80.10	
Na ₂ O	0.85	0.36	1.22	0.67	0.94	0.30	1.56	0.99	0.74	0.18	1.11	0.70	0.74	0.20	0.68	0.14	0.66	0.29	0.75	0.08	0.72	0.06	0.59	0.05	0.88	0.34	38.05	
K ₂ O	2.54	2.90	3.74	3.43	2.79	2.75	3.64	3.27	2.34	2.68	3.65	3.19	2.33	2.55	2.34	2.76	2.39	2.63	2.40	1.41	2.57	2.52	2.34	2.41	2.76	2.71	98.30	
SO ₃	1.00	1.26	1.23	2.20	1.48	1.37	2.63	4.43	2.33	5.39	0.92	1.19	0.90	1.43	1.36	1.27	1.13	0.99	7.66	3.49	2.39	2.24	5.68	0.64	2.39	1.99	83.25	
P ₂ O ₅	0.10	0.09	0.09	0.08	0.16	0.09	0.11	0.07	0.12	0.07	0.11	0.08	0.10	0.17	0.09	0.06	0.09	0.06	0.13	0.07	0.10	0.08	0.11	0.08	0.11	0.08	76.44	

^a Ash percentages estimated from ultimate analysis data.

variation exists among the individual samples, these make up, on average, around 58% and 27% respectively of the coal ashes for both the ROM and clean coal materials. The remainder of the ash constituents are represented by Fe₂O₃, CaO, K₂O and SO₃, with lesser but still significant proportions of TiO₂, MgO and Na₂O, and a very minor proportion of P₂O₅.

The percentages of most of these oxides are similar in the respective ashes of both the ROM and clean coal samples. However, for reasons discussed in Section 3.5 (below), the average percentages of both Fe₂O₃ and Na₂O are lower in the clean coal ashes than in the ashes of the ROM materials.

3.4. Relations between mineral matter and ash chemistry

The chemical composition of the (high-temperature) coal ash implied by the mineralogical data in Table 3 was calculated from the mineral percentages and inferred mineral compositions, following procedures discussed by Ward et al. (1999). This process included allowance for loss of water of hydration from the clay minerals and hydrous sulphates, loss of CO₂ from the carbonates, and conversion of pyrite, where present, to hematite. Plots showing the relationship between the percentages of each major element oxide inferred from the XRD data to the actual percentages of the same oxides determined directly by XRF analysis are given in Fig. 4. Each plot shows the percentage of the relevant oxide in the ash of each sample indicated by each of the two methods, together with a diagonal line on which the points would fall if equal percentages were determined by both techniques.

The data points for SiO₂ and Al₂O₃ (Fig. 4A and B) fall close to but slightly above the diagonal equality line, suggesting an overall high level of consistency between the results of the two techniques but a slight over-estimation of these elements from the mineralogical data. The points for Fe₂O₃ (Fig. 4C) are somewhat more scattered, but are generally parallel to the diagonal line. However, they all plot below the equality line, suggesting that the XRD analysis has under-estimated the proportion of iron-bearing phases. Underestimation of Fe₂O₃ may have occurred because some of the iron in the mineral matter occurs in phases such as the illite and/or I/S, which were assumed to be Fe-free in calculating the inferred ash chemistry. Unrecognised replacement of Al by Fe in these minerals, coupled with replacement of Si by Al, could also explain the slight over-estimation of SiO₂ and Al₂O₃ by the XRD analysis mentioned above. Alternatively, some of the iron in the coals may occur in a non-crystalline form (e.g. amorphous material or colloidal iron staining), which could not be detected by the XRD technique.

The plots for CaO, MgO, K₂O, Na₂O and SO₃ (Fig. 4D-H) show scattered values, but an overall broad correlation with the equality line. For MgO (Fig. 4E) the data points for the two samples containing significant proportions of dolomite (CR 17 and CR 18) plot close to the equality line, but the XRD data appear to have under-estimated the percentages of MgO for a number of other samples. As with the Fe₂O₃ discussed above, this may indicate that some Mg is also incorporated in the illite and I/S component. A similar pattern is indicated for SO₃ (Fig. 4H), possibly arising from difficulties in quantitative XRD analysis due to low crystallinity in some of the sulphate components.

Although many of the points on the K₂O plot (Fig. 4F) also lie close to the equality line, some, particularly those with relatively high K₂O percentages, plot slightly above that line. This may be because calculation of the inferred chemistry assumed complete saturation of K⁺ ions in the interlayer positions of the illite and I/S components, whereas in sedimentary materials incomplete saturation of these layers with K⁺, or partial replacement of interlayer K⁺ with other ions, is commonly involved.

3.5. Changes in mineral matter with beneficiation

One of the main objects of this study was to assess whether the overall reduction in the percentages of ash associated with beneficiation of

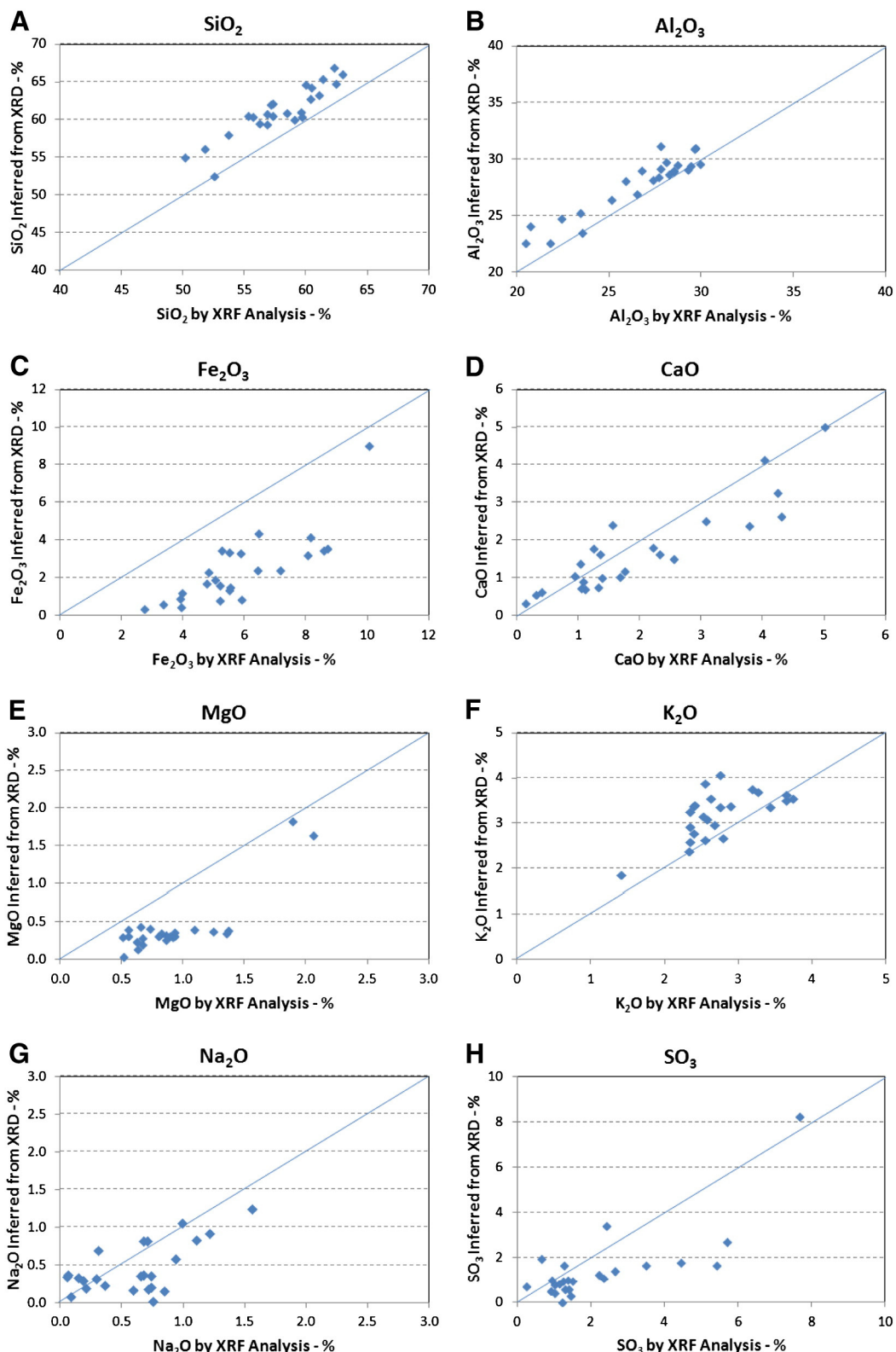


Fig. 4. Plots showing percentages of major element oxides in coal ashes inferred from XRD data compared to percentages on the same oxides determined from XRF analysis of the ash from the same coal samples. A) SiO₂; B) Al₂O₃; C) Fe₂O₃; D) CaO; E) MgO; F) K₂O; G) Na₂O; H) SO₃. Diagonal line in each plot represents equality of both values.

the ROM coals (Table 2) has been accompanied by any changes in the nature of the mineral matter. Table 3 indicates that, despite the reductions in the proportion of mineral matter in the clean coals compared to the ROM materials, similar proportions of most minerals are present in the LTAs of the individual ROM and corresponding clean coal samples,

suggesting that little change has taken place in the actual nature of the mineral matter components. More specifically, the average percentages of quartz, kaolinite, illite, I/S, feldspar, dolomite, and bassanite plus gypsum in the mineral matter of the clean coals indicated in Table 3 are between 80 and 120% of the corresponding average percentages

for the ROM materials. Averages for siderite (20%), anatase (70%) and rutile (240%) lie well outside this range, but these phases, where present, each make up less than 2% of the mineral matter in the samples, and significant levels of scatter are associated with the individual determinations.

By contrast, the average percentage of pyrite in the clean-coal samples is about 66% of the average for the ROM materials. An even greater contrast is apparent if the percentages of jarosite are added to those of the pyrite, with the combined average for the clean coals being only 38% of the ROM value. The average percentage of (total) sulphur

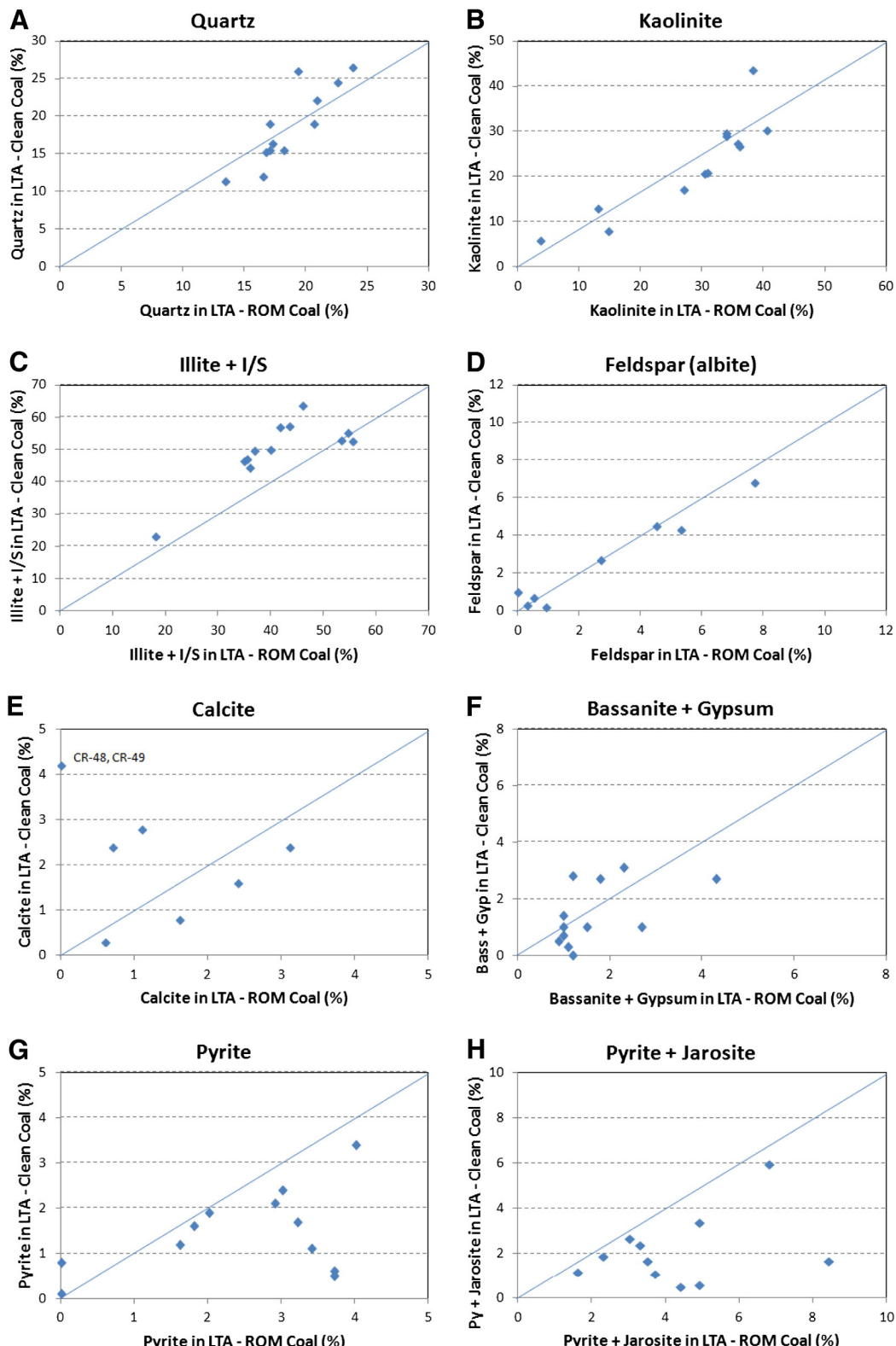


Fig. 5. Plots showing percentages of key minerals in LTA of clean coals against percentages in LTA of ROM coal samples. A) quartz; B) kaolinite; C) illite + illite/smectite; D) feldspar (albite); E) calcite; F) bassanite + gypsum; G) pyrite; H) pyrite + jarosite. Diagonal line represents equal percentages in LTA of both fractions.

in the clean coals is around 69% of the average percentage in ROM materials (Table 2), suggesting that, in removing pyrite from the ROM coals, the beneficiation processes have reduced the total sulphur content to a similar extent.

The greater abundance of jarosite in the ROM samples relative to the clean coals probably reflects a greater degree of oxidation of pyrite in

the ROM materials, due to exposure either before sampling or during storage (Oliveira et al., 2012). Any of such jarosite, if present in the ROM coal supplied to the preparation plant, would probably have been washed away during the beneficiation process. The presence of jarosite nevertheless suggests that an even greater abundance of pyrite would have been present in the ROM materials if the oxidation had not

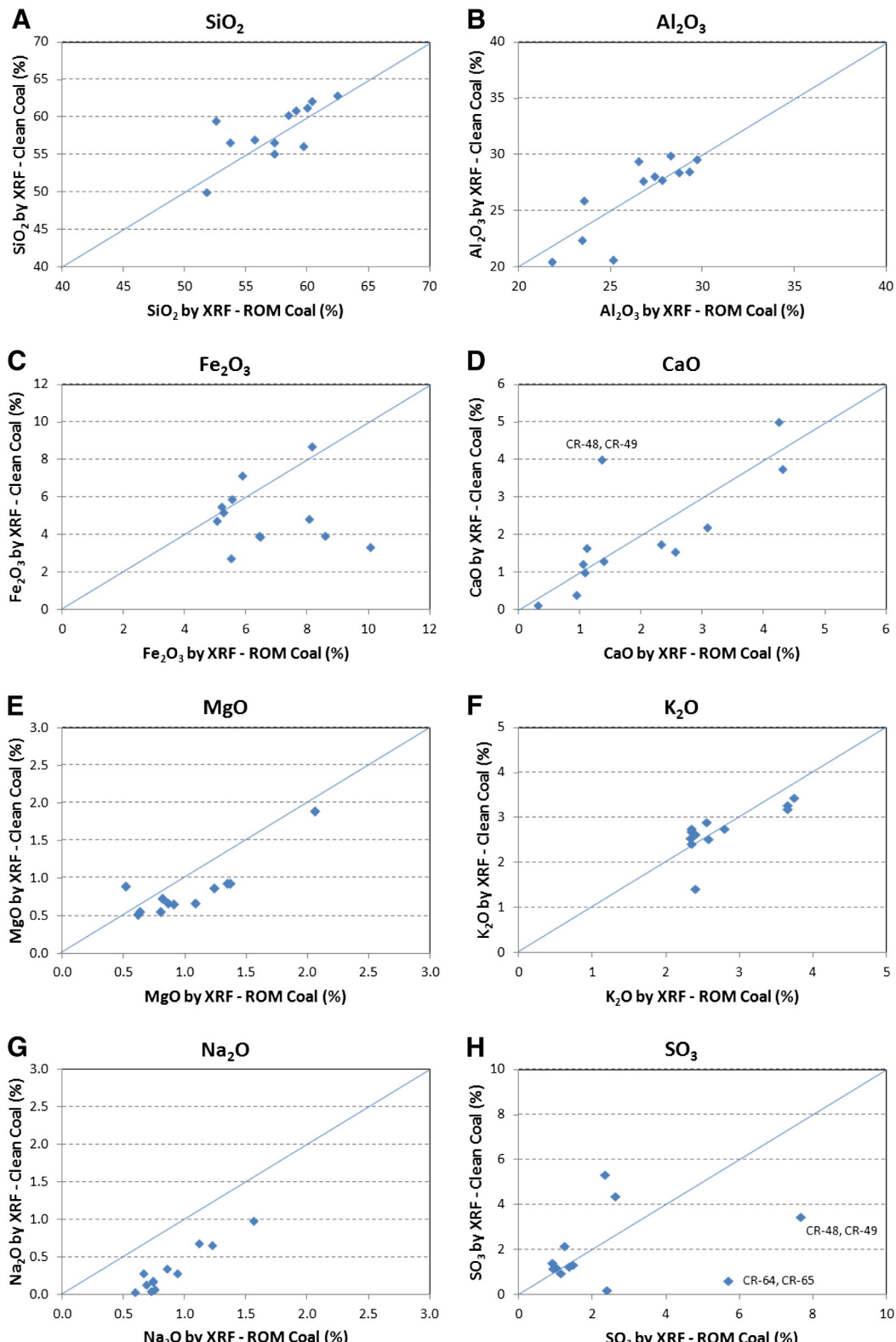


Fig. 6. Plots showing percentages of major element oxides in ash of clean coals against percentages in ash of ROM coal samples. A) SiO_2 ; B) Al_2O_3 ; C) Fe_2O_3 ; D) CaO ; E) MgO ; F) K_2O ; G) Na_2O ; H) SO_3 . Diagonal line in each plot represents equal percentages in ash of both fractions.

Table 5

Mineralogy of whole-coal samples (wt. %).

Sample	CR-01	CR 02	CR-05	CR 06	CR 09	CR 10	CR-15	CR 16	CR-17	CR 18	CR-23	CR 24	CR-35	CR 36	CR 40	CR 41	CR-42	CR 43	CR 48	CR 49	CR-57	CR 58	CR-64	CR 65	Average	Average	Clean %	
	ROM	Clean	ROM	clean	of ROM																							
Quartz	10.2	6.1	17.6	13.6	11.7	5.4	14.9	11.4	9.0	4.8	11.5	13.0	9.3	5.7	9.3	5.9	10.5	9.5	16.9	8.3	17.1	9.9	13.5	9.0	12.5	8.4	67.2	
Kaolinite	24.6	12.1	10.1	7.2	21.5	9.2	2.3	2.5	23.7	11.5	8.7	4.0	17.4	10.6	14.6	6.5	19.0	10.3	30.8	16.3	27.8	15.5	28.3	14.7	18.9	10.3	54.4	
Illite	9.7	7.7	14.1	8.1	8.0	5.1	10.5	10.5	9.2	5.5	10.9	11.1	4.0	10.4	5.8	7.6	7.0	7.8	11.6	5.0	8.6	7.7	17.1	7.7	9.6	8.0	83.5	
Illite/smectite	12.7	12.2	27.4	21.3	21.6	20.3	24.3	12.2	14.7	13.2	21.4	16.5	16.5	7.8	19.0	16.4	19.8	20.6	3.0	3.7	20.1	16.6	10.6	18.1	18.2	14.7	80.7	
Albite	0.0	0.0	4.1	2.4	1.9	1.2	4.8	2.9	0.2	0.1	2.7	2.2	0.5	0.1	0.4	0.0	0.6	0.0	0.0	0.0	0.0	0.5	0.4	0.4	1.3	0.8	58.4	
Pyrite	1.2	0.8	1.4	0.9	2.4	0.5	2.0	0.7	2.0	1.0	2.4	1.7	0.8	0.4	2.0	0.2	2.3	0.2	0.0	0.3	0.0	0.1	2.3	1.1	1.6	0.7	39.9	
Jarosite	0.2	0.0	0.9	0.6	0.2	0.0	0.2	0.0	0.2	0.0	0.5	0.0	0.0	0.0	0.6	0.0	0.4	0.0	13.8	0.0	6.9	0.8	3.1	2.1	1.9	0.2	12.8	
Calcite	0.0	0.0	0.0	0.2	0.8	1.2	1.5	0.7	0.5	1.0	0.0	1.3	1.6	0.9	0.9	0.3	0.4	0.1	0.0	1.6	0.0	0.0	0.0	0.0	0.0	0.5	0.7	123.2
Dolomite	0.5	0.0	0.2	0.0	0.0	0.0	0.0	0.0	0.0	3.8	2.6	0.0	0.0	0.0	0.1	0.0	0.0	0.0	0.0	0.3	0.0	0.0	0.0	0.0	0.0	0.4	0.3	69.2
Siderite	0.0	0.0	0.0	0.0	0.9	0.0	0.0	0.0	0.7	0.3	0.0	0.0	0.3	0.0	0.1	0.0	0.2	0.0	0.0	0.0	0.0	0.0	0.0	0.0	0.0	0.2	0.0	13.8
Anatase	0.9	0.0	0.8	0.5	0.9	0.5	0.6	0.3	0.8	0.6	0.5	0.0	0.5	0.3	0.8	0.4	0.7	0.4	1.2	0.0	0.8	0.7	0.7	0.7	0.8	0.4	48.3	
Rutile	0.2	0.0	0.4	0.0	0.0	0.5	0.0	0.4	0.6	0.1	0.0	0.0	0.0	0.1	0.1	0.0	0.0	0.0	0.8	0.1	0.1	0.2	0.4	0.1	0.2	0.1	160.9	
Bassanite	0.7	1.1	0.8	0.8	1.1	0.4	1.4	1.3	1.2	1.1	0.7	0.0	0.5	0.2	0.5	0.4	0.6	0.3	0.8	1.0	0.2	0.2	0.5	0.7	0.6	87.0		
Gypsum	0.0	0.0	0.0	0.0	0.0	0.0	0.0	0.0	0.0	0.0	0.0	0.0	0.0	0.0	0.0	0.0	0.0	0.0	2.7	0.0	0.7	0.0	2.0	0.0	0.4	0.0	0.0	
Illite + I/S	22.4	19.9	41.4	27.8	29.6	25.4	34.8	22.8	23.9	18.7	32.3	27.6	20.5	18.2	24.8	24.1	26.7	28.5	14.6	8.8	28.7	24.2	27.6	25.8	27.7	22.5	81.3	
Pyrite + jarosite	1.4	0.8	2.3	0.8	2.6	0.5	2.2	0.7	2.2	1.0	2.9	1.7	0.8	0.4	2.7	0.2	2.7	0.2	13.8	0.3	6.9	0.9	5.3	3.3	3.6	0.9	24.0	
Bassanite + Gypsum	0.7	1.1	0.8	1.3	1.1	0.4	1.4	1.3	1.2	1.1	0.7	0.0	0.5	0.2	0.5	0.4	0.6	0.3	3.5	1.0	0.9	0.2	2.1	0.5	1.1	0.7	60.9	

Table 6

Major element chemistry of whole-coal samples (wt. %).

Sample	CR 01	CR 02	CR 05	CR 06	CR 09	CR 10	CR 15	CR 16	CR 17	CR 18	CR 23	CR 24	CR 35	CR 36	CR 40	CR 41	CR 42	CR 43	CR 48	CR 49	CR 57	CR 58	CR 64	CR 65	Average	Average	Clean %
	ROM	Clean	ROM	clean	of ROM																						
SiO ₂	27.14	18.46	43.56	32.18	37.98	21.02	32.86	24.61	27.15	18.35	32.53	26.75	25.72	16.26	27.09	19.62	32.61	25.82	42.26	23.78	49.63	28.08	41.50	26.85	35.03	23.35	66.65
Al ₂ O ₃	14.07	9.63	16.36	11.47	18.01	11.19	11.98	8.23	15.06	10.42	13.54	8.89	12.49	8.18	13.33	9.66	16.36	12.19	18.95	10.34	22.27	13.56	20.72	13.10	16.22	10.65	65.67
Fe ₂ O ₃	2.47	1.79	3.53	2.44	3.34	1.94	3.53	1.59	4.22	1.77	3.16	3.07	2.48	1.74	4.18	1.35	3.08	1.18	8.09	1.34	5.44	1.80	6.31	4.11	4.08	2.00	48.99
MnO	0.02	0.01	0.01	0.02	0.04	0.01	0.05	0.04	0.08	0.08	0.01	0.01	0.03	0.01	0.02	0.01	0.01	0.01	0.01	0.01	0.01	0.01	0.01	0.01	0.03	0.02	71.94
TiO ₂	0.65	0.51	0.66	0.46	0.80	0.55	0.48	0.34	0.72	0.62	0.52	0.40	0.63	0.46	0.71	0.56	0.79	0.62	0.92	0.42	1.03	0.67	0.90	0.67	0.74	0.53	71.77
CaO	0.51	0.33	0.77	0.85	1.62	0.58	2.36	1.51	2.22	1.83	0.57	0.53	1.38	0.65	1.13	0.60	0.77	0.56	1.09	1.60	0.27	0.06	0.72	0.19	1.21	0.80	66.53
MgO	0.52	0.22	0.96	0.48	0.58	0.24	0.68	0.35	1.08	0.69	0.73	0.40	0.39	0.20	0.40	0.25	0.45	0.24	0.42	0.36	0.52	0.23	0.49	0.26	0.63	0.33	52.49
Na ₂ O	0.40	0.12	0.85	0.34	0.60	0.11	0.86	0.40	0.39	0.07	0.60	0.30	0.33	0.06	0.33	0.05	0.37	0.12	0.61	0.03	0.60	0.03	0.46	0.02	0.54	0.13	24.93
K ₂ O	1.20	0.94	2.61	1.75	1.78	1.03	2.00	1.31	1.23	0.98	1.97	1.37	1.05	1.14	0.95	1.33	1.12	1.93	0.56	2.16	1.16	1.81	1.14	1.68	1.08	64.42	
SO ₃	0.47	0.41	0.86	1.13	0.94	0.51	1.44	1.78	1.22	1.97	0.50	0.51	0.41	0.42	0.66	0.44	0.63	0.42	6.17	1.39	2.01	0.11	4.40	0.30	1.46	0.80	54.55
P ₂ O ₅	0.05	0.03	0.06	0.04	0.10	0.03	0.06	0.03	0.06	0.03	0.05	0.02	0.05	0.06	0.05	0.05	0.03	0.08	0.02	0.11	0.03	0.08	0.04	0.07	0.03	50.09	

Table 7

Trace element concentrations by inductively-coupled plasma mass spectrometry (ppm of coal unless otherwise indicated).

Sample	CR 1 ROM	CR 2 Clean	CR 5 ROM	CR 6 Clean	CR 9 ROM	CR 10 Clean	CR 15 ROM	CR 16 Clean	CR 17 ROM	CR 18 Clean	CR 23 ROM	CR 24 Clean	CR 35 ROM
Ash %	47.4	32.5	69.8	51.1	63.7	37.4	54.9	40.2	52.4	36.6	53.9	43.0	44.9
Li	9.71	46.06	44.73	36.24	28.8	20.83	23.27	70.37	71.89	42.21	34.67	17.59	49.05
Be	7.38	3.93	4.7	3.87	3.16	2.92	3.2	5.86	4.35	4.15	3.71	2.37	3.64
B	52.81	27.49	175.52	47.45	30.72	4.92	12.23	24.04	21.33	7.01	24.14	21.35	36.08
Sc	7.65	17.04	14.3	16.9	10.25	7.44	9.99	16.79	21.31	18.05	11.55	6.73	13.75
Ti	894	3409	4369	3141	2735	643	2932	4949	4893	1057	3301	1518	3642
V	70.4	136.4	91.57	131.8	67.14	48.81	69.01	124.1	119.1	111.4	87.29	44.07	112.0
Cr	13.56	81.23	51.29	75.74	34.63	26.46	36.34	66.56	137.1	58.58	41.43	20.09	58.87
Mn	205.9	40.61	118.8	114.6	115.6	88.48	466	358.1	900.8	632.1	70.65	55.05	223.2
Co	7.71	7.76	10.22	9.51	7.9	6.88	7.59	16.47	11.93	7.36	7.79	5.91	9.61
Nb	8.33	33.8	43.54	32.67	30.89	9.04	30.76	47.04	44.23	7.47	35.26	15.24	36.23
Ni	21.35	16.1	17.37	21.31	12.65	16.42	13.48	27.72	48.36	13.27	14.07	10.64	19.22
Cu	15.15	17.14	19.84	20.13	12.53	16.71	16.79	32.06	24.92	13.30	19.07	15.75	19.68
Zn	200.91	309.98	242.23	104.87	82.03	376.26	82.22	170.4	128.4	87.15	131.62	26.46	210.8
Ga	6.48	16.64	23.27	14.19	14.42	8.38	15.43	24.63	22.77	15.47	17.63	7.44	16.64
Ge	<0.8	9.0	4.3	10.2	3.0	2.0	3.4	5.2	6.8	<0.8	5.4	3.1	8.6
As	27.76	10.86	20.26	12.97	12.94	10.48	14.07	12.76	16.02	7.67	8.21	6.58	13.74
Se	1.63	3.16	3.68	3.9	2.46	2.15	2.52	4.79	5.7	3.43	3.32	2.91	3.68
Rb	7.47	43.78	134.0	39.62	84.3	27.16	89.26	81.07	54.93	40.27	95.82	50.57	44.78
Sr	37.9	92.61	117.99	38.65	79.17	39.95	137.2	116.2	115.7	52.45	240.4	153.3	59.23
Y	48.11	36.83	30.37	37.15	29.88	25.32	25.34	34.7	33.9	19.05	28.46	19.19	29.99
Zr	55.12	302.6	155.6	385.2	130.1	182.4	133.5	355.1	377.6	221.5	132.4	65.48	300.5
Mo	1.61	3.54	3.03	2.57	2.20	1.33	2.05	3.74	4.33	2.28	2.45	1.65	2.64
Cd	<0.8	<0.8	0.97	<0.8	<0.8	0.84	<0.8	<0.8	<0.8	<0.8	<0.8	<0.8	0.84
Sn	1.35	5.61	4.65	4.19	3.31	1.29	3.33	5.17	5.13	3.4	3.98	1.55	4.03
Sb	<0.8	1.09	1.74	0.59	1.03	<0.8	0.67	1.17	0.86	<0.8	<0.8	<0.8	<0.8
Cs	4.91	7.96	23.51	7.69	16.29	7.24	19.12	15.14	8.4	6.89	12.34	8.70	7.72
Ba	117.9	276.8	1250	93.61	678.5	123.4	196.0	1036	529.0	324.0	678.6	302.7	167.7
La	17.11	35.03	33.63	35.97	29.09	26.66	25.85	37.52	34.66	20.47	28.77	16.01	28.61
Ce	51.92	96.24	87.44	101.5	76.51	79.60	67.57	102.9	92.52	9.49	74.8	43.96	74.33
Pr	5.39	9.37	8.38	10.01	7.43	8.07	6.44	9.76	8.86	6.07	7.06	4.32	7.12
Nd	24.67	41.14	36.13	44.69	32.57	37.02	27.76	43.05	38.84	27.05	30.41	19.35	30.78
Sm	6.25	9.16	7.54	9.98	6.93	8.42	5.96	9.44	8.34	6.02	6.43	4.37	6.58
Eu	<0.8	1.23	1.01	1.35	0.86	1.11	<0.8	1.35	1.16	0.82	0.83	<0.8	0.9
Gd	6.63	8.61	7.16	9.32	6.39	7.53	5.58	9.05	7.9	5.43	6.14	4.13	6.51
Tb	0.96	1.06	0.89	1.12	0.82	0.87	0.8	1.12	1.01	0.8	0.8	0.8	0.83
Dy	6.06	6.08	5.13	6.29	4.78	4.49	4.16	6.13	5.72	3.45	4.69	3.11	4.93
Ho	1.28	1.18	1.01	1.2	0.97	0.82	0.82	1.14	1.11	0.8	0.94	0.8	0.98
Er	3.24	3	2.67	3.07	2.58	2	2.17	2.86	2.84	1.55	2.48	1.6	2.51
Tm	<0.8	<0.8	<0.8	<0.8	<0.8	<0.8	<0.8	<0.8	<0.8	<0.8	<0.8	<0.8	<0.8
Yb	3.20	3.42	3.08	3.56	3.11	2.15	2.55	3.18	3.33	1.73	2.95	1.81	2.8
Lu	<0.8	<0.8	<0.8	<0.8	<0.8	<0.8	<0.8	<0.8	<0.8	<0.8	<0.8	<0.8	<0.8
Hf	1.59	8.73	6.2	8.13	4.27	2.48	4.17	7.97	9.41	4.78	4.2	1.93	6.37
Ta	<0.8	7.34	11.71	5.19	5.47	0.82	5.98	10.16	8.53	<0.8	6.47	2.05	5.33
W	<0.8	4.16	6.36	3.54	4.06	0.95	5.02	6.50	8.85	<0.8	6.38	2.46	3.98
Tl	2.08	1.76	1.99	1.50	1.27	1.41	1.72	2.25	2.30	1.08	1.34	1.08	1.35
Pb	29.17	21.19	61.93	28.27	42.93	19.71	32.74	74.17	36.39	16.24	28.39	12.65	30.15
Bi	<0.8	<0.8	<0.8	<0.8	<0.8	<0.8	<0.8	1.18	0.87	<0.8	<0.8	<0.8	<0.8
Th	10.08	14.84	17.81	14.97	11.96	11.68	12.56	21.22	43.26	36.98	14.83	7.97	12.67
U	3.71	7.93	5.10	5.01	4.87	5.89	4.29	15.96	16.80	12.84	5.66	2.71	4.12

taken place. Removal of any jarosite would also serve to reduce the total sulphur content of the clean coal products, compared to that of the ROM materials.

The relationships between the individual components in the mineral matter of the ROM and clean coals are further illustrated in Fig. 5, where the individual percentages of each mineral in the LTA of the corresponding pairs of samples are plotted against each other. The data points for quartz, kaolinite, illite + I/S and feldspar (Fig. 5A to D) plot close to the diagonal line representing equal percentages in each group of samples. There is, however, possibly an indication from Fig. 5B and C that kaolinite tends to be more abundant in the LTA of the ROM coals than in the LTA of the clean coals, and that illite and I/S tend to be more abundant in the LTA of the clean coals than in the LTA of the ROM materials.

The points for calcite (Fig. 5E) are more scattered, but with the exception of one outlier (CR 48 and CR 49) falls on each side of the equality line. The outlier value has, however, affected the overall average; as indicated in Table 3 the average percentage of calcite in the LTA of the clean coals is around 200% of the average value for the

ROM samples. A similar scattered plot is indicated for bassanite plus gypsum (Fig. 5F). The points for pyrite (Fig. 5G) and pyrite plus jarosite (Fig. 5H) plot mainly if not entirely below the equality line, confirming a systematic reduction in the proportion of pyrite in the coal by the beneficiation processes.

Fig. 6 provides a similar set of plots based on the percentages of major elements in the ashes of the respective pairs of coal samples. Data points for SiO₂, Al₂O₃, MgO and K₂O (Fig. 6A, B, E, F) fall close to the equality line; this is consistent with the similarity in quartz, illite and I/S in the mineral matter of the corresponding ROM and clean-coal samples. Many of the points for Fe₂O₃ (Fig. 6C) plot below the equality line, suggesting a similar relationship to that shown for pyrite in Fig. 5E. Other data points, however, plot close to the equality line, suggesting that, despite the differences in pyrite, at least some of the Fe in the samples also occurs in the illite and I/S, as discussed in Section 3.4 above.

The data points for CaO and SO₃ (Fig. 6D and H) show a broad scatter around the equality line. For one pair of samples (CR 48 and CR 49) CaO

CR 36	CR 40	CR 41	CR 42	CR 43	CR 48	CR 49	CR 57	CR 58	CR 64	CR 65	Average ROM	Average clean	Clean % of ROM
Clean	ROM	Clean											
29.4	48.70	34.4	55.9	42.8	80.5	39.9	84.0	46.1	77.4	47.3	61.1	40.1	65.5
65.37	46.01	31.24	44.24	46.29	48.85	27.82	87.16	52.58	79.85	41.63	47.35	41.52	87.7
5.01	4.75	4.76	3.71	4.70	2.20	5.82	2.85	3.37	3.64	3.53	3.94	4.19	106.3
33.49	17.31	15.23	13.74	24.4	505.8	72.45	32.64	15.21	428.3	19.16	112.6	26.02	23.1
16.39	16.95	16.06	9.83	16.03	14.22	8.98	14.92	17.4	17.61	14.92	13.53	14.39	106.4
4640	4638	3528	3736	4150	5482	2033	6773	4096	5919	3805	4109	3081	75.0
119.4	141.4	130.3	94.97	117.4	119.2	64.82	108.5	145.4	99.79	117.6	98.36	107.6	109.4
66.98	80.66	76.23	52.77	67.25	60.44	28.79	55.40	74.4	55.56	64.45	56.50	58.90	104.2
174.3	113.0	97.61	74.97	103.0	10.69	39.43	14.24	13.97	38.80	24.44	196.05	145.14	74.0
12.43	12.43	8.32	8.90	6.48	1.43	4.14	1.87	5.36	12.05	9.21	8.29	8.32	100.4
46.79	41.98	32.26	33.47	36.10	50.17	22.32	57.34	37.05	51.56	34.09	38.65	29.49	76.3
23.88	20.58	17.30	15.37	14.33	5.18	12.33	6.20	16.72	16.96	16.49	17.57	17.21	98.0
26.41	22.94	14.12	18.90	16.4	48.16	19.24	16.57	23.07	38.39	28.55	22.75	20.24	89.0
108.2	249.1	78.7	113.0	71.23	40.95	133.3	63.2	57.88	129.1	101.4	139.5	135.5	97.1
23.76	20.84	16.88	17.77	20.74	25.96	14.80	31.60	19.10	29.37	18.36	20.18	16.70	82.7
2.7	7.23	8.52	5.14	8.01	4.21	8.13	3.32	5.71	4.33	9.14	4.71	6.05	128.3
13.46	16.83	7.92	11.40	7.98	44.54	7.10	67.48	27.23	28.00	24.18	23.44	12.43	53.0
3.91	3.99	3.45	3.25	7.75	7.99	2.53	10.12	9.03	5.19	7.69	4.46	4.56	102.2
68.99	55.18	48.27	47.35	56.34	87.05	27.05	94.89	50.85	76.37	46.14	72.62	48.34	66.6
110.9	108.1	74.23	133.4	109.9	140.8	93.18	122.6	45.52	113.78	45.41	117.18	81.02	69.1
31.56	33.28	35.88	21.10	29.89	23.93	44.53	27.98	31.78	25.85	28.94	29.85	31.24	104.6
277.8	236.8	228.1	153.4	178.4	185.6	105.6	158.5	220.9	171.4	244.5	182.6	230.7	126.4
3.39	3.24	2.19	2.40	1.90	5.47	1.77	5.31	2.81	4.88	3.66	3.30	2.57	77.8
<0.8	<0.8	<0.8	<0.8	<0.8	<0.8	0.82	<0.8	<0.8	<0.8	<0.8	0.82	0.81	98.5
4.94	5.16	4.57	3.99	4.13	5.28	3.06	5.77	4.55	5.17	4.05	4.26	3.88	90.9
1.43	0.71	<0.8	<0.8	<0.8	1.43	0.7	2.78	0.89	1.38	1.14	1.15	0.92	79.8
10.23	10.56	9.76	9.00	10.69	10.83	6.06	11.49	8.77	11.47	8.22	12.14	8.95	73.7
402.9	533.7	370.8	770.2	548.3	406.4	117.9	413.2	225.9	502.4	289.2	520.4	342.7	65.9
38.19	37.74	39.27	24.18	35.86	38.03	20.24	48.87	32.16	40.04	32.24	32.22	30.80	95.6
106.5	102.0	108.9	61.92	95.23	94.49	53.4	123.3	86.68	102.8	83.98	84.13	80.70	95.9
10.49	9.72	10.68	6.15	9.02	8.50	5.28	11.15	8.26	9.52	7.95	7.98	8.27	103.7
45.92	41.99	47.26	26.47	38.72	34.89	23.56	46.46	35.4	39.51	34.06	34.21	36.44	106.5
9.99	8.88	10.61	5.70	8.12	6.67	5.49	8.96	7.35	8.02	7.16	7.19	8.01	111.4
1.33	1.19	1.47	<0.8	1.10	0.84	<0.8	1.10	0.94	1.04	0.95	0.94	1.10	116.9
8.91	8.15	10.0	5.19	7.38	5.87	5.94	7.75	6.63	7.04	6.51	6.69	7.45	111.4
1.02	1.00	1.19	<0.8	0.89	<0.8	0.82	0.86	0.84	0.84	<0.8	0.87	0.94	108.8
5.51	5.70	6.43	3.66	5.09	3.99	5.37	4.60	5.04	4.51	4.76	4.83	5.15	106.6
1.04	1.12	1.21	<0.8	1.02	<0.8	1.13	0.89	1.03	0.85	0.95	0.96	1.03	106.5
2.64	2.93	3.06	1.88	2.64	2.11	3.01	2.32	2.74	2.23	2.49	2.50	2.56	102.3
<0.8	<0.8	<0.8	<0.8	<0.8	<0.8	<0.8	<0.8	<0.8	<0.8	<0.8	<0.8	<0.8	100.0
2.89	3.41	3.51	2.16	3.12	2.46	3.19	2.64	3.24	2.59	2.92	2.86	2.89	101.3
<0.8	<0.8	<0.8	<0.8	<0.8	<0.8	<0.8	<0.8	<0.8	<0.8	<0.8	<0.8	<0.8	100.0
6.98	7.06	6.22	4.49	5.35	5.83	3.21	5.28	6.38	5.29	5.87	5.35	5.67	106.0
8.67	6.33	4.53	4.87	6.13	9.02	3.97	10.05	5.45	9.45	5.22	7.00	5.01	71.6
9.02	5.46	4.20	4.35	4.76	6.36	1.98	8.09	4.46	7.46	4.34	5.60	3.93	70.2
2.39	2.92	1.90	2.03	1.74	4.59	<0.8	3.31	1.22	3.51	2.41	2.37	1.63	68.8
33.34	39.82	15.01	33.67	12.79	108.7	16.98	219.8	54.24	87.33	52.9	62.58	29.79	47.6
0.91	<0.8	<0.8	<0.8	<0.8	1.36	<0.8	1.37	0.88	1.34	<0.8	0.95	0.85	89.7
19.39	16.9	15.96	12.13	17.07	17.18	10.39	17.31	14.8	20.64	14.05	17.28	16.61	96.1
9.08	5.56	5.06	3.77	4.90	4.65	4.70	4.75	4.53	6.34	5.86	5.80	7.04	121.3

appears to be more abundant in the ash of the clean coal than of the ROM material, reflecting variations in the abundance of calcite as discussed above. The percentage of SO₃ retained in the ash, by contrast, appears to be greater for two of the ROM samples (CR 48 and CR 64), possibly reflecting a greater abundance of gypsum in the relevant materials (Table 3).

The plot for Na₂O (Fig. 6G) shows a relatively strong trend parallel to but below the equality line, indicating consistently higher proportions of Na₂O in the ashes of the ROM coals than in the ashes of the corresponding clean-coal materials. Without mineralogical data this might be interpreted as a reduction in the feldspar (albite) content of the mineral matter with beneficiation. However, the proportion of feldspar in the mineral matter of the clean coals is similar to that of the ROM materials (Table 3, Fig. 5D), and the difference indicated in Fig. 6G cannot be ascribed to such a source. It is therefore suggested that the reduction in Na₂O shown for the clean coal ashes reflects removal of exchangeable Na from the illite and I/S, brought about by immersion in water during the beneficiation processes.

3.6. Minerals and major elements as fractions of whole-coal samples

Tables 5 and 6 provide data on the mineral matter and major element oxides, expressed as percentages of the individual whole-coal samples. When considered on a whole-coal basis (Table 5), the average proportions of quartz, kaolinite, illite + I/S and bassanite + gypsum in the clean coals are between 55 and 80% of the average proportions of the same minerals in the ROM samples. This is similar to the change in the average proportion of LTA in the two groups of materials, and confirms that the relative abundance of these components in the mineral matter is not significantly affected by the preparation processes.

In contrast, the average percentages of pyrite, jarosite and pyrite + jarosite in the clean coals, when considered on a whole-coal basis, represent only 45%, 12% and 25%, respectively, of the average percentages in the ROM materials; this confirms the selective removal of these components from the coal during beneficiation. Similar comparisons for other minerals, such as feldspar, dolomite, calcite, anatase and rutile, are unreliable due to the low percentages of these

components in the coals; indeed, the percentages of these minerals in many ROM and clean-coal samples are below the relevant detection limits.

Using a similar approach, Table 6 indicates that the average percentages of most major elements (expressed as oxides) in the clean coal samples (SiO_2 , Al_2O_3 , TiO_2 , CaO , K_2O , SO_3), calculated to a whole-coal basis, are between 60 and 80% of the respective average values for the ROM materials. This is consistent with the observation in Table 4 that the average ash percentage for the clean coals is around 66% of the average ash percentage for the ROM samples. By contrast, the average percentage of Fe_2O_3 (whole-coal basis) in the clean coals is only 50% of the average percentage in the ROM materials. As discussed above, this is consistent with the overall reduction in pyrite content produced by beneficiation.

The percentages of MgO and P_2O_5 , on a whole-coal basis, in the clean coals are also around 50% of the average for the ROM coals; however, the individual percentages are generally low (<1% for MgO and <0.2% for P_2O_5), so that trends are difficult to discern. Although not producing a clear trend, the individual values for MgO in the coal ash, as indicated in Fig. 6E, are also slightly lower for some of the clean-coal samples than for the ROM materials.

The average percentage of Na_2O in the clean coals is only around 25% of the average for the ROM samples. As discussed above, this is also apparent in the chemistry of the coal ashes, and may represent the result of cation exchange in the clay minerals associated with the beneficiation processes.

4. Trace element concentrations in ROM and clean-coal samples

Concentrations of trace elements in the ROM and clean coal samples are presented in Table 7. In addition to data on the individual samples, the tabulation lists the average concentration of each element in the 12 ROM and 12 clean coals of the sample series. The average concentration of each element in the 12 clean coals has also been expressed as a fraction (percentage) of the average concentration of the same element in the 12 ROM coals, to provide a simple basis for evaluating the impact of the beneficiation processes on the overall trace element characteristics.

4.1. Elements with concentrations reduced by beneficiation

The concentrations of number of elements in the clean coals, such as Ba, Cs, Mn, Nb, Rb, Sr, Ta, Ti, Tl and W, are between 60 and 80% of the respective average concentrations in the ROM samples. Since the average ash yield or mineral matter content of the clean coals is around 66% of the average for the ROM coals, and the average percentages of major components in the clean coals (SiO_2 , Al_2O_3 , CaO , K_2O) on a whole-coal basis are also between 60 and 80% of the average percentages in the ROM materials, the difference in concentration of these trace elements between the two groups may be related to the overall reduction in mineral matter or ash produced by the beneficiation processes. These trace elements may therefore be associated with the main minerals in the coals, which in this case are the clay mineral components. Many are lithophile elements, and have been shown in other studies (e.g. Dai et al., 2012; Ward et al., 1999) to be associated with clays and other aluminosilicate phases.

A few trace elements, such as As, B and Pb, show an even greater reduction associated with beneficiation, having average concentrations in the clean coals that represent 55%, 26% and 50%, respectively, of the average in the ROM materials (Table 5). Arsenic and Pb are generally regarded as chalcophile elements, and are commonly associated with sulphide phases (Diehl et al., 2012; Finkelman, 1981; Kolker, 2012; Swaine, 1990; Ward et al., 1999). The additional reduction in their concentration may thus be due to preferential removal of pyrite by beneficiation, as discussed in Section 3.5 above. Indeed, if a reduction of 67% in the mineral matter content is produced, on average, by beneficiation, and the average percentage of pyrite in that mineral matter is

also reduced by 67% (Table 3), the overall average reduction in pyrite as a fraction of the total coal in each case would be around 50%. This is consistent with the reduction of 45% on a whole-coal basis indicated in Table 5, and similar to the reduction in average As and Pb concentrations indicated in Table 7.

Plots of the relationships between the concentrations of As and Pb in the coal and the ash percentages for the whole sample suite (Fig. 7A and B) show a positive correlation, at least for those samples with ash greater than 60%. This suggests a relationship between these elements and the coal mineral matter. Plots of the same concentrations against the percentage of pyrite plus jarosite in the coal (Fig. 7B and D) also show a scattered but overall positive correlation, confirming the association of As and Pb with the pyrite in that mineral matter.

Boron concentrations are typically high in coals deposited under marine conditions (Dai et al., 2005, 2013; Goodarzi and Swaine, 1994; Swaine, 1990). The element often shows an organic affinity (Gluskoter et al., 1977; Riley et al., 2012; Ward, 1980), in which case the B concentration would be expected to increase in the clean coals of the present study, relative to the corresponding ROM materials. However, B in coal may also be associated with illite (Bohor and Gluskoter, 1973), or possibly with small concentrations of minerals such as tourmaline (Boyd, 2002), and in such cases its concentration should be lower in the clean coals than the equivalent ROM samples.

Three of the ROM coals in the present study (CR 5, CR 48, CR 64) have unusually high B concentrations (>100 ppm), with the concentrations being substantially reduced in the corresponding clean coal products. This suggests a strong mineral affinity. The average B concentration for the other ROM materials is 20.3 ppm and that for the corresponding clean coals is 16.7 ppm, with the latter representing 82.4% of the average ROM concentration. This may suggest a mixed affinity for B in most of the coals for the present sample suite. The individual results in Table 7 indicate that the concentration of B is usually, but not always lower in the clean coals than in the corresponding ROM materials. Where it is lower in the clean coal the B probably has a more dominant mineral affinity, and where it is higher the B may have a more dominant organic affinity.

Fig. 7E suggests a positive correlation of B with ash percentage (i.e. a mineral affinity), although this is mainly due to the three coals with high B concentrations (CR 5, CR 48 and CR 64). No significant correlation appears to be indicated between the B concentrations and the ash percentages for the other coal samples. Fig. 7F shows no significant correlation between the B concentration and the percentage of illite + I/S in the whole-coal samples (Table 5), even for the samples with high B concentrations. The apparent correlation of B with ash and the lack of correlation of B with illite + I/S thus suggests that the high B concentrations in samples CR 5, CR 58 and CR 64 may be due to the presence of tourmaline in the ROM materials.

4.2. Elements with concentrations increased by beneficiation

For three of the elements in Table 7, Ge, U and Zr, the average concentrations in the clean coals are significantly higher than in the ROM materials (i.e. >120% of the average ROM values). In these cases the element might be associated in some way with the organic matter, which would give rise to an increase in concentration as the proportion of mineral material is reduced. Plots of the relation between the concentration of these elements and the ash percentage of the coal samples, as indicated by ultimate analysis, are given in Fig. 8A–C. These do not, however, show any consistent trend that would confirm such a relationship for the coals of the sample suite.

Evaluation of the individual sample pairs in Table 7 indicates that the concentration of Ge is increased in the clean coal for eight of the 12 sites, but decreased, sometimes quite substantially, in the remaining four. Many authors, including Gluskoter et al. (1977), Finkelman (1981), Zhuang et al. (2006) and Dai et al. (2012), indicate that Ge in coal

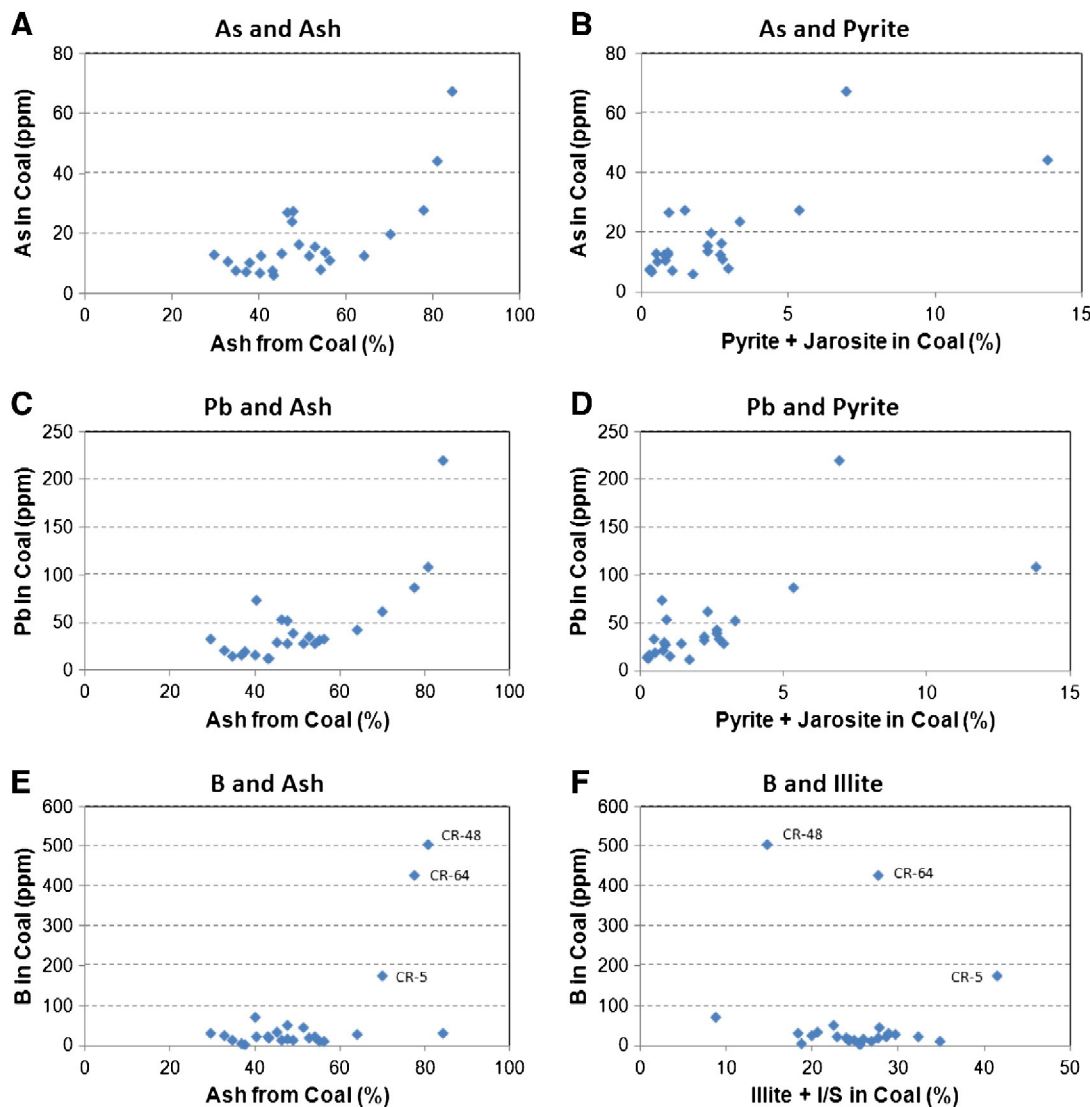


Fig. 7. Plots showing relationships of As and Pb concentrations with ash and pyrite. A) As and ash; B) As and pyrite + jarosite in coal; C) Pb and ash; D) Pb and pyrite + jarosite in coal.

commonly has a strong organic affinity; if so, this would be consistent with the increase associated with beneficiation for many of the sites in the present study. However, the variability in Table 7 suggests that the extent of any such affinity may vary from coal to coal, depending on the sample source. Detailed float–sink studies of fine-crushed coal by Ward (1980) indicated that the mode of Ge occurrence in Australian coals may be variable, with an organic association in some coals and a mineral association in others. Mastalerz and Drobniak (2012) also suggest that Ge in Indiana coals may be associated with either the minerals (clays, pyrite) or the organic matter.

Although Fig. 8D suggests a scattered but broadly positive correlation between the concentrations of the two elements, the pattern shown by U and Zr in Table 7 is also variable for the sample suite. Despite the overall increases suggested by the average values, only five of the 12 sample pairs show an increase in U with beneficiation, and six of the pairs show an increase in Zr, when examined on a site-by-site basis. The averages for Zr are also influenced by high concentrations in some of the clean-coal samples (CR 2, CR 6, CR 10).

Finkelman (1981) suggests that much of the uranium in coal appears to be organically bound, although a substantial proportion may be also associated with accessory minerals such as zircons and rare-earth phosphates. Such a mixed occurrence is consistent with the variable partitioning between ROM and clean coals observed in the present

study, and with the poor correlation to ash percentage as indicated by Fig. 8B.

The indication in Table 7 of a greater abundance of Zr in the clean coals relative to the ROM materials is surprising; this element is generally regarded as having a strong mineral affinity, especially in higher-rank coals (Finkelman, 1981). However, if the data for the three sample pairs with highest Zr concentrations in the clean-coal samples are excluded (CR-1/CR-2, CR-5/CR-6, CR-15/CR-16), the average concentrations for the ROM and clean coals are 154 and 144 ppm, respectively, making the average Zr concentration in the clean coals very similar to that in the ROM materials. The overall trend in the relation between Zr and ash (Fig. 8C) also does not support a consistent correlation, either positive or negative.

Euhedral zircon crystals approximately 5 μm in diameter have been observed during SEM examination of ROM and clean coal samples from the present study (Fig. 9). These may represent the main mode of Zr occurrence within the coal samples. The exact mode of occurrence of such crystals may vary; if they are preferentially associated with the organic-rich parts of the coal seams, possibly due to removal of less-stable constituents in the original peat-forming environment, they could be partitioned with the clean coal fractions and give rise to an apparent organic affinity in the coarse-crushed coals from the preparation plants. Although the mode of Zr occurrence in the coals requires

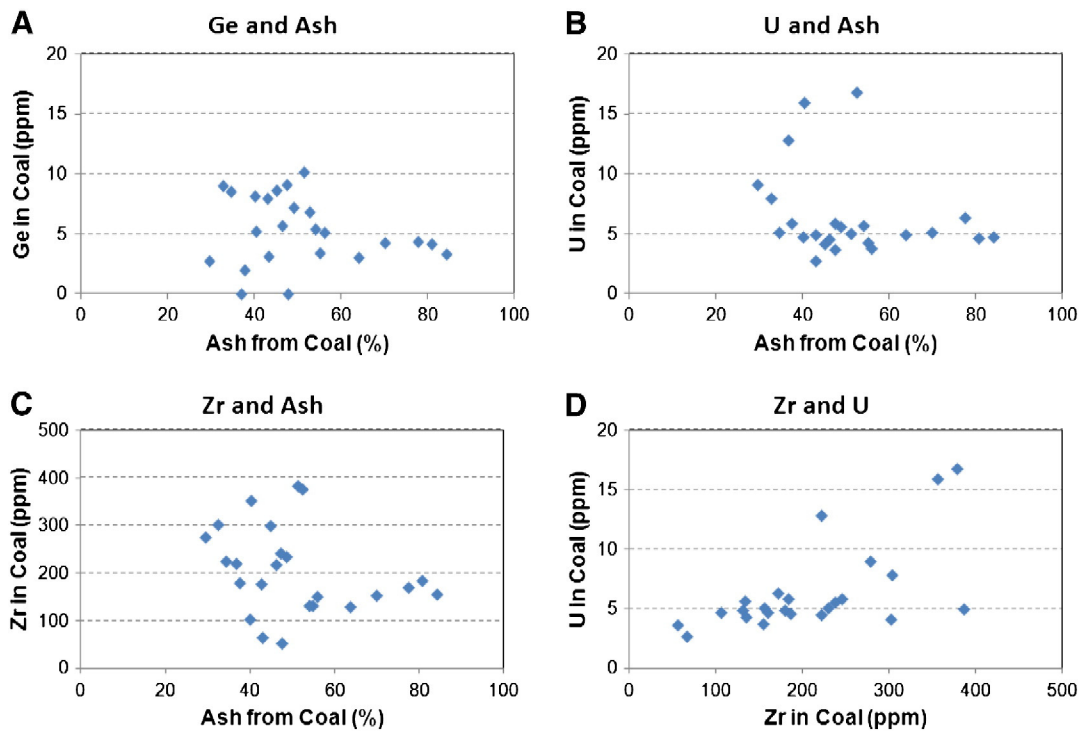


Fig. 8. Plots showing relationships involving trace element components: A) Ge and ash; B) U and ash; C) Zr and ash; D) U and Zr. Ash percentages in each case are inferred from ultimate analysis data.

additional investigation, the averages for the majority of the sample pairs, and the absence of a trend in Fig. 8C, suggest a relatively even partitioning of such crystals between the mineral-rich and organic-rich fractions for most of the sites studied. The possible correlation between Zr and U indicated in Fig. 8D may also suggest an association of U with the zircon components.

4.3. Elements with concentrations unaffected by beneficiation

For the remainder of the trace elements in Table 7, the average concentrations in the clean coal are similar to the averages in the ROM materials, with average concentrations in the clean coals representing between 80 and 110% of the averages in the ROM samples. These elements, moreover, represent the great bulk of the trace elements analysed for the study. Despite the general reduction in the proportion of mineral matter, and also variation in some cases on a site-by-site basis, the average concentrations of these elements do not appear to have been significantly changed by the beneficiation processes. They are probably partitioned, at least at the particle sizes used in commercial preparation, more or less evenly between the mineral-rich and organic-rich components.

5. Conclusions

Comparison of ROM and clean coal products from Santa Catarina preparation plants shows significant reductions in ash, mineral matter and total sulphur percentages associated with beneficiation, and also in the relative proportions of pyrite within the mineral matter. With the exception of pyrite, the mineral matter of the clean coals, as determined by quantitative X-ray diffraction, is similar to that of the respective ROM materials, with abundant quartz, kaolinite, illite and interstratified illite/smectite, and minor proportions of calcite and other accessory phases, and appears to have been little changed by coal preparation.

Although at least some of the pyrite in the coals appears to be in frambooidal form, and therefore intimately associated with the organic matter, the reduction in pyrite content for the clean coal LTAs may

indicate that a significant part of the pyrite in the ROM coals is also relatively coarse-grained and/or associated in some way with the mineral-rich particles in the crushed coals supplied to the preparation plants. The similarities in relative proportions of the other minerals in the LTA of the respective ROM and clean-coal samples, and also the great abundance in both fractions of illite and I/S, indicate that the clay-rich material is intimately admixed with the coal, as might be expected from frequent influx of detrital sediment into the original peat-forming environment, and with the exception of pyrite is not readily liberated from the organic components at the top sizes used in the beneficiation processes.

The reduction in pyrite within the mineral matter is accompanied by a small reduction in the proportion of Fe₂O₃ within the coal ash, although some of the Fe in the coal also appears to be associated with clay minerals such as illite and illite/smectite. A reduction in the proportion of Na₂O in the ash is also noted for the clean coal samples; since the proportions of feldspar (albite) in the respective LTAs remain relatively constant, this may reflect ion-exchange processes in the clay minerals associated with immersion in water during beneficiation.

Comparison of the ROM and clean coal samples indicates that the concentrations of most trace elements are either similar in the two types of material, or are reduced in the clean coal by a similar proportion to the overall reduction in mineral matter content (LTA percentage). The concentrations of As and Pb are reduced to a greater extent, consistent with the reduction in pyrite associated with beneficiation, and plots of their concentration against pyrite on a whole-coal basis confirms that these elements are associated with the pyrite in the ROM materials. The concentration of B also decreases substantially with beneficiation in some of the sample pairs, possibly indicating an association with tourmaline in the relevant ROM materials, but in other most cases is similar in the respective ROM and clean-coal samples.

Some elements, such as Ge, U, and possibly Zr, have higher average concentrations in the clean coals than in the ROM materials, suggesting an association, at least in part, with the organic matter. This does not necessarily mean that the elements are incorporated within the organic material; they may occur in mineral phases that are more intimately

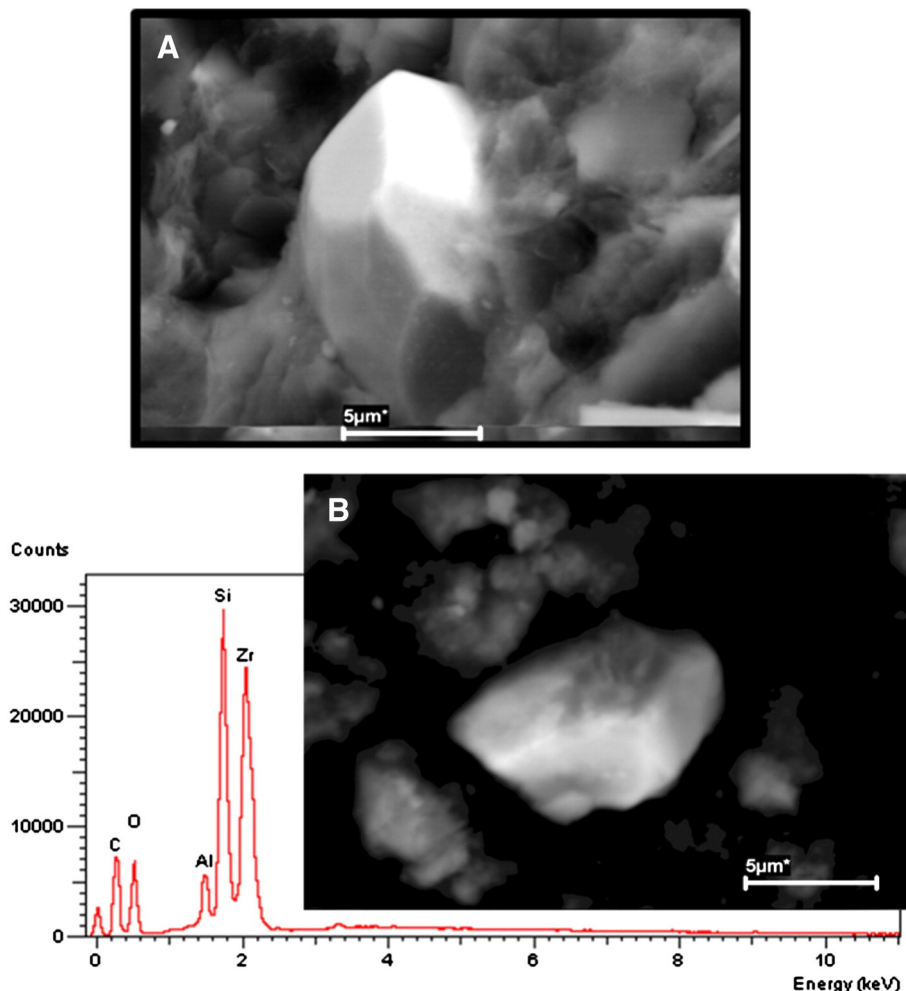


Fig. 9. SEM images of euhedral zircon crystals in (A) ROM (CR 9) and (B) clean coal (CR 10) samples. The EDX spectrum for sample CR 10, representing zircon with minor kaolinite, is also shown.

admixed with the maceral components. The relation to ash percentage suggests that the association for these elements in the different coal deposits may be split between the organic-rich and the mineral-rich components, at least at the particle sizes used in the beneficiation processes.

Acknowledgements

Thanks are extended to David French, Mihaela Grigore and David Jacyna, of CSIRO Energy Technology, for assistance with ashing of the coal samples, and to Irene Wainwright, of the UNSW Analytical Centre, for provision of the XRF analyses. Many thanks are also extended to the relevant coal companies for providing the samples used in the study. Shifeng Dai and an anonymous referee are thanked for their constructive comments on the manuscript.

Luis F.O. Silva and Marcos L.S. Oliveira benefited from a scholarship financed by the National Council of Technological and Scientific Development (Conselho Nacional de Desenvolvimento Científico e Tecnológico—CNPq). The work was financially supported by the CNPq, the Fundação de Amparo à Pesquisa do Estado do Rio Grande do Sul (FAPERGS), and Centro Universitário Lasalle-Canoas (UNILASALLE).

References

- Agência Nacional de Energia Elétrica (ANEEL) (Brasil), 2012. Relatório ANEEL 2011. Agência Nacional de Energia Elétrica, Brasília (108 pp.).
- American Society for Testing Materials (ASTM), 1991. Standard Practice for Preparing Coal Samples for Microscopical Analysis by Reflected Light. ASTM Standard D 2797-91. American Society for Testing and Materials, West Conshohocken, PA (3 pp.).
- American Society for Testing Materials (ASTM), 1996. Standard Test Methods for Collection of a Gross Sample of Coal. ASTM Standard D2234-89. American Society for Testing and Materials, West Conshohocken, PA (10 pp.).
- Bohor, B.P., Gluskoter, H.J., 1973. Boron in illite as a paleosalinity indicator of Illinois coals. *Journal of Sedimentary Petrology* 43, 945–956.
- Boyd, R.J., 2002. The partitioning behaviour of boron from tourmaline during ashing of coal. *International Journal of Coal Geology* 53, 43–54.
- Bryers, R.W., 1996. Fireside slagging, fouling, and high-temperature corrosion of heat-transfer surface due to impurities in steam-raising fuels. *Progress in Energy and Combustion Science* 22, 29–120.
- Clarke, L.B., Sloss, L.L., 1992. Trace Element Emissions From Coal Combustion and Gasification. IEA Coal Research, Series IEACR/49.IEA Clean Coal Centre, London.
- Dai, S., Chou, C.-L., Yue, M., Luo, K., Ren, D., 2005. Mineralogy and geochemistry of a late Permian coal in the Dafang Coalfield, Guizhou, China: influence from siliceous and iron-rich calcic hydrothermal fluids. *International Journal of Coal Geology* 61, 241–258.
- Dai, S., Wang, X., Seredin, V.V., Hower, J.C., Ward, C.R., O'Keefe, J.M.K., Huang, W., Li, T., Li, X., Liu, H., Xue, W., Zhao, L., 2012. Petrology, mineralogy, and geochemistry of the Ge-rich coal from the Wulantuga Ge ore deposit, Inner Mongolia, China: new data and genetic implications. *International Journal of Coal Geology* 90–91, 72–99.
- Dai, S., Zhang, W., Seredin, V.V., Ward, C.R., Hower, J.C., Song, W., Wang, X., Li, X., Zhao, L., Kang, H., Zheng, L., Wang, P., Zhou, D., 2013. Factors controlling geochemical and mineralogical compositions of coals preserved within marine carbonate successions: a case study from the Heshan Coalfield, southern China. *International Journal of Coal Geology* 109–110, 77–100.
- de Souza, K.F., Sampaio, C.H., Kussler, J.A.T., 2012. Washability curves for the lower coal seams in Candiota Mine – Brazil. *Fuel Processing Technology* 96, 140–149.
- Departamento Nacional de Produção Mineral (DNPM), 2010. Anuário Mineral Brasileiro 2010, vol. 1 (Brasília, 871 pp.).
- Diehl, S.F., Goldhaber, M.B., Koenig, A.E., Lowers, H.A., Ruppert, L.F., 2012. Distribution of arsenic, selenium, and other trace elements in high pyrite Appalachian coals:

- evidence for multiple episodes of pyrite formation. *International Journal of Coal Geology* 94, 238–249.
- Feil, N., Sampaio, C.H., Wotruba, H., 2012. Influence of jig frequency on the separation of coal from the Bonito seam – Santa Catarina, Brazil. *Fuel Processing Technology* 96, 22–26.
- Finkelman, R.B., 1981. Modes of Occurrence of Trace Elements in Coal. US Geological Survey Open File Report 81-99 (301 pp.).
- Frazer, F.W., Belcher, C.B., 1973. Quantitative determination of the mineral matter content of coal by a radio-frequency oxidation technique. *Fuel* 52, 41–46.
- Gluskoter, H.J., 1965. Electronic low temperature ashing of bituminous coal. *Fuel* 44, 285–291.
- Gluskoter, H.J., Ruch, R.R., Miller, W.G., Cahill, R.A., Dreher, G.B., Kuhn, J.K., 1977. Trace elements in coal: occurrence and distribution. *Illinois State Geological Survey Circular* 499 (154 pp.).
- Goodarzi, F., Swaine, D.J., 1994. Paleoenvironmental and environmental implications of the boron content of coals. *Geological Survey of Canada Bulletin* 471, 1–46.
- Goodarzi, F., Swaine, D.J., 1995. Environmental Aspects of Trace Elements in Coal. Kluwer Academic Publishers, Dordrecht (312 pp.).
- Holz, M., Ade, M.B., Kalkreuth, W., 1999. Coal Seam Petrology Analyzed Within a Sequence Stratigraphy Framework: Preliminary Results From the Early Permian Rio Bonito Formation of Southernmost Brazilian Gondwanaland. In: Lemos de Souza, M.J., Marques, M.M., Fernandes, J.P. (Eds.), Proceedings and Papers, 2nd Symposium on Gondwana Coals, Porto, 1998. Faculdade de Ciências do Porto, Departamento de Geologia, Memória, 5, pp. 25–36.
- Hower, J.C., Blanchard, L.J., Robertson, J.D., 1998. Magnitude of minor element reduction through beneficiation of Central Appalachian coals. *Coal Preparation* 19, 213–229.
- Huggins, F.E., Seidu, L.B.A., Shah, N., Huffman, G.P., Honaker, R.Q., Kyger, J.R., Higgins, B.L., Robertson, J.D., Pal, S., Serha, M.S., 2009. Elemental modes of occurrence in an Illinois #6 coal and fractions prepared by physical separation techniques at a coal preparation plant. *International Journal of Coal Geology* 78, 65–76.
- Kalkreuth, W., Sherwood, N., Cioccarelli, G., Corrêa da Silva, Z., Silva, M., Zhong, N., Zufa, L., 2004. The application of FAMM (Fluorescence Alteration of Multiple Macerals) analyses for evaluating rank of Parana' Basin coals, Brazil. *International Journal of Coal Geology* 57, 167–185.
- Kalkreuth, W., Holz, M., Kern, M., Machado, G., Mexias, A., Silva, M.B., Willett, J., Finkelman, R., Burger, H., 2006. Petrology and chemistry of Permian coals from the Paraná Basin: 1. Santa Terezinha, Leão-Butiá and Candiota Coalfields, Rio Grande do Sul, Brazil. *International Journal of Coal Geology* 68, 79–116.
- Klepzig, M.C., 2001. Palinologia Aplicada à Reconstituição das Unidades de Paisagem e Dinâmica das Turfeiras Formadoras dos Carvões Permianos do Rio Grande do Sul, Brasil. (Tese Doutorado) Inst. Geociências, UFRGS.
- Kolker, A., 2012. Minor element distribution in iron disulfides in coal: a geochemical review. *International Journal of Coal Geology* 94, 32–43.
- Koukouzas, N., Ward, C.R., Li, Z., 2010. Mineralogy of lignites and associated strata in the Mavropigi field of the Ptolemais Basin, northern Greece. *International Journal of Coal Geology* 81, 182–190.
- Marcello, R.R., Galato, S., Peterson, M., Riella, H.G., Bernardin, A.M., 2008. Inorganic pigments made from the recycling of coal mine drainage treatment sludge. *Journal of Environmental Management* 88, 1280–1284.
- Mastalerz, M., Drobniak, A., 2012. Gallium and germanium in selected Indiana coals. *International Journal of Coal Geology* 94, 302–313.
- Mastalerz, M., Padgett, P.L., 1999. From in situ coal to the final coal product: a case study of the Danville Coal Member (Indiana). *International Journal of Coal Geology* 41, 107–123.
- Matjcie, R.H., Li, Z., Ward, C.R., French, D., 2008. Chemical composition of glass and crystalline phases in coarse gasification ash. *Fuel* 87, 857–869.
- Matjcie, R.H., Ward, C.R., Li, Z., 2012a. Mineralogical transformations in coal feedstocks during carbon conversion, based on packed bed combustor tests, Part 1: bulk coal ash studies. *Coal Combustion and Gasification Products* 4, 45–54.
- Matjcie, R.H., Ward, C.R., Li, Z., 2012b. Mineralogical transformations in coal feedstocks during carbon conversion, based on packed bed combustor tests, Part 2: behaviour of individual particles. *Coal Combustion and Gasification Products* 4, 55–67.
- Milaní, E.J., França, A.B., Schneider, R.L., 1994. Bacia do Paraná. In: Feijó, F.J. (Ed.), artas estratigráficas das bacias sedimentares brasileiras. Rio de Janeiro, Boletim de Geociências da Petrobras, vol. 8 (1), pp. 69–82.
- Moore, F., Esmaeili, A., 2012. Mineralogy and geochemistry of the coals from the Karmozd and Kiasar coal mines, Mazandaran province, Iran. *International Journal of Coal Geology* 96–97, 9–21.
- Norrish, K., Hutton, J.T., 1969. An accurate X-ray spectrographic method for the analysis of a wide range of geological samples. *Geochimica et Cosmochimica Acta* 33, 431–453.
- Oliveira, M.L.S., Ward, C.R., French, D., Hower, J.C., Querol, X., Silva, L.F.O., 2012. Mineralogy and leaching characteristics of beneficiated coal products from Santa Catarina, Brazil. *International Journal of Coal Geology* 94, 314–325.
- Pires, M., Querol, X., 2004. Characterization of Candiota (south Brazil) coal and combustion by-products. *International Journal of Coal Geology* 60, 57–72.
- Querol, X., Fernandez-Turiel, J.L., Lopez-Soler, A., 1995. Trace elements in coal and their behaviour during combustion in a large power station. *Fuel* 74, 331–343.
- Querol, X., Whateley, M.K.G., Fernandez-Turiel, J.L., Tuncali, E., 1997. Geological controls on the mineralogy and geochemistry of the Beyazari lignite, central Anatolia, Turkey. *International Journal of Coal Geology* 33, 255–271.
- Querol, X., Klika, Z., Weiss, Z., Finkelman, R.B., Alastuey, A., Juan, R., Lopez-Soler, A., Plana, F., Kolker, A., Chenery, S.R.N., 2001. Determination of element affinities by density fractionation of bulk coal samples. *Fuel* 80, 83–96.
- Quick, W.J., Irons, R., 2002. Trace element partitioning during the firing of washed and untreated power station coals. *Fuel* 81, 665–672.
- Quispe, D., Pérez-López, R., Silva, L.F.O., Nieto, J.M., 2012. Changes in mobility of hazardous elements during coal combustion in Santa Catarina power plant (Brazil). *Fuel* 94, 495–503.
- Rao, C.P., Gluskoter, H.J., 1973. Occurrence and distribution of minerals in Illinois coals. *Illinois State Geological Survey Circular* 476 (56 pp.).
- Reifenstein, A.P., Kahraman, H., Coin, C.D.A., Calos, N.J., Miller, G., Uwins, P., 1999. Behaviour of selected minerals in an improved ash fusion test: quartz, potassium feldspar, sodium feldspar, kaolinite, illite, calcite, dolomite, siderite, pyrite and apatite. *Fuel* 78, 1449–1461.
- Rietveld, H.M., 1969. A profile refinement method for nuclear and magnetic structures. *Journal of Applied Crystallography* 2, 65–71.
- Riley, K.W., French, D.H., Farrell, O.P., Wood, R.A., Huggins, F.E., 2012. Modes of occurrence of trace and minor elements in some Australian coals. *International Journal of Coal Geology* 94, 214–224.
- Sampaio, C.H., Tavares, L.M.M., 2005. Beneficiamento Gravimétrico: Uma introdução aos processos de concentração mineral e reciclagem de materiais por densidade. 1. ed., Porto Alegre, Editora UFRGS, vol. 1. 603 pp.
- Sampaio, C.H., Aliaga, W., Pacheco, E.T., Petter Filho, E.A., Wotruba, H., 2008. Coal beneficiation of Candiota mine by dry jigging. *Fuel Processing Technology* 89, 198–202.
- Sampaio, C.H., Duarte, C., Miltzarek, G.L., 2011. Characterization and uses of a southern Brazilian coal. *Proceedings of XIV Balkan Mineral Processing Congress, Tuzla, Library Dervis Susic Tuzla*, 2011, vol. 2, pp. 652–655.
- Senior, C.L., Zeng, T., Che, J., Ames, M.R., Sarofim, A.F., Olmez, I., Huggins, F.E., Shah, N., Huffman, G.P., Kolker, A., Mroczkowski, S., Palmer, C., Finkelman, R., 2000. Distribution of trace elements in selected pulverized coals as a function of particle size and density. *Fuel Processing Technology* 63, 215–241.
- Silva, L.F.O., Ward, C.R., Hower, J.C., Izquierdo, M., Waanders, F., Oliveira, M.L.S., Li, Z., Hatch, R.S., Querol, X., 2010. Mineralogy and leaching characteristics of coal ash from a major Brazilian power plant. *Coal Combustion and Gasification Products* 2, 51–65.
- Silva, L.F.O., Sampaio, C.H., Guedes, A., Fdez-Ortiz de Vallejuelo, S., Madariaga, J.M., 2012. Multianalytical approaches to the characterisation of minerals associated with coal and the diagnosis of their potential risk by using combined instrumental microspectroscopic techniques and thermodynamic speciation. *Fuel* 94, 52–63.
- Standards Australia, 2000. Higher Rank Coal–Mineral Matter and Water of Constitution. Australian Standard 1038 Part 22. (20 pp.).
- Swaine, D.J., 1990. Trace Elements in Coal. Butterworth, London (278 pp.).
- Taylor, J.C., 1991. Computer programs for standardless quantitative analysis of minerals using the full powder diffraction profile. *Powder Diffraction* 6, 2–9.
- Thomas, L., 2002. Coal Geology, 2nd edition. John Wiley and Sons, Chichester, UK (384 pp.).
- Vamvaka, D., Mistakidou, E., Drakonaki, S., Fosclos, A., Kavouridis, K., 2001. Ash quality of a beneficiated lignite from Ptolemais Basin, northern Greece. *Energy & Fuels* 15, 1181–1185.
- Vassilev, S.V., Eskenazy, G.M., Vassileva, C.G., 2001. Behaviour of elements and minerals during preparation and combustion of the Pernik coal, Bulgaria. *Fuel Processing Technology* 72, 103–129.
- Wagner, N.J., Tlotengl, M.T., 2012. Distribution of selected trace elements in density fractionated Waterberg coals from South Africa. *International Journal of Coal Geology* 94, 225–237.
- Wang, W., Qin, Y., Wei, C., Li, Z., Guo, Y., Zhu, Y., 2006. Partitioning of elements and macerals during preparation of Antaibao coal. *International Journal of Coal Geology* 68, 223–232.
- Ward, C.R., 1980. Mode of occurrence of trace elements in some Australian coals. *Coal Geology* 2, 77–98.
- Ward, C.R., Spears, D.A., Booth, C.A., Staton, I., Gurba, L.W., 1999. Mineral matter and trace elements in coals of the Gunnedah Basin, New South Wales, Australia. *International Journal of Coal Geology* 40, 281–308.
- Ward, C.R., French, D., Riley, K., Stephenson, L., Farrell, O., Li, Z., 2011. Element leachability from a coal stockpile and associated coastal sand deposits. *Fuel Processing Technology* 92, 817–824.
- Zhuang, X., Querol, X., Alastuey, A., Juan, R., Plana, F., Lopez-Soler, A., Du, G., Martynov, V.V., 2006. Geochemistry and mineralogy of the Cretaceous Wulantuga high-germanium coal deposit in Shengli coal field, Inner Mongolia, northeastern China. *International Journal of Coal Geology* 66, 119–136.